Optimierung, Modifizierung und Charakterisierung therapeutisch aktiver D-Peptide zur Behandlung der Alzheimerschen Demenz

Inaugural-Dissertation

zur Erlangung des Doktorgrades
der Mathematisch-Naturwissenschaftlichen Fakultät
der Heinrich-Heine-Universität Düsseldorf

Vorgelegt von
Antonia Nicole Klein
aus Westerland

Düsseldorf, Mai 2015

Aus dem Institut für Physikalische Biologie
der Heinrich-Heine Universität Düsseldorf

Gedruckt mit der Genehmigung
der Mathematisch-Naturwissenschaftlichen Fakultät
der Heinrich-Heine-Universität Düsseldorf

Referent: Prof. Dr. Dieter Willbold
Korreferent: Prof. Dr. Georg Groth

Tag der mündlichen Prüfung: 15.09.2015

Inhaltsverzeichnis

Tabellenverzeichnis

Abbildungsverzeichnis

Kurzfassung

Bei Protein-Fehlfaltungskrankheiten werden amyloide Strukturen als Ursache für das Entstehen und das Fortschreiten der Krankheit diskutiert. Bei diesen Krankheiten handelt es sich sowohl um neuronale, also auch nichtneuronale Erkrankungen, wie z. B. die Alzheimersche Demenz (AD) und Diabetes Typ II.

Die Selbstaggregation von Aβ-Monomeren gilt als eins der Schlüsselereignisse in der Entstehung der AD. Aktuelle Forschungsergebnisse zeigen, dass Aβ-Oligomere zur Entstehung und dem Fortschreiten der AD führen. Die Inhibierung der Bildung und/oder die Entfernung der Aβ-Oligomere stellen daher vielversprechende therapeutische Ansätze dar. Diese Ansätze wurden durch das mittels Spiegebild-Phagendisplay selektierte D-enantiomere Peptid D3 verwirklicht. D3 ist u. a. in der Lage *in vitro* Aβ-Oligomere zu eliminieren und zeigt in verschiedenen AD Mausmodellen eine therapeutische Effektivität.

Ziel der hier vorliegenden Arbeit war die systematische Optimierung der Aminosäuresequenz von D3 bezüglich der Bindung der D3-Derivate an verschiedene Aβ-Spezies. Anschließend wurden die so selektierten D3-Derivate auf ihre Effektivität Aβ-Oligomere zu eliminieren untersucht.

Im ersten Teil dieser Arbeit wurden ausgehend von der Aminosäuresequenz des Peptids D3 Peptide selektiert, die mit einer höheren Affinität an HFIP-vorbehandeltes Aβ, bestehend hauptsächlich aus Aβ-Monomeren, binden. Mit Hilfe von Peptid-Mikroarrays wurden die D3-Derivate DB1 bis DB5 identifiziert und selektiert. DB3 wurde detailliert *in vitro* charakterisiert. Es bindet an Aβ-Monomere und -Oligomere mit einer mikromolaren Affinität. Die Aggregation von Aβ wird durch DB3 inhibiert und toxische Aβ-Oligomere eliminiert. Des Weiteren werden vorgebildete Aβ-Aggregate durch DB3 zerstört. Um den therapeutischen Effekt von DB3 zu steigern, wurde ein Tandempeptid (DB3DB3) entworfen, das einer C- zu N-terminalen Verknüpfung von zwei einzelnen DB3-Peptiden entspricht. Der *in vitro* Wirkungsgrad wurde durch diese Verdoppelung des Peptides im Vergleich zum einfachen DB3 verstärkt. Dies wird z. B. durch eine 40 x höhere Affinität von DB3DB3 an Aβ-Monomere und -Oligomere und einer 750 x geringeren mittleren effektiven Konzentration (EC_{50}) der Inhibierung der Aβ-Aggregation im Vergleich zu DB3 deutlich.

Zur gezielten Stabilisierung von Aβ-Monomeren und somit einer Inhibierung der Aβ-Aggregation ist eine spezifische Bindung des therapeutischen Wirkstoffs an Aβ-Monomere wichtig. Unter Verwendung von definierten Aβ-Spezies wurde im zweiten Teil dieser Arbeit eine zwei-Schritt-Prozedur mit Peptid-Mikroarrays durchgeführt. Mit dieser Methode wurden sieben weitere D3-Derivate (ANK1 bis ANK7), die mit einer hohen Afftinität und Spezifität an Aβ-Monomere binden, selektiert und *in vitro* charakterisiert. Die D3-Derivate ANK1 bis ANK7 binden an Aβ-Monomere mit einer submikromolaren Affinität, inhibieren die Aggregation von Aβ und eliminieren toxische Aβ-Oligomere ohne den Anteil von Aβ-Monomeren signifikant zu reduzieren. In Folge dessen wird durch die ANK-Peptide die Aβ-induzierte Zytotoxizität auf neuronale Zellen reduziert. Die ANK-Peptide sind in ihrer *in vitro* Wirkung effizienter als D3 und die DB-Peptide. ANK6 reduziert zusätzlich den Prion-ähnlichen Seeding-Mechanismus, wandelt zuvor gebildete Aβ-Aggregate in amorphe, unstrukturierte Aggregate um und verbessert die kognitiven Fähigkeiten von transgenen-APPSwDI Mäusen.

Abstract

Amyloid structures are discussed to be the cause of protein misfolding diseases. Those neuronal and non-neuronal diseases are associated with the misfolding of peptides or proteins and their aggregation to toxic or dysfunctional species, e. g. Alzheimer's disease (AD) and Typ II diabetes.

One hallmark of AD is the aggregation of Aβ monomers to Aβ fibrils via different intermediates. Aβ oligomers are discussed to be responsible for the development and progression of AD. Promising strategies for a causal therapy of AD is to inhibit the aggregation of Aβ monomers into toxic Aβ oligomers or to eliminate them. This approach was realized with the D-enantiomeric peptide D3, which was selected via mirror image phage display. D3 is able to eliminate Aβ oligomers *in vitro* and has therapeutic effect in different AD mouse models.

Goal of this work was to systematically optimize the amino acid sequence of D3 according to the binding ability of the resulting D3 derivatives to different Aβ species. The hereby selected D3 derivatives were analyzed regarding their ability to eliminate Aβ oligomers.

Within the first part of this work, the D-peptide D3 was optimized regarding its binding affinity to HFIP pretreated Aβ, consisting mainly of Aβ monomers. By using peptide microarrays, the D3 derivatives DB1 to DB5 were identified and selected. DB3 is able to bind to monomeric and oligomeric Aβ with a submicromolar affinity, inhibits the Aβ aggregation, eliminates Aβ oligomers, reduces the Aβ-induced celltoxicity and disassembles preformed Aβ aggregates. By generating a head-to-tail tandem peptide of DB3, termed DB3DB3, the beneficial effects of DB3 were increased, as shown for example by a 40 fold higher affinity to Aβ monomers and oligomers and a 750 fold decreased EC_{50} for inhibiting Aβ aggregation.

In order to stabilize Aβ monomers and inhibit their aggregation, highly specific binding to Aβ monomers can be expected to be beneficial. This was addressed in the second part of this work. Seven D3 derivatives, termed ANK1 to ANK7 were identified and selected by a two-step-procedure using peptide microarrays. ANK1 to ANK7 bind with submicromolar affinity to Aβ monomers, inhibit the Aβ aggregation, eliminate Aβ oligomers and reduce the Aβ-introduced celltoxicity. Regarding all these properties, ANK1 to ANK7 are more effective than D3 and the DB-peptides. ANK6 is able to reduce the Aβ seeding potential, to convert preformed Aβ aggregates into unstructured, amorphic aggregates and to enhance cognitive abilities of tg-APPSwDI mice.

1. Einleitung

1.1. Amyloide Fehlfaltungskrankheiten

Für die Funktion von Proteinen ist eine korrekte dreidimensionale Struktur essentiell. Werden Proteine fehlgefaltet und nicht durch natürliche Proteolyse abgebaut, können Proteinaggregate entstehen und Aggregationskrankheiten, wie die Alzheimersche Demenz (AD), die Parkinsonkrankheit (PD), Chorea Huntington (HD) und Amyotrophe Lateralsklerose (ALS) ausgelöst werden. Die Ursachen, die zu pathologischen Proteinfehlfaltungen führen, sind bisher ungeklärt (Carrell *et al.*, 1997).

Bisher wurden 40 amyloide Krankheiten identifiziert, darunter die in Abbildung 1 genannten neuronalen Krankheiten, aber auch nichtneuronale Erkrankungen, wie Diabetes Typ II. Die zur Fehlfaltung neigenden Peptide und Proteine werden auf Grund einer genetisch vererbbaren Mutation oder spontan fehlgefaltet, verlieren so ihre physiologische Funktion oder wirken toxisch. In Folge dessen aggregieren die Peptide und Proteine zu Ablagerungen, die als amyloide Aggregate bezeichnet werden (Chiti *et al.*, 2006).

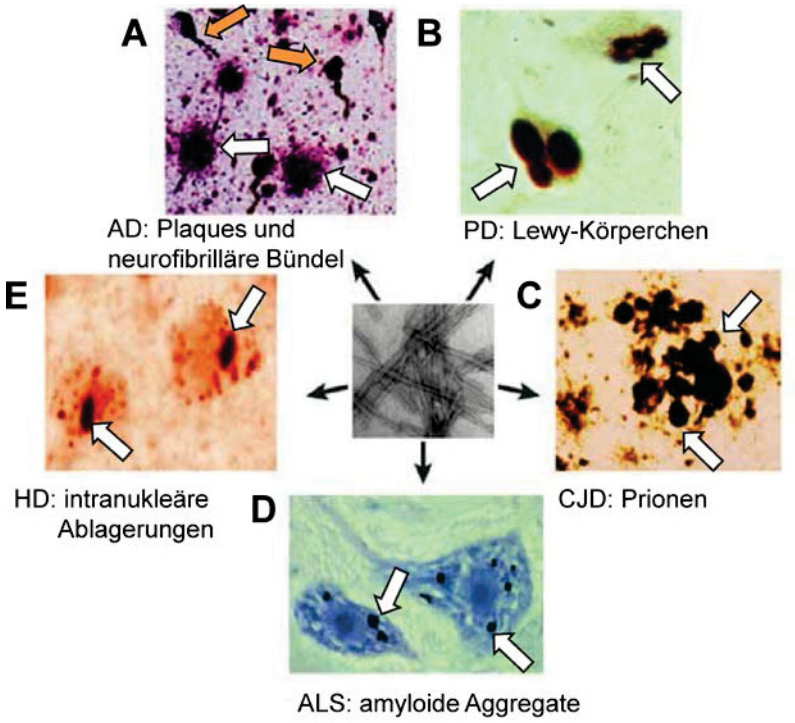

Abbildung 1| Zerebrale Ablagerungen in neurodegenerativen Erkrankungen.

A) Die pathologischen Hauptmerkmale der Alzheimerschen Demenz (AD) sind amyloide Plaques, bestehend hauptsächlich aus Amyloid-β-Peptid (weiße Pfeile), und neurofibrilläre Bündel, die hyperphosphoryliertes Tau-Protein (gelbe Pfeile) enthalten. B) Zytoplasmatische Aggregate, sogenannte Lewy-Körperchen, bestehend aus α-Synuclein, sind typischerweise in den Neuronen von Parkinson-Erkrankten (PD) zu finden. C) Extrazelluläre Prionen kommen in verschiedenen Hirnarealen bei der Creutzfeld-Jakob-Krankheit (CJD) vor. D) Bei Patienten mit Amyotropher Lateralsklerose (ALS) bestehen diese amyloiden Aggregate z. B. aus Superoxid-Dismutase 1. E) Intrazelluläre Aggregate bestehend aus Huntingtin kennzeichnen die Chorea Huntington (HD) Pathologie. Die Struktur der Proteinaggregate (Abbildung in der Mitte) ist bei all diesen Krankheiten sehr ähnlich und besteht aus fibrillären Netzwerken. Abbildung nach Soto (2003).

Amyloide Aggregate besitzen eine geordnete Struktur mit cross-β-Faltblättern, an die die Farbstoffe Kongorot und Thioflavin T binden (Puchtler *et al.*, 1965, Levine, 1993). Cross-β-Struktur entsteht durch die Ausbildung von β-Faltblättern entlang der Fibrillenachse (Nelson *et al.*, 2005). Im Elektronenmikroskop sind typische fibrilläre Strukturen mit geraden, unverzweigten, etwa 10 nm breiten Fibrillen zu erkennen (Abbildung 1, Mitte). Des Weiteren sind amyloide Aggregate besonders resistent gegenüber proteolytischer Degradation (Soto, 2003).

Bei neurodegenerativen Erkrankungen kommt es infolge dieser fehlgefallteten Proteine, der Ausbildung von amyloiden Aggregaten und weiteren

pathologischen Veränderungen im Gehirn, zu Beeinträchtigungen in kognitiven Fähigkeiten, wie z. B. bei: abstraktem Denken, erlernten Bewegungen, Emotionen, Erinnerungen und anderen Fähigkeiten.

Amyloide Aggregate erhöhen des Weiteren die Wahrscheinlichkeit der sexuellen Übertragung von dem humanen Immundefizienz-Virus (HIV). Mit einer durchschnittlichen Wahrscheinlichkeit von 0,0011 % pro Geschlechtsverkehr ist das Risiko einer Mann-zu-Frau intravaginalen Übertragung des HIV-1 sehr niedrig (Gray *et al.*, 2001). Ein Teil der prostataspezifische saure Phosphatase (engl. *Prostatic acidic phosphatase*, PAP), der SEVI (engl. *semen-derived enhancer of viral infection*) genannt wird, bildet in Sperma amyloide Strukturen und steigert die sexuelle Übertragungseffizienz (Münch *et al.*, 2007, Olsen *et al.*, 2010). Dabei erleichtert die intrinsisch positive Ladung der SEVI-Fibrillen das Anlagern und Fusionieren von Virionen mit den Zielzellen, möglicherweise durch Neutralisieren der negativen Ladung von Virionen und der damit verbundenen Reduzierung der Abstoßung der Virionen mit den Zellmembranen der Zielzellen (Roan *et al.*, 2009). Eine präventive Strategie, um die Übertragung von HIV-1 zu verhindern, stellen Inhibitoren dar, welche die amyloiden Strukturen der SEVI-Fibrillen zerstören.

1.2. Die Alzheimersche Demenz

1.2.1. Epidemiologie der Alzheimerschen Demenz

Die AD ist eine neurodegenerative Erkrankung mit zunehmendem Verlust des Kurzzeit-Gedächtnisses und anderen kognitiven Fähigkeiten, verbunden mit zum Teil drastischen Persönlichkeits- und Verhaltensänderungen (Mattson, 2004). Mit 60 bis 80 % zählt AD, gefolgt von der vaskulären Demenz mit 15 %, zu den häufigsten Demenzformen.

Wenige Prozent der an AD erkrankten Personen leiden an der „familiären Alzheimerschen Demenz“ (fAD), die in der Regel bereits vor dem 65. Lebensjahr auftritt. Es sind mehr als 150 verschiedene Mutationen bekannt, die als Ursache für die fAD gelten und hauptsächlich im Presenilin-1 (PS-1) Gen auf Chromosom 14 oder im Gen für das Amyloid-Vorläufer-Protein (APP) auf Chromosom 21 lokalisiert sind. Im Gegensatz dazu wurde 2012 eine Genmutation im APP Gen

entdeckt, die vor kognitiven Beeinträchtigungen allgemein und AD schützt (Jonsson *et al.*, 2012).

Der größte Risikofaktor der AD ist das Lebensalter. Mehr als 95 % der AD Erkrankungsfälle gehören zur sporadischen AD (sAD), die ab einem Lebensalter von 65 Jahren auftritt. Das Risiko an AD zu erkranken verdoppelt sich ab dem 65. Lebensjahren alle fünf Jahre, sodass ab einem Alter von 90 jeder Dritte erkrankt ist (Qiu *et al.*, 2009). Da die Lebenserwartung stetig ansteigt und die Gesellschaft im Durchschnitt immer älter wird, gewinnt AD zunehmend an gesellschaftlicher und wirtschaftlicher Bedeutung. Laut Prognosen wird die Anzahl an Demenzerkrankten von über 36 Mio. im Jahr 2010 auf über 115 Mio. Erkrankte im Jahr 2050 weltweit ansteigen (Abbildung 2). Jährlich kommen 4,3 Mio. neue Fälle hinzu (Prince *et al.*, 2013, Ferri *et al.*, 2005).

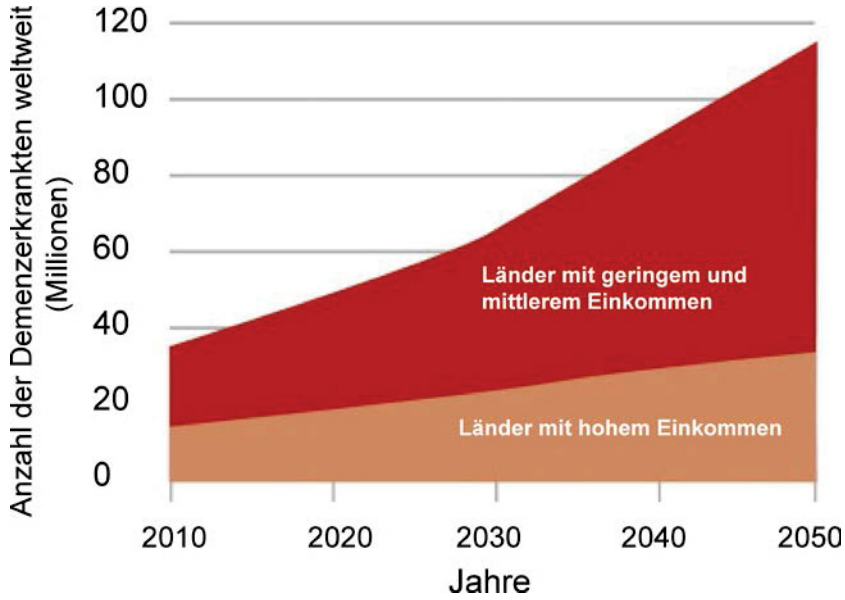

Abbildung 2| Prognose der Demenzerkrankten weltweit von 2010 bis 2050.

2010 gab es etwa 36 Mio. an Demenz erkrankte Personen. Diese Zahl wird bis 2050 voraussichtlich auf über 115 Mio. Demenzerkrankte ansteigen. Davon kommen aktuell 58 % der Demenzerkrankten aus Ländern mit niedrigem oder mittlerem Einkommen. Dieser Anteil wird bis 2050 auf voraussichtlich 71 % ansteigen. Dies steht in Zusammenhang mit einem geringen Bildungsstandard in diesen Ländern. Abbildung nach Prince *et al.* (2013).

Neben dem Alter werden weitere Risikofaktoren für die Entwicklung von AD diskutiert, wie ungesunde Ernährung, wenig Sport, geringe Bildung und häufige Schädel-Traumata (Mayeux, 2003, Beydoun *et al.*, 2014).

Trotz intensiver Forschung (circa 106.000 verschiedene Publikationen zum Thema AD wurden bereits veröffentlicht, Stand Pubmed März 2015) kann AD erst *post mortem* zweifelsfrei bestimmt werden. Zu Lebzeiten wird eine Ausschlussdiagnose mit Hilfe von neurophysiologischen Tests und bildgebenden Verfahren, wie Computertomografie (CT) und Magnetresonanztomografie (MRT) durchgeführt. Genauere Diagnosemethoden, wie Positronen-Elektronen-Tomographie (PET)-Aufnahmen von pathologischen Amyloid-β- und Tau-Ablagerungen oder die Detektion von Biomarkern über das Blut oder Liquor, befinden sich noch in der Entwicklung (Ikonomovic *et al.*, 2008, Blennow *et al.*, 2010, Zhang *et al.*, 2012, Wang-Dietrich *et al.*, 2013).

Des Weiteren existiert keine kausale Therapie, die den Krankheitsverlauf verlangsamen oder gar stoppen kann (Shelanski *et al.*, 2015). Auf mögliche therapeutische Ansätze, die aktuell erforscht und/oder entwickelt werden, wird in Kapitel 1.2.4 detailliert eingegangen.

1.2.2. Pathologie

Das klinische Krankheitsbild von AD kann durch drei pathologische Merkmale beschrieben werden: die Abnahme des Hirnvolumens, das Auftreten von extrazellulären Plaques und das Auftreten von intrazellulären, neurofibrillären Bündeln (Abbildung 3) (Nelson *et al.*, 2012).

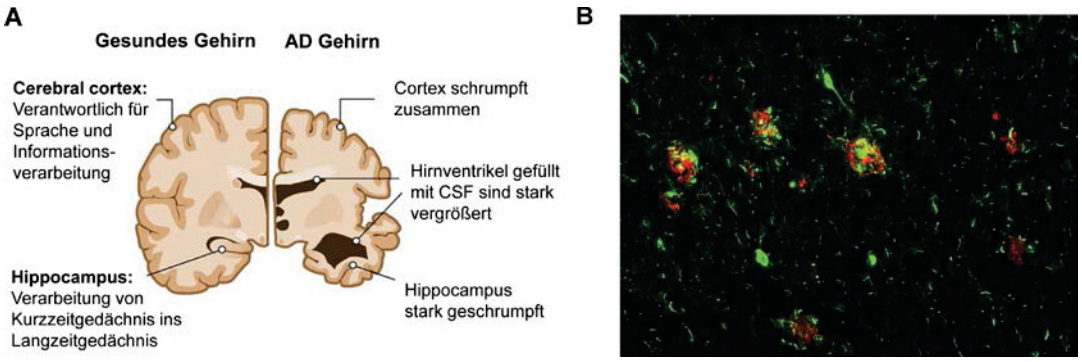

Abbildung 3| Charakteristische Merkmale der AD.

A) Schematische Darstellung eines Gehirns einer gesunden Person (links) und einer an der AD erkrankten Person (rechts). Die Abnahme des Gehirnvolumens ist eine Folge des Schrumpfens von Cortex und Hippocampus. Gleichzeitig vergrößern sich die Hirnventrikel. Quelle: Alzheimer Association. B) *Post mortem* Aufnahmen von Immunfärbungen extrazellulärer Plaques, bestehend hauptsächlich aus Amyloid-β-Peptid, gefärbt in rot und intrazellulären neurofibrillären Bündeln, bestehend aus hyperphosphoriliertem Tau, gefärbt in grün. Quelle: Jakob-Roetne *et al.* (2009)

Durch den fortschreitenden Verlust von Nervenzellen und Synapsen, hauptsächlich im Hippocampus und den Kortex-Regionen (Abbildung 3A), nimmt das Hirnvolumen bei AD-Erkrankten stark ab. Diese Gehirnregionen sind zuständig für Lern- und Erinnerungsprozesse. Die Hirnventrikel gefüllt mit Zerebrospinalflüssigkeit (CSF) sind stark vergrößert.

Neben den neurodegenerativen Prozessen kommt es zu extrazellulären Ablagerungen von Aggregaten aus Aβ-Peptiden, welche in Kapitel 1.2.3 näher beschrieben werden, und von intrazellulären Ablagerungen von neurofibrillären Bündeln (NFTs), bestehend aus dem Mikrotubuli-bindenden Protein Tau (Abbildung 3B) (Jakes *et al.*, 1991, Glenner *et al.*, 1984, Masters *et al.*, 1985).

Tau stabilisiert Mikrotubuli in neuronalen Axonen, wodurch die Funktion von Mikrotubuli beim axonalen Transport und als zytoskelettales Elemente beim Aufbau der Axone gewährleistet wird (Cleveland *et al.*, 1977). Die physiologische Funktion von Tau wird durch seine Phosphorylierung gesteuert (Johnson *et al.*, 2004). Bei AD und frontolateralen Demenz wird Tau hyperphosphoryliert, in Folge dessen die Bindung an Mikrotubuli inhibiert wird (Grundke-Iqbal *et al.*, 1986, Cleveland *et al.*, 1977). Hyperphosporiliertes Tau aggregiert zu abnormalen Fasern (PHFs), die eine helikale Struktur aufweisen. Die PHFs bilden in Neuronen und anderen zerebralen Zellen wiederum höher vernetzte

Aggregate, sogenannte neurofibrilläre Bündel (NFTs). Der Krankheitsverlauf der AD korreliert mit dem Grad der Tauopathie (Braak *et al.*, 1991).

1.2.3. Amyloid-β-Peptid

Bildung und Regulation von Aβ

Hauptbestandteil der extrazellulären Plaques ist das Amyloid-β-Peptid (Aβ), das während unserem gesamten Leben kontinuierlich durch enzymatische Proteolyse vom Amyloid-Vorläufer-Protein (engl. *amyloid precourser protein*, APP) generiert wird (Abbildung 4). APP ist ein 110 bis 130 kDa großes Typ I transmembran Glykoprotein, mit einer membranständigen Domäne, einem extrazellulären glykosylierten N-Terminus und einem kurzen intrazellulären C-Terminus (Zhang *et al.*, 2011). Das APP-Gen ist auf Chromosom 21 lokalisiert.

APP kann durch zwei Wege proteolytisch gespalten werden. Bei dem amyloiden Prozessierungsweg wird APP am resultierenden N-Terminus von Aβ durch das Enzym β-Sekretase geschnitten. Anschließend wird das resultierende Fragment durch den γ-Sekretase-Komplex am resultierenden C-Terminus prozessiert. Da der γ-Sekretase-Komplex verschiedene Schnittstellen innerhalb der Transmembrandomäne von APP erkennt, entstehen verschiedene Aβ-Isoformen mit einer Länge von 30 bis 51 Aminosäuren (Abbildung 4) (Olsson *et al.*, 2014).

Eine alternative APP-Prozessierung, auch als der nicht-amyloide Prozessierungsweg bekannt, erfolgt durch die α-Sekretase (De Strooper, 2010). Die α-Sekretase verhindert die Bildung von Aβ, da APP innerhalb der Aβ-Sequenz geschnitten wird.

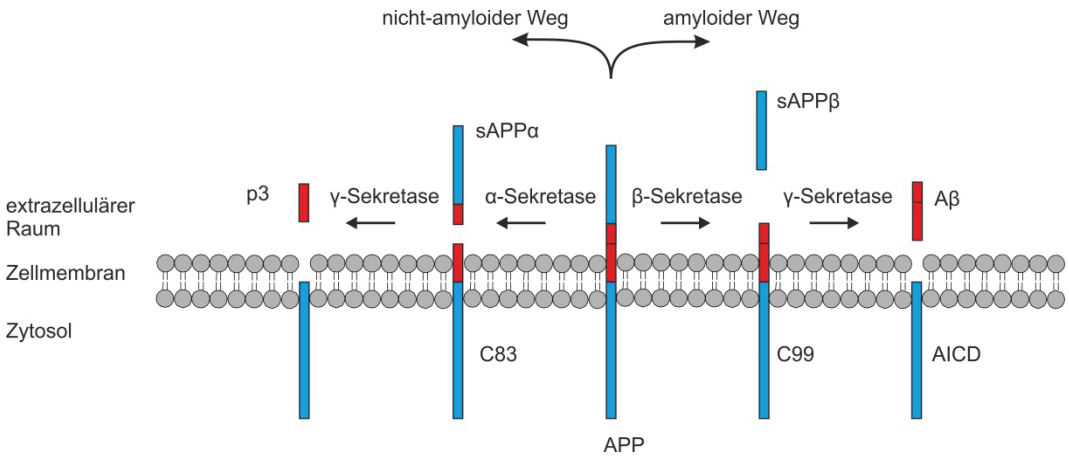

Abbildung 4| APP-Prozessierung.

Die Prozessierung von APP erfolgt auf zwei Wegen. Bei dem amyloiden Weg wird APP zunächst durch die β-Sekretase in sAPPβ und ein membranständiges C99-Fragment gespalten und anschließend durch die γ-Sekretase in Aβ und die intrazelluläre APP-Domäne (*APP intracellular domain*, AICD). Bei dem nicht-amyloiden Prozessierungsweg spaltet die α-Sekretase innerhalb der Aβ-Sequenz und generiert ein extrazelluläres sAPPα-Fragment und ein membranständiges C83-Fragment. Anschließend spaltet die γ-Sekretase ein p3-Fragment vom C83-Fragment ab. Abbildung nach Querfurth *et al.* (2010).

Monomeres Aβ ist ein 4,5 kDa großes, amphipathisches Peptid mit einem hydrophilen N-Terminus und einem hydrophoben C-Terminus. Aβ-Monomere neigen zur Selbstaggregation. Als häufigste Form tritt Aβ im menschlichen Gehirn mit einer Länge von 40 (Aβ(1-40)) und 42 Aminosäuren (Aβ(1-42)) auf. Obwohl der Unterschied nur aus zwei zusätzlichen C-terminalen Aminosäuren (Ala und Ile) besteht, neigt Aβ(1-42) deutlich stärker zur Selbstaggregation als Aβ(1-40) und besitzt eine höhere Toxizität auf neuronale Zellen (Selkoe, 2001). Neben der unterschiedlichen Prozessierung von APP führen auch posttranslationale Modifikationen von Aβ, z. B. die Bildung von Pyroglutamat bei Aβ(3-x) oder die Phosphorylierung von Ser8 und Ser26, zu einem veränderten Aggregationsverhalten von Aβ (Saido *et al.*, 1995, Kumar *et al.*, 2011).

Die physiologische Funktion von monomerem Aβ ist nicht detailliert geklärt. Berichtet wird, dass monomeres Aβ eine neuroprotektive Funktion hat, als antimikrobielles Peptide im angeborenen Immunsystem und bei der Induzierung von proinflammatorischen Aktivitäten bei einer Vielzahl von Mikroben wirkt (Soscia *et al.*, 2010, Giuffrida *et al.*, 2009).

Aβ wird u. a. durch Neprilysin, das Insulin abbauende Enzym (IDE), das Endothelin-Konversionsenzym und Plasmin abgebaut (Eckman *et al.*, 2005). Neprilysin ist eine Membran-assoziierte Zink-Endopeptidase, die Aβ-Monomere und -Oligomere abbaut (Kanemitsu *et al.*, 2003). IDE, eine Thiolmetalloendopeptidase, baut kleine Peptide, wie Insulin und monomeres Aβ ab (Qiu *et al.*, 1998).

Des Weiteren stellt sich im Blut und Gehirn ein Gleichgewicht von Aβ über die Blut-Hirn-Schranke (engl. *blood brain barrier*, BBB) ein. Aβ wird über das *low-density lipoprotein receptor related protein* (LRP1) durch die BBB aus dem Gehirn transportiert und in der Leber oder Niere abgebaut. Ins Gehirn wird Aβ über den *receptor for advanced glycation endproducts* (RAGE) transportiert (Deane *et al.*, 2009, Deane *et al.*, 2003).

Aβ-Oligomere und deren pathologische Effekte

In der Literatur werden eine Vielzahl von verschiedenen synthetischen und im menschlichen Organismus vorkommenden Aβ-Aggregationsformen diskutiert, unter anderem Protofibrillen, ringförmige Strukturen, Aggregationskeime, aus Aβ bestehende diffuse Liganden (ADDLs), sowie globuläre und amyloide Fibrillen (Abbildung 5). Im Allgemeinen werden Aβ-Oligomere, die u. a. als Dimer, Tetramer oder als größere Dodecamere (Aβ*56) *in vivo* auftreten, für die Enstehung und den Krankheitsverlauf von der AD verantwortlich gemacht. Die Konzentration von Aβ-Oligomeren korreliert stärker mit dem Krankheitsverlauf als die Konzentration von Aβ-Fibrillen (McLean *et al.*, 1999, Hartley *et al.*, 1999). Aβ-Fibrillen stellen eine Reservoir von löslichen, toxischen Aβ-Oligomeren dar und/oder haben eine protektive Funktion (Haass *et al.*, 2007).

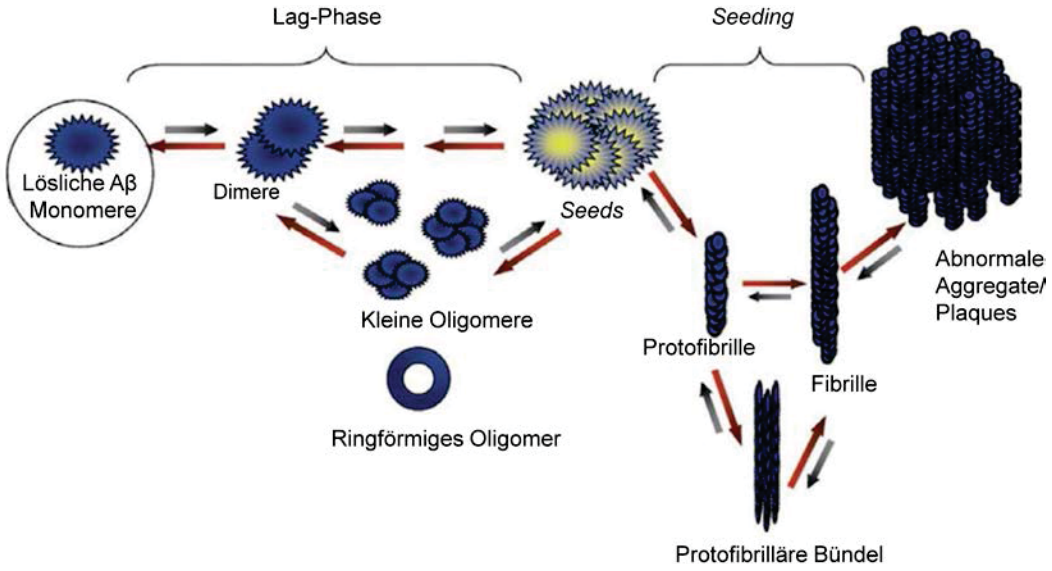

Abbildung 5| Aggregation von Aβ.

Lösliche Aβ-Monomere aggregieren zu Dimeren und kleinen löslichen Oligomeren. Im Folgenden aggregieren Aβ-Oligomere zu Protofibrillen, Fibrillen und größeren abnormalen Aggregaten. Die Aggregationsreaktion kann unterteilt werden in eine Lag-Phase, bei der die Bildung der Aβ-Oligomere als *Seeds* (Aggregationskeim) die zeitlimitierende Reaktion darstellt, gefolgt von einer Seeding-Phase (beschleunigten Aggregations-Phase). Nebenprodukte stellen kleine und ringförmige Oligomere dar. Es ist bisher nicht klar, ob sie zu *On-* oder *Off-Pathways* gehören. Abbildung modifiziert nach Finder *et al.* (2007).

Die Lag-Phase der Aβ-Aggregation kann durch die Zugabe von vorgebildeten Aβ-Aggregationskeimen, auch *Seeds* genannt, reduziert werden. Dies wird als ein Prion-ähnlicher aggregationskeimgeförderter Mechanismus, auch *Seeding* genannt, diskutiert (Cohen *et al.*, 2013, Petkova *et al.*, 2005). Die Bildung von *Seeds*, welche aus Aβ-Oligomeren besteht, ist der limitierende Faktor und wird durch eine Lag-Phase bei der Aggregation von Aβ-Monomeren zu Fibrillen deutlich. Der *Seeding*-Mechanismus ist hoch spezifisch, andere amyloiden Strukturen können die Aggregation von Aβ nicht auslösen (O'Nuallain *et al.*, 2004). Nach der Lag-Phase folgt eine schnelle Wachstumsphase der Aβ-Aggregate.

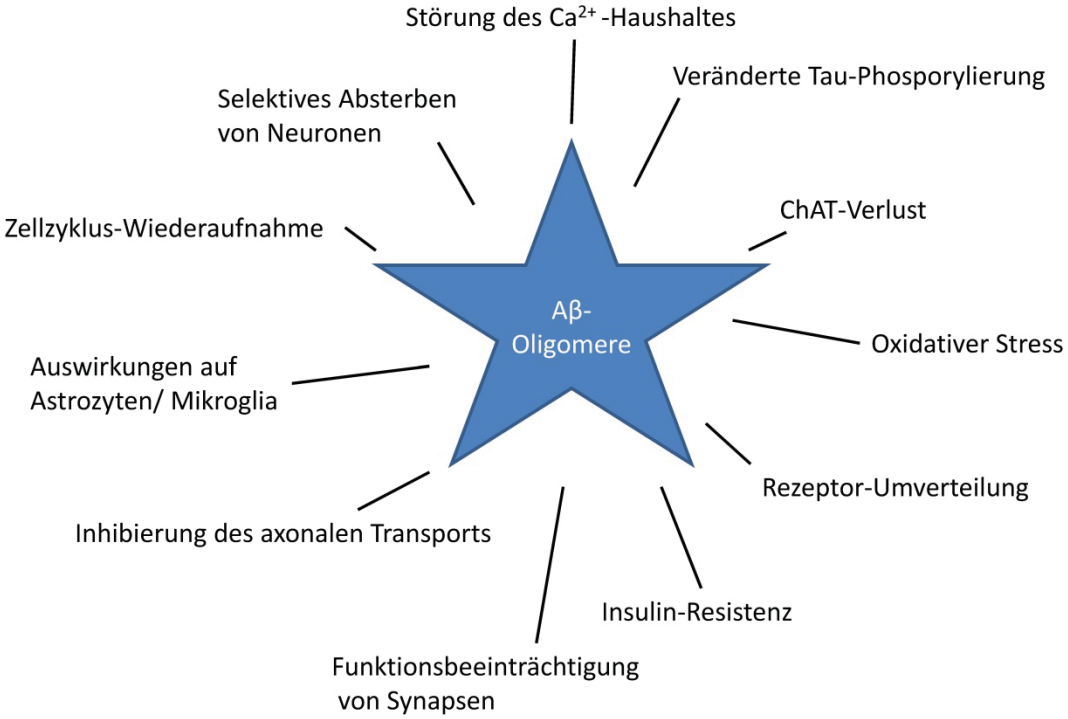

Abbildung 6| Direkter und indirekter Einfluss von Aβ-Oligomere auf die Pathologie von AD.

Aβ-Oligomere führen zur Störung des Ca^{2+}-Haushaltes durch Ausbilden von Membranporen, verändern die Tau-Phosporylierung und inhibieren somit den axionalen Transport. Durch die Aktivierung von inflammatorischen Signalwegen werden Astrozyten und Migroglia aktiviert und Neuronen und Synapsen sterben ab bzw. verlieren ihre Funktion (Sondag *et al.*, 2009, White *et al.*, 2005). Aβ-Oligomere induzieren oxidativen Stress, der zum Verlust der Aktivität der Cholinacetyltransferase (ChAT) führt (Butterfield, 2002, Nunes-Tavares *et al.*, 2012). Des Weiteren haben Aβ-Oligomere einen Einfluss auf Insulin und den Zellzyklus (Varvel *et al.*, 2009, Seward *et al.*, 2013, Zhao *et al.*, 2008). Abbildung nach Viola *et al.* (2015).

Die Bildung von toxischen Aβ-Oligomeren führt zu einer Reihe von Ereignissen auf immunologische und neuronale Funktionen (Abbildung 6). Unter anderem wird eine inflammatorische Reaktion von Mikroglia und Astrocyten auslöst. Neuritische und neuronale Dysfunktionen führen zum Verlust von Nervenzellen und Synapsen (Goure *et al.*, 2014, Itagaki *et al.*, 1989).

Vaskuläre Veränderungen führen zu einer beeinträchtigten Funktion von Blutgefäßen. Dadurch wird der Transport von Nährstoffen zu den Neuronen verringert und der Aβ-Abbau über die BBB aus dem Gehirn reduziert (Iadecola, 2004).

Aβ-Oligomere inhibieren die Langzeit-Potenzierung (LTP), verstärken Langzeit-Depression (LTD) und reduzieren die dendritische Dornen Dichte (Shankar *et al.*, 2008). Zusätzlich hat das C-terminale Fragment von APP evtl. einen beschleunigenden Effekt auf die Entstehung synaptische Dysfunktion und den Verlust von Synapsen in der AD (Oster-Granite *et al.*, 1996).

Aβ-Oligomere wirken auf den N-Methyl-D-Aspartat-Rezeptor (NMDAR) (J. J. Li, Dolios, Wang, & Liao, 2014; S. Li et al., 2009), der indirekt durch den Transport von Ca^{2+} in die Synapsen und die damit verbundene Aktivierung von verschiedenen Signalwegen, für die LTD verantwortlich ist. Aβ-Oligomere aktivieren den NMDAR, wodurch die Ca^{2+}-Aufnahme erhöht, die Glutamataufnahme verringert und das LTD verstärkt wird.

Die toxische Wirkung von Aβ-Oligomeren beruht des Weiteren auch auf der Induktion von oxidativem Stress. Aβ-Oligomere interagieren mit reduzierenden Metallen, z. B. Fe^{2+} und Cu^{+} und bilden H_2O_2. In Membrannähe werden dadurch Lipide peroxidiert und die Bildung von 4-hyroxynonenal (4HNE) induziert. Dies ist ein toxisches Aldehyd, das Cystein, Lysin und Histidin in Proteinen kovalent modifiziert, z. B. Membrantransporter, Rezeptoren, GTP-bindende Proteine und Ionenkanäle, und so ihre Funktion beeinträchtigt (Mattson, 2004). Des Weiteren haben Aβ-Oligomere einen Einfluss auf den zellulären Energiestoffwechsel.

Es konnte gezeigt werden, das Aβ in die Zellmembran inkorporiert und dort Poren bildet. Durch diese Poren kann Ca^{2+} in die Zellen diffundieren und Apoptose ausgelöst (Lashuel *et al.*, 2002, Quist *et al.*, 2005, Poojari *et al.*, 2013).

In Fachveröffentlichungen wird diskutiert, dass Aβ-Oligomere eine verstärkte Tau-Phosphorylierung bewirken, wodurch der axonale Transport inhibiert wird (Jin *et al.*, 2011, Rhein *et al.*, 2009).

Amyloid-β-Kaskaden-Hypothese

Die Aβ-Kaskaden-Hypothese besagt, dass ein Ungleichgewicht von Aβ-Produktion und -Abbau zur Neurodegeneration und Demenz führt (Abbildung 7) (Blennow *et al.*, 2006). Bei einer neueren Version der Aβ-Kaskaden-Hypothese werden die kleineren, löslichen, am stärksten toxischen Aβ-Oligomere als

Ursache der AD angesehen. Ausgelöst durch einen bisher unbekannten Faktor kommt es zu einer erhöhten extrazellulären Gesamt-Aβ-Bildung, einem veränderten Aβ(1-40)/Aβ(1-42) Verhältnis und/oder einem gestörten Abbau von Aβ (Kuperstein *et al.*, 2010). Die daraus resultierende Aggregation von Aβ ist eines der Schlüsselereignisse in der Entstehung der AD. Die intrazelluläre Aggregation von Aβ führt zu der Bildung von verschiedenen koexistierenden Aβ-Aggregationsformen (Abbildung 5). Die Aβ-Oligomerisierung führt über mehrere Zwischenereignisse zur Demenz (Jin *et al.*, 2011).

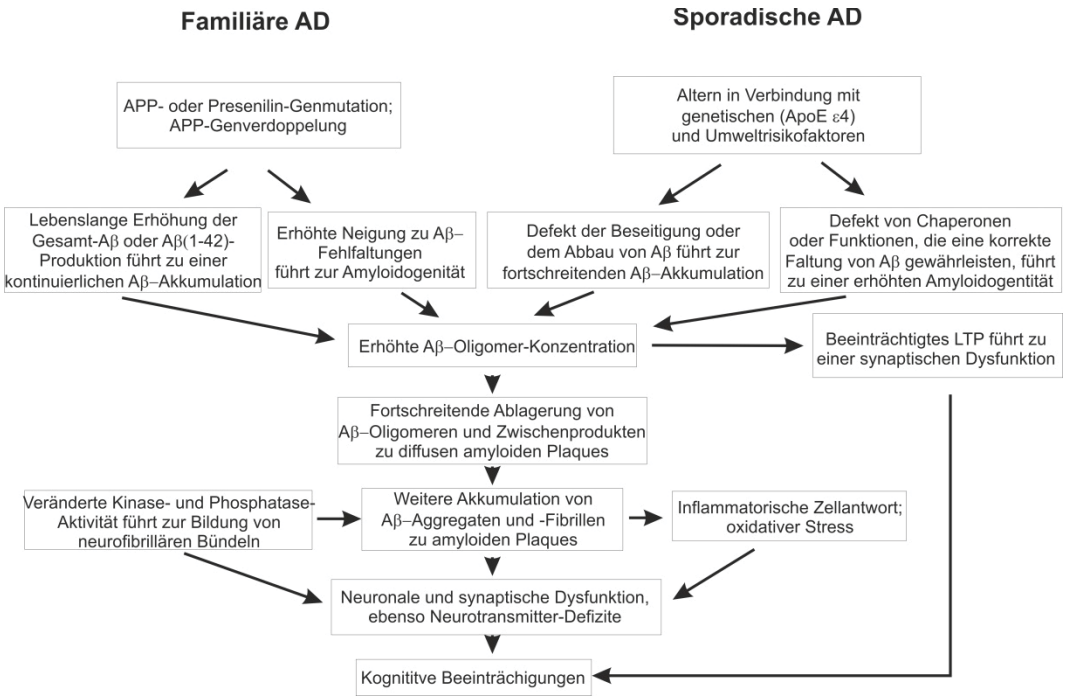

Abbildung 7| Schematische Übersicht der Amyloid-β-Kaskaden-Hypothese.

Ein Ungleichgewicht zwischen Aβ-Produktion und -Abbau im Gehirn resultiert in einer erhöhten Konzentration an Aβ-Peptid und führt zur Entstehung der AD, mit neuronaler Degeneration und Demenz im weiteren Krankheitsverlauf. Bei der fAD wurde eine erhöhte Gesamt-Aβ- oder Aβ(1-42)-Produktion festgestellt. Bei der sAD gibt es Hinweise auf einen gestörten Aβ-Abbau. In fAD und sAD führt eine erhöhte Neigung zur Oligomerisierung und Aggregierung von Aβ. Verlust von Synapsen und der Krankheitsverlauf von AD korreliert mit der Konzentration an Aβ-Oligomeren. Als Folge der erhöhten Konzentration von Aβ-Oligomeren wird das LTP im Hippocampus inhibiert, wodurch die Synapsenfunktion gestört wird. Des Weiteren wird Tau hyperphosphoriliert und neurofibrilläre Bündeln gebildet, sowie inflammatorischer und oxidativer Stress ausgelöst. Abbildung nach Blennow *et al.* (2010).

1.2.4. Therapeutische Ansätze

Palliative Therapie

In den 1980er Jahren galt ein Mangel an Acetylcholin als Auslöser für die AD. Aus dieser Hypothese sind die heutigen zugelassenen Medikamente Donepezil, Rivastigmin und Galatamin entstanden, die allerdings, wie wir heute wissen, nur die Symptome behandeln, nicht die Ursachen. Sie können den symptomatischen Krankheitsverlauf bis zu zwei Jahre verlangsamen (Courtney *et al.*, 2004, Bullock *et al.*, 2005). Memantine ist ein weiteres zugelassenes AD Medikament. Es inhibiert die Aktivierung des NMDA-Repetors, die durch die glutaminerge Dysfunktion ausgelöst wird und zu eine intrazellulären Akkumulation von Ca^{2+}-Ionen führt. Zusätzlich nehmen viele AD-Patienten antipsychotische Medikamente und Antidepressiva (Brodaty *et al.*, 2003, Masterman, 2003).
In den letzten zwei Jahrzehnten wurden auf Basis der Amyloid-β-Kaskaden-Hypothese und mit Hilfe von transgenen Mausmodellen einige kausal wirkende Medikamente entwickelt, von denen aber bislang keines in allen Phasen der klinischen Prüfung erfolgreich getestet wurde. Zugrundeliegende therapeutische Ansätze sind dabei β- und γ-Sekretase-Inhibitoren, Immuntherapien durch Aβ Antikörper, Aggregationsmodulatoren von Aβ und Tau-basierte Therapien (Abbildung 8). Andere ursächliche therapeutische Ansätze, wie eine Cholesterol-basierte Therapie, Metallkomplexbildung mit Cu^{2+}- und Zn^{2+}-Ionen und Inhibierung von synaptotoxischen und neurodegenerativen Effekten werden hier nicht weiter diskutiert, sind aber auch mögliche Ansätze (Hardy *et al.*, 2002).

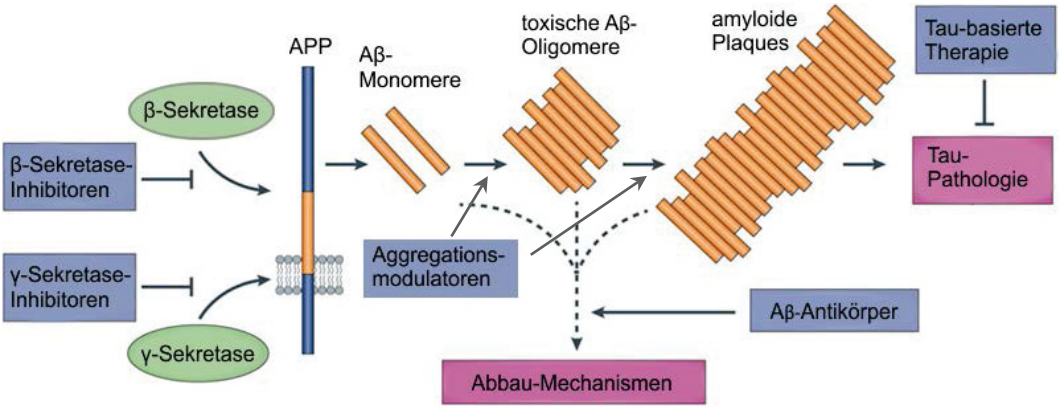

Abbildung 8| Die Amyloid-Kaskaden-Hypothese und mögliche therapeutische Ansätze.

Schematische Darstellung möglicher therapeutischer Strategien bei der Amyloid-Vorläufer-Protein (APP) Prozessierung (durch β- und γ-Sekretase-Inhibitoren), der Aβ-Aggregation (durch Aggregationsmodulatoren und -inhibitoren oder Aβ-Immuntherapie) oder der Tau-Pathologie (Tau-basierte Therapie). Kombinationen der möglichen Therapien ist die vielversprechendste Strategie. Abbildung modifiziert nach Mullard (2012).

Sekretase-Inhibitoren

Ein therapeutischer Ansatz ist die Reduktion der Bildung von Aβ durch Inhibition der Sekretasen. Wie in Kapitel 1.2.3 gezeigt, wird Aβ durch die β- und γ-Sektretasen generiert.

Eine Inhibierung der γ-Sekretase gestaltet sich schwierig, da die γ-Sekretase über 100 Substrate besitzt, u. a. das Protein Notch (De Strooper *et al.*, 1999). Notch ist ein Rezeptor, der bei der Entwicklung von Geweben und Embryonen mit verantwortlich ist (Andersson *et al.*, 2011). Die Inhibierung der γ-Sekretase muss zur Vermeindung von Off-Target Effekten deshalb sehr spezifisch für die APP-Prozessierung sein (Lundkvist *et al.*, 2007). Die klinischen Studien der γ-Sekretase-Inhibitoren Semagacestat (LY-450139) und Svagacestat (BMS-708163) wurden abgebrochen, weil keine Verbesserung der kognitiven Fähigkeiten erreicht wurde und es zu Off-Target-basierten Nebenwirkungen auf Grund der Gesamtinhibierung der γ-Sekretase kam. Neue Strategien für γ-Sekretase-Inhibitoren sind nicht die aktive Domäne zu blockieren, sondern die substratandockenden Domäne, die spezifisch für APP ist (Wolfe, 2006) und die Adenosintriphosphate (ATP)- Bindungsdomäne zu blockieren. Letztere moduliert selektiv die APP-Prozessierung (Fraering *et al.*, 2005).

Die Entwicklung von Sekretase-Inhibitoren verlagert sich immer mehr auf β-Sekretase (BACE) Inhibitoren. Zwei Beispiele für aktuell in klinischen Phasen befindenden BACE1-Inhibitoren sind E2609 und MK-8931. MK-8931 ist ein von Merck lizenziertes kleines Molekül, bei dem in der Phase I bis zu 94 % Reduktion von Aβ(1-40) in CSF bei einer zwei wöchigen Studie beobachtet wurde (Forman *et al.*). E2609 erreichte in der Phase I 46 - 80 % Reduktion von Aβ in CSF bei einer Verabreichung über 2 Wochen. Allerdings haben Studien gezeigt, dass auch BACE1 andere Substrate, z. B. Neuregulin 1 (NRG1), besitzt (Savonenko *et al.*, 2008), und BACE1-knockout-Mäuse Verhaltensstörungen entwickeln. Derzeit werden weitere klinische Studien im Menschen mit BACE1-Inhibitoren durchgeführt.

Immuntherapie

Ein weiterer therapeutischer Ansatz zur Behandlung von AD ist die Immuntherapie. Bei einer Immuntherapie wird durch Antikörper z. B. gegen Aβ eine Immunantwort ausgelöst und Aβ abgebaut. Unterschieden werden hierbei aktive und passive Immunisierungen.

Bei der aktiven Immunisierung wird Aβ oder Teile von Aβ als Immunogen verabreicht, die Produktion von eigenen Antikörpern gegen dieses Aβ-Immunogen, dass durch die Antikörper erkannt wird, anregt und Aβ abgebaut (Schenk *et al.*, 1999). Die aktive Immunisierung ist allerdings mit Risiken verbunden. Eine klinische Studie der Phase II eines Aβ(1-42)-Vakzines wurde auf Grund einer mit T-Helferzellen assoziierten, autoimmunen Meningoenzephalitis bei 6 % der Patienten abgebrochen (Orgogozo *et al.*, 2003).

Bei der passiven Immunisierung werden Antikörper verabreicht, die die T-Zell-Antwort aktivieren (Bard *et al.*, 2000). Im Folgenden werden Medikamente der passiven Immuntherapie vorgestellt, die sich in der klinischen Prüfung befinden.

Solanezumab und Bapineuzumab sind zwei humanisierte monoklonale IgG1 Antikörper, die gegen Aβ gerichtet sind. Solanezumab bindet an die mittlere Domäne von monomerem Aβ (Bard *et al.*, 2003), Bapineuzumab bindet den N-Terminus von Aβ. Beide Antikörper konnten in der klinischen Phase III keine

generelle klinische Verbesserung oder deutlichen Krankheitsveränderungen zeigen (Doody *et al.*, 2014, Salloway *et al.*, 2014, Wisniewski *et al.*, 2015).

BIIB37, auch bekannt unter dem Namen Aducanumab, ist ein Antikörper, der aggregiertes Aβ erkennt. Aducanumab wurde durch umgekehrte translationale Medizin (*reverse translational medicine*) aus gesunden, alten Spendern gewonnen. Dieser humane Antikörper bindet an ein konformationelles Epitop von Aβ und erkennt keine Aβ-Monomere. Bei einer klinischen Studie IB mit diesem Antikörper konnte ein therapeutischer Effekt gegen AD beim Menschen beobachtet werden (Sheridan, 2015) [http://www.alzforum.org/therapeutics/aducanumab].

Aβ-Aggregations- und Abbaumodulatoren

Bei der Modulation der Aβ-Aggregation wird das Ziel verfolgt, die Konzentration der pathogene Aβ-Oligomere oder generell Aβ-Aggregaten zu reduzieren. Dies kann erfolgen durch die Inhibierung der Bildung oder durch das Entfernen von Aβ-Oligomeren oder Aβ-Aggregaten (Knowles *et al.*, 2014).

Einige natürliche Substanzen, zum Beispiel Kurkuma und Epigallocatechingallat (EGCG), zeigen eine inhibierende Eigenschaft auf die Aβ-Aggregation (Begum *et al.*, 2008, Ehrnhoefer *et al.*, 2008). Die meisten dieser Substanzen sind Farbstoff- oder Phenolderivate und binden unspezifisch an eine Vielzahl von Biomolekülen.

Durch die Interaktion von Aβ mit kleinen Molekülen, wie heterozyklische Aminopyrazole oder Peptide, wie z. B. D3 (wird im weiteren Verlauf dieses Kapitels detaillierter eingeleitet), werden die amyloidogenen Eigenschaften von Aβ verändert (Nagel-Steger *et al.*, 2010, Funke *et al.*, 2010, Kirsten *et al.*, 1997, Rzepecki *et al.*, 2004).

Es wurden einige kleine Peptide entwickelt, sogenannte β-Faltblattbrecher, die auf der Selbsterkennungssequenz von Aβ, der mittleren hydrophoben Region ^{17}LVFF^{20}, basieren (Sciarretta *et al.*, 2006). Der β-Faltblattbrecher iAβ5p (Ac-LPFFD-NH_2) konnte in zwei verschiedenen transgenen AD-Mausmodellen die Aβ-Plaque-Belastung und zerebralen Schädigungen reduzieren (Permanne *et al.*, 2002).

Ein weiterer therapeutischer Ansatz ist, den Abbau von Aβ zu fördern. Im Gehirn wird Aβ hauptsächlich durch Neprilysin und IDE abgebaut (vgl. Kapitel 1.2.3). Die Aktivität von Neprilysin und IDE nimmt während des Alterns und bei der AD ab (Wang *et al.*, 2003, Caccamo *et al.*, 2005). Mit Hilfe von Medikamenten kann die Aktivität dieser Proteasen gesteigert und somit der Abbau von Aβ gefördert werden (Cabrol *et al.*, 2009).

D-Peptide

Ein Vorteil von Peptiden gegenüber Antikörpern ist ihre geringe Größe und damit verbundene effizientere Bioverfügbarkeit. Besonders synthetische Peptide besitzen eine geringere Immunogenität als Proteine und nicht-körpereigene Antikörper (McGregor, 2008). Des Weiteren sind Peptide günstiger in der Herstellung, besitzen eine höhere Aktivität pro Masseneinheit, eine höhere Lagerungsstabilität und zeigen eine geringe Wechselwirkung mit anderen Medikamenten (Vlieghe *et al.*, 2010).

Das größte Problem von Peptiden ist allerdings eine schnelle Degradation und mangelnde Permeabilität über biologische Barrieren, wie die Blut-Hirn-Schranke. Dies führt zu kurzen *in vivo* Halbwertszeiten (im Allgemeinen < 30 min) und geringen oralen Bioverfügbarkeiten (1 - 2 % der verabreichten Gesamtmenge) (Lee *et al.*, 1989, Bocci, 1989).

Um die Proteaseresistenz von Peptiden zu steigern können die normalerweise in L-enantiomerer Konformation vorliegenden Aminosäuren teilweise oder komplett gegen D-enantiomere Aminosäuren austauscht werden (Powell et al., 1993). Eine weitere Strategie ist das Verwenden von nicht-natürlich vorkommenden Aminosäuren. Die Bioverfügbarkeit kann durch chemische Modifikation verbessert werden, z. B. führt die C-terminale Polyamidierung zu einer höheren BBB Permeabilität von Peptiden (Poduslo *et al.*, 1999).

D3 (s. Tabelle 1) ist ein dodecameres, D-enantiomeres Peptid, welches durch einen Spiegelbild-Phagendisplay mit Selektion gegen monomeres und möglicherweise kleine oligomere Aβ(1-42)-Spezies identifiziert wurde (Wiesehan, 2003; Wiesehan, 2008; van Groen, 2008).

Tabelle 1| Aminosäuresequenz von D3.
Die Aminosäuresequenz (Ein-Buchstaben-Code) von D3 und die chemischen Eigenschaften der Aminosäuren sind dargestellt. Gekennzeichnet wurden saure Aminosäuren (D und E) in rot, basische Aminosäuren (K und R) in blau, polar, ungeladene Aminosäuren (G, S, T, N, Q und C) in grün, hydrophobe Aminosäuren (A, I, L, M, V, und P) in schwarz und aromatische Aminosäuren (F, H, Y und W) in grau. Da alle Aminosäuren des D3-Peptids in D-enantiomerer Konformation sind, wurden die Buchstaben klein geschrieben.

Peptid	Aminosäuresequenze
D3	rprtrlhthrnr

In vitro Studien haben gezeigt, dass D3 die Bildung von Aβ-Fibrillen inhibiert, die zytotoxische Wirkung von Aβ(1-42) reduziert und Aβ-Aggregate möglicherweise in nicht-amyloide, nicht-fibrilläre und nicht-toxische Aggregate umwandelt. Es reduziert den Anteil an Aβ-Oligomere und verschiebt das Gleichgewicht zu größeren Aβ-Aggregaten ohne den Anteil an Aβ-Monomere zu reduzieren (Funke *et al.*, 2010). D3 bindet an amyloide Plaques und bevorzugt an Aβ-Oligomere (Bartnik *et al.*, 2009, van Groen *et al.*, 2009). Mit Hilfe eines *in vitro* Models konnte gezeigt werden, das D3 die BBB passieren kann (Liu *et al.*, 2009).

In silico Studien deuten darauf hin, dass D3 mit den negativ geladenen Gruppen von Aβ interagiert. Dadurch wird die Ladung der Oberfläche von Aβ kompensiert. Dies führt zu einer Reduktion der Löslichkeit und fördert die Aβ-Aggregation (Funke *et al.*, 2010, Olubiyi *et al.*, 2012).

In vivo reduziert D3 die Aβ-Plaque-Menge und zerebrale Inflammation in transgenen Mäusen (APPSwe/PSΔE9) nach Applikation direkt ins Gehirn. Durch orale Applikation wurden die kognitiven Fähigkeiten verbessert und neuroinflammatorische Prozesse reduziert (Funke *et al.*, 2010, van Groen *et al.*, 2013, van Groen *et al.*, 2008).

Durch rationales Wirkstoffdesign wurden weitere D3-Derivate, z. B. RD2, entwickelt und *in vitro* charakterisiert (Olubiyi *et al.*, 2014) [http://www.alzforum.org/news/conference-coverage/d-peptides-drugs-protein-therapy-approaching-phase-1-trials]. Ein weiteres D3-Derivat wurde durch die

Verknüpfung von D3 als molekulare Erkennungsdomäne mit einem Aminopyrazol als β-Faltblattbrecher entwickelt. Dieses D3-Derivat zeigt eine gesteigerte *in vitro* Wirksamkeit im Vergleich zu D3 (Müller-Schiffmann *et al.*, 2010).

1.3. Screeningverfahren zur Medikamentenentwicklung

Medikamente können durch Screening von Datenbanken zur Identifizierung von Bindungsliganden an ein spezielles Zielprotein entwickelt werden. Eine Screeningmethode ist die Phagendisplay-Methode (Scott *et al.*, 1990, Devlin *et al.*, 1990). Phagen exprimieren die Aminosäuresequenz eines Peptids, Proteins oder Teile von Proteinen als Fusionskonstrukt zusammen mit dem Hüllprotein auf der Phagenoberfläche. Diese Aminosäuresequenz ist ebenfalls im Phagengenom inseriert (Smith *et al.*, 1997). Bei der Phagendisplay-Methode werden Phagenbibliotheken mit über 1 Mrd. verschiedenen Peptidsequenzen in Lösung zu einem immobilisierten Zielprotein gegeben. Die Liganden bleiben bei einem Waschschritt an dem Zielprotein gebunden, alle anderen Phagen werden durch waschen entfernt. Nach verschiedenen Selektionsrunden wird ein Einzelphage isoliert und die Peptidsequenz, die an das Zielprotein bindet, durch Sequenzierung des Phagengenoms identifiziert.

Eine Abwandlung der klassischen Phagendisplay-Methode ist das Spiegelbild-Phagendisplay. Dabei wird gegen den Spiegelbild der Ziel-Moleküle selektiert. Ein Peptid mit der so identifizierten Aminosäure-Sequenz, in der aber alle Aminosäure Reste D-enantiomere Aminosäuren darstellen, binden dann an das Original-Zielmolekül (Funke *et al.*, 2009, Schumacher *et al.*, 1996).

Eine weitere Hochdurchsatzmethode um viele Liganden-Studien gleichzeitig durchzuführen, sind Mikroarrays. Mikroarray ist ein Oberbegriff für eine ganze Reihe von verschiedenen Arrayformaten und Anwendungen. Mit Hilfe von DNA-, RNA-, Protein-, Lysat- und Peptid-Mikroarrays lassen sich ganze Genom-, Proteom-, Transkiptom- und Metabolismusstudien durchführen (Schena *et al.*, 1995, Zhu *et al.*, 2003, Leivonen *et al.*, 2009, Foong *et al.*, 2012). Der große Vorteil von Mikroarrays ist die Automatisierung, Parallelisierung und Minimalisierung von den zuvor genannten Studien, da mehrere tausend verschiedene Liganden auf einer Oberfläche immobilisiert werden, wobei jeder Liganden einzeln in einem kleinen definierten Bereich (*Spot*) vorliegt. Durch ein

Experiment können somit tausende von Einzelnachweisen parallel durchgeführt werden.

Neben den Arrayformaten, die sich hinsichtlich des Liganden, der auf dem Array immobilisiert ist, und der Anwendung unterscheiden, wird zusätzlich zwischen Makro- und Mikroarrays unterschieden. Makroarrays weisen wenige Spots pro Array auf und das Trägermaterial des Arrays besteht häufig aus einer Membran, z. B. Cellulose. Sie besitzen typischerweise 20 Spots pro cm^2, wobei ein Spot einen Durchmesser von 2 - 3 mm hat. Mikroarrays haben eine hohe Anzahl an Spots pro Array und als Trägermaterial dienen häufig Glasobjektträger, wie sie in der Mikroskopie verwendet werden. Sie besitzen 200 Spots pro cm^2 mit einem Spotdurchmesser kleiner als 1 mm (Katz *et al.*, 2011).

In Abbildung 9 ist der Aufbau von Peptid-Mikroarrays schematisch dargestellt. Bei Peptid-Mikroarrays sind Peptide kovalent auf Objektträgern immobilisiert (Fodor *et al.*, 1991). Der Analyt wird in Lösung auf den Objektträger gegeben.

Es gibt verschiedene Verfahren um eine Interaktion von immobilisierten Liganden und freien Analyten zu detektieren. Bei der markierungsbasierten Detektion wird der Analyt direkt markiert oder über ein mehrstufiges Detektionssystem (z. B. mit einem sekundären Antikörper) nachgewiesen. Erfolgt die Detektion über Fluoreszenz wird diese mit einem Laserscanner gemessen. Nachteil dieser Detektionsmethode ist, dass möglicherweise die Bindestelle des Liganden durch den Farbstoff blockiert wird. Dieses Problem tritt bei der markierungsfreien Detektion nicht auf (Lokate *et al.*, 2007).

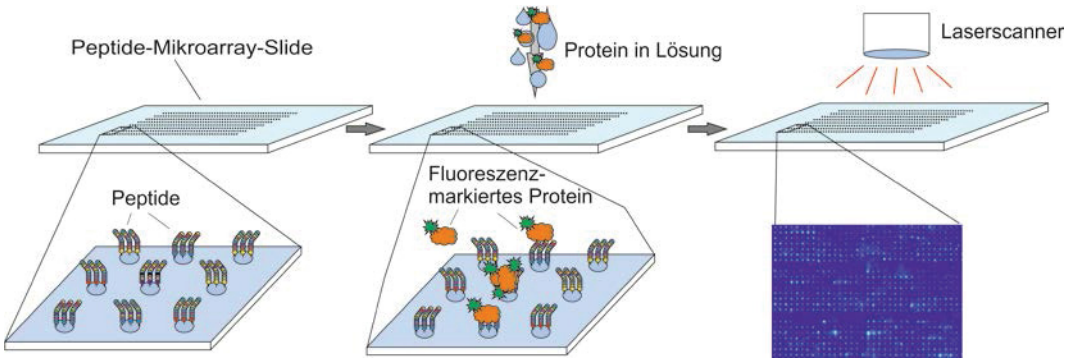

Abbildung 9| Aufbau von Peptid-Mikroarrys.

Identische Peptide werden in einem 100 µm breiten Bereich kovalent an einen Standard-Mikroskopie-Objektträger immobilisiert. Auf einem Mikroarray-Objektträger können so über 1000 verschiede Peptide immobilisiert werden (links). Nach der Immobilisierung wird der Peptid-Mikroarray-Objektträger mit Substrat inkubiert (Mitte). Das Substrat kann mit einem Fluorochrom markiert sein. In diesem Fall kann die Detektion mit einem Laserscanner erfolgen (rechts).

Peptid-Mikroarrays haben einen breiten Anwendungsbereich, z. B. beim Erstellen von Enzymprofilen (Kinase- und Protease-Screening), Affinitätsprofilen (Epitopmapping und *Proteinfingerprints*) und in der Diagnostik (Andresen *et al.*, 2006).

Viele bei einem Screening identifizierte Substanze werden nach generellen Wirksamkeitsstudien durch rationales Wirkstoffdesign hinsichtlich ihrer Funktion und pharmakokinetischen Eigenschaften chemisch optimiert, zum Beispiel durch N- oder C-terminale Modifizierung um die Bioverfügbarkeit zu steigern (Vlieghe *et al.*, 2010).

2. Zielsetzung dieser Arbeit

Trotz intensivster Forschung gibt es für die AD kein kausal wirkendes Medikament. Als Ursache von AD wird aktuell die Bildung von toxischen Aβ-Oligomeren diskutiert. Als effektivste Behandlungsstrategie wird daher die Inhibierung der Bildung oder die Eliminierung von Aβ-Oligomeren angesehen. In vorherigen Arbeiten in unserer Arbeitsgruppe wurden mittels Spiegelbild-Phagendisplay D-enantiomere Peptide entwickelt. D3 wurde durch die Selektion gegen HFIP-vorbehandeltes Aβ, bestehend überwiegend aus Aβ-Monomeren, identifiziert und bindet bevorzugt an Aβ-Oligomere. Im AD-Mausmodell zeigte D3 eine nachweisbare therapeutische Eignung.

Hauptziel dieser Arbeit war die systematische Optimierung der D3-Aminosäuresequenz bezogen auf die Bindung an verschiedene Aβ-Spezies. Als Hochdurchsatzmethode sollten Peptid-Mikroarrays verwendet werden. Die Selektion von möglichen optimierten D3-Derivaten sollte auf Basis einer erhöhten Affinität gegenüber HFIP-vorbehandeltes Aβ und einer erhöhten Affinität sowie Spezifität an Aβ-Monomere erfolgen. Dazu sollte eine Prozedur mit Peptid-Mikroarrays etabliert werden.

Im Anschluss sollten die neu selektierten D3-Derivate durch verschiedene biochemische und biophysikalische Methoden charakterisiert und ihre *in vitro* Effektivität mit D3 verglichen werden. Für weitere *in vitro* und *in vivo* Studien sollte ein vielversprechender Kandidat ausgewählt werden.

3. Ergebnisse

3.1. Publizierte Ergebnisse

3.1.1. Optimization of the all-D peptide D3 for Aβ oligomer eliminiation

Einzureichen bei: PlosOne

Impact Factor (2013): 3.534

Eigener Anteil: 80 %

Entwicklung und Durchführung der Peptid-Mikroarray-Studien, Durchführung des Thioflavin T-Assay, QIAD-Assays und transmissionselektronenmikroskopischen Aufnahmen, Schreiben des Manuskripts

Optimization of the all-D peptide D3 for Aβ oligomer elimination

Antonia Nicole Klein[1], Tamar Ziehm[1], Markus Tusche[1], Johan Buitenhuis[2], Dirk Bartnik[1], Annett Boeddrich[3], Thomas Wiglenda[3], Erich Wanker[3], Susanne Aileen Funke[1,4], Oleksandr Brener[1,5], Lothar Gremer[1,5], Janine Kutzsche[1], Dieter Willbold[1,5,*]

[1] Institute of Complex Systems, Structural Biochemistry (ICS-6), Research Center Jülich, 52425 Jülich, Germany

[2] Institute of Complex Systems, Soft Matter (ICS-3), Research Center Jülich, 52425 Jülich, Germany

[3] Neuroproteomforschung und Molekulare Mechanismen Neurodegenerativer Erkrankungen, Max-Delbrück-Centrum für Molekulare Medizin, Berlin, Germany

[4] Bioanalytik, Fakultät angewandte Naturwissenschaften, Hochschule für angewandte Wissenschaften Coburg, 96450 Coburg

[5] Institut für Physikalische Biologie, Heinrich-Heine-Universität Düsseldorf, 40225 Düsseldorf, Germany

*Correspondence: d.willbold@fz-juelich.de

Abstract

The aggregation of amyloid-β (Aβ) is suspected to be the crucial event in Alzheimer's disease (AD). Especially small neurotoxic oligomers of Aβ are thought to be responsible for the development and progression of the disease. Therefore, their elimination is a promising objective for a causal therapy of AD.

Starting from the well characterized D-enantiomeric peptide D3, we identified D3 derivatives, which bind monomeric Aβ. The underlying hypothesis is that ligands, which bind monomeric Aβ, can be expected to stabilize Aβ monomers within the various equilibria with Aβ assemblies, which ultimately should lead to elimination of Aβ oligomers. One of the hereby identified D-peptide, called DB3, and a head-to-tail tandem of DB3, named DB3DB3, were studied in more detail. We could show that both compounds (i) inhibit the formation of Thioflavin T-positive fibrils, (ii) bind to Aβ monomers with micromolar affinities, (iii) eliminate Aβ oligomers, (iv) reduce Aβ-induced cytotoxicity and (v) disassemble preformed Aβ aggregates. The beneficial effects of DB3 were topped by the tandem peptide DB3DB3 which showed highly enhanced efficacy. Our approach yielded Aβ monomer stabilizing ligands that can now be used to investigate, whether this is a suitable therapeutic strategy.

Introduction

Each year, there are 4.2 million new cases of dementia worldwide with Alzheimer's disease (AD) being the most common cause and up to now there is no causal treatment for AD available [1, 2].

Intracellular neurofibrillary tangles (NFTs), consisting of hyperphosphorylated tau, and extracellular plaques, consisting predominantly of amyloid-β (Aβ), are the major pathological hallmarks of AD. The cleavage of the amyloid precursor protein (APP) by the β- and γ-secretases results in the release of Aβ. Because neither the N- nor the C-terminal cleavage is homogeneous, various species of Aβ are formed. The most abundant species of Aβ is Aβ(1-40), consisting of 40 amino acids. The second most dominant species is Aβ(1-42) [3, 4].

According to the amyloid cascade hypothesis, the aggregation of Aβ is considered to be responsible for the development and the progression of AD. Various Aβ aggregate species have been described, including Aβ oligomers and Aβ protofibrils [5]. Especially the soluble, toxic Aβ oligomers are thought to be responsible for damage of synaptic plasticity, formation of free radicals, disequilibrium of intracellular calcium distribution, chronic inflammation and increased phosphorylation of tau [6, 7]. Thus, the inhibition of Aβ oligomerization or the elimination of Aβ oligomers are promising treatment strategies for the development of a causal therapy of AD.

We have previously selected the 12mer all-D-enantiomeric peptide D3 via mirror image phage display [8, 9]. *In vitro*, D3 binds to amyloid plaques, reduces Aβ aggregation to regular fibrils, eliminates Aβ oligomers, and converts preformed fibrils into non-amyloidogenic, non-fibrillar, non-toxic aggregates [10-14]. *In vivo*, the plaque load and cerebral inflammation of transgenic mice is reduced after injection of D3 into the brain and cognitive impairment of transgenic mice is improved after oral application [10, 15, 16].

In the present study, we screened for D3 derivatives with optimized efficiency. To allow screening for various derivatives, we used peptide microarrays, as they allow miniaturization, parallelization and automatization and enable high throughput screenings [17, 18]. In addition, non-natural amino acids and linker groups, like biotin or fluorescein, can be introduced easily.

We screened more than 600 different D3 derivatives for their ability to bind monomeric Aβ and characterized the five most promising candidates with respect to their ability to prevent Aβ fibril formation. For further optimization, the most promising D3 derivative DB3 was modified by designing a head-to-tail tandem peptide, called DB3DB3. Both peptides were characterized in more detail regarding their affinity to Aβ monomers and their efficiency to eliminate Aβ oligomers.

Material and Methods

Peptides

Aβ(1-42), N-terminally biotinylated Aβ(1-42) and FITC-Aβ(1-42) were purchased from Bachem (Heidelberg, Germany). D3 (rprtrlhthrnr), DB1 (rpitrlhtdrnr), DB2 (rpittlqthqnr), DB3 (rpitrlrthqnr), DB4 (rprtrlrthqnr), and DB5 (rpitrlqtheqr) were purchased from JPT (Berlin, Germany). DB3DB3 (rpitrlrthqnrrpitrlrthqnr) was purchased from peptides&elephants (Potsdam, Germany). All D-peptides consisted of D-enantiomeric amino acids, were C-terminally amidated and more than 95 % pure.

HFIP pretreatment of Aβ(1-42)

For monomerization Aβ(1-42), N-terminally biotinylated Aβ(1-42) and FITC-Aβ(1-42) were dissolved in 1,1,1,3,3,3-hexafluoroisopropanol (HFIP) overnight to a final concentration of 1 mg/ml and aliquoted. HFIP was evaporated by vacuum concentration (Concentrator 5301, Eppendorf, Germany) for 20 min and the aliquots were stored at -20 °C until further usage.

Peptide Microarrays

Pepspot membranes

In a first generation peptide array, every position of the 12 amino acid residue D-peptide D3 was replaced against all 20 naturally occurring amino acids in their D-enantiomeric conformation. The nitrocellulose membrane spotted with these 240 different peptides (JPT, Berlin, Germany) was blocked using TBS pH 7.4 with 10 % v/v blocking solution (Roche, Basel, Switzerland) for 2.5 h at room temperature. After 5 min washing with TBS and 0.1 % v/v Tween 20 (TBS-T), the membrane was incubated with 5 µM Aβ(1-42) in 10 mM sodium phosphate buffer pH 7.4 for 1 h. The potential of all 240 derivatives to bind monomeric Aβ was measured by applying 6E10 (BioLegend, San Diego, USA, diluted 1:10.000 in TBS pH 7.4) and a horseradish peroxidase (HRP)-conjugated goat anti-mouse antibody (Fisher Scientific, Schwerte, Germany, diluted 1:10.000 in TBS pH 7.4). The membrane was washed with TBS-T pH 7.4 for 2 h. HRP activity was measured after incubation with HRP substrate (Pierce, Waltham, USA) by using a ChemiDoc 200 detection system (Bio-Rad Laboratories, Munich, Germany) and the ImageLab software (Bio-Rad Laboratories, Hercules, Munich, Germany).

Pepscan

For the second generation a peptide microarray was produced by Pepscan (Lelystad, Netherlands).

For the Pepscan chip, the peptides were covalently coupled on glass slides in triplicate (spots with diameter of 100 µm). Slides were incubated with 5 µM FITC-Aβ(1-42) in 10 mM sodium phosphate buffer pH 7.4 for 1 h at room temperature with gentle agitation. After incubation, the slides were washed three times with TBS-T for 10 min, three times with water for 10 min and subsequently dried using a stream of nitrogen gas.

Fluorescence intensity of FITC-Aβ(1-42) bound to the peptide spots on the slides was measured using a FLA800 fluorescence image system (Fujifilm Medical Systems USA Inc, Stamford, USA) with a slide carrier employing a 473 nm laser for excitation. Digital images were recorded at 5 µm resolution. The fluorescence was analyzed using the software AIDA Array Metrix (Raytest, Staubenhardt, Germany). Signals were integrated for each spot (diameter 80 µm). Background signal was detected from local dot rings width at a diameter of 150 µm and background ring width of 30 µm and subtracted from the peptide spot signal.

Thioflavin T (ThT) Assay

20 µM Aβ(1-42) was mixed with 20 µM Thioflavin T (ThT) and 31 µg/ml DB3 or DB3DB3 within 10 mM sodium phosphate buffer pH 7.4. The assay was performed using a non-binding 96 well plate (Greiner Bio-One, Frickenhausen, Germany). ThT fluorescence was measured every 15 min at λ_{ex} = 440 nm and λ_{em} = 490 nm in a temperature-controlled plate reader (Polarstar Optima, BMG, Offenburg, Germany) at 37 °C with 1 min agitation before every measurement. Each value was background corrected using the ThT fluorescence of a solution without Aβ(1-42) but containing the peptide.

Biolayer interferometry (BLI)

BLI experiments were performed using an Octet RED96 instrument (fortéBIO, PALL Life Science, Menlo Park, USA). N-terminally biotinylated Aβ(1-42) was dissolved in HFIP, lyophilized and dissolved in 2 mM aqueous sodium hydroxide (1 mg/ml) in order to destroy any pre-existing aggregates. The Aβ(1-42) solution was neutralized by dilution in running buffer (20 mM sodium phosphate buffer pH 7.4) to a final concentration of 20 µg/ml and directly immobilized on Super Streptavidin biosensors (SSA) (fortéBIO, PALL Life Science, Menlo Park, USA) to a final of 3 nm. Ligand biosensors and reference biosensors were quenched with 20 µg/ml biotin for 7 min.

For K_D determinations, the binding of a dilution series of DB3 (200 µM, 100 µM, 50 µM, 25 µM, 12.5 µM, 6.25 µM, 3.125 µM) or DBDB3 (20 µM, 10 µM, 5 µM, 2.5 µM, 1.25 µM, 0.625 µM, 0.3125 µM) was detected in parallel to the ligand biosensors and reference biosensors. A separate buffer cycle was used for double referencing. For evaluation, steady state response

levels were plotted against the applied peptide concentrations and fitted according to Langmuir´s 1:1 binding model (Hill function with n = 1, OriginPro 8.5G, OriginLab, Northampton, USA).

QIAD assay

The quantitative determination of interference with Aβ(1-42) aggregate size distribution (QIAD) was performed as described before [14]. In brief, 80 µM Aβ(1-42) was incubated in 10 mM sodium phosphate buffer pH 7.4 for 4.5 h at 22 °C with 600 rpm agitation. Aβ(1-42) aggregation was continued for additional 40 min with or without DB peptide. The hereby obtained partial size distribution was analyzed by applying a density gradient centrifugation. 100 µl of the incubated sample were placed on top of a gradient with 5 to 50 % iodixanol (Optiprep, Axis-shield, Oslo, Norway) and separated at 259.000 x g for 3 h at 4 °C using an ultracentrifuge (Optima MAX-XP, Beckman Coulter, Brea, USA). Fourteen fractions à 140 µl were taken from top to bottom. The pellet was dissolved by adding 60 µl of 6 M guanidine hydrochloride to the centrifugation tube. After boiling for 5 min, the dissolved pellet sample was collected. The samples were stored at -80 °C until further use.

For quantification of the Aβ(1-42) amount in each fraction, a reversed phase high performance liquid chromatography (RP-HPLC) was performed using a Zorbax SB-300 C8 column (Agilent, Böblingen, Germany) connected to an Agilent 1260 Infinity system using 30 % (v/v) acetonitrile with 0.1 % (v/v) trifluoroacetic acid (TFA) as mobile phase with a flow of 1 ml/min and a column temperature of 80 °C. The applied sample volume was 20 µl. The UV absorption at 214 nm was measured. For quantification of the Aβ(1-42) amount, the area under the peak representing Aβ(1-42) was calculated and the molar concentration was determined using a calibration curve.

For additional control and visualization of the Aβ content in each fraction a 16 % tricine-SDS-PAGE was performed and Aβ(1-42) was visualized by silver staining according to Schagger [19].

MTT cell viability assay

Rat pheochromocytoma PC12 cells (Leibniz Institute DSMZ, Braunschweig, Germany) were cultivated in DMEM medium supplemented with 10 % fetal bovine serum and 5 % horse serum. 10.000 cells per well were seeded on collagen-coated 96 well plates (Gibco, Life technology, Carlsberg, USA) and incubated in a 95 % humidified atmosphere with 5 % CO_2 at 37 °C for 24 h. To yield oligomeric Aβ, monomerized Aβ(1-42) was preincubated for 4.5 h in natriumphosphate buffer at 21 °C and 600 rpm agitation. Then, DB peptide was added at different concentrations and incubated for further 40 min at 21 °C and 600 rpm agitation before addition to the PC12 cells. Final concentrations were 1 µM Aβ(1-42) and 0, 2, 1, or 5 µM DB3 or half of the molar peptide concentrations of DB3DB3. The PC12 cells were further incubated for 24 h in 95 %

humidified atmosphere with 5 % CO_2 at 37 °C after adding the Aβ-peptide mixture. Cell viability was then measured using the Cell proliferation Kit I (MTT) (Roche, Basel, Switzerland) according to manufacturer's instruction. The absorbance of the formazan product was determined by measuring the absorption at 570 nm after subtracting the absorption at 660 nm. For absorption measurements, the Polarstar Optima plate reader (BMG, Offenburg, Germany) was used. All results were normalized to cells that were treated with buffer only.

Aβ Aggregation inhibition ELISA

Freshly dissolved monomeric Aβ(1-42) (400 nM in 500 mM Tris-buffer pH 7.4) was incubated with and without DB peptides in different concentrations (0.01, 0.05, 0.1, 0.5, 1, 5, 10, 50 and 100 µM for DB3 or half of the molar concentrations in case of DB3DB3) in a humidity chamber for 23 h at 37 °C. The aggregation was analyzed by an enzyme-linked immunosorbent assay (ELISA). NP27 antibody in bicarbonate/carbonate buffer was used to coat the ELISA plate overnight. Then the plate was washed in PBS-Tween buffer (1x PBS + 0.05 % Tween) and blocked for 2 h at room temperature with 5 % casein buffer. After washing, Aβ aggregate solutions were added to the plate and incubated for 1 h at room temperature. The plate was washed again and bound Aβ aggregates were detected by biotinylated 6E10/HRP-avidin mediated immunoreaction (BioLegend, San Diego, USA) using TMB as detection reagent. Each value was background corrected which were derived from ELISA of samples without capture antibody and normalized to the control without peptide (0 % no inhibition, 100 % full inhibition). Mean value and standard error were calculated from three independent experiments. EC_{50} was calculated by fitting the data to a logistic dose response function.

Aβ Aggregate disassembly ELISA

Freshly dissolved monomeric Aβ(1-42) (400 nM in 500 mM Tris-buffer pH 7.4) was incubated in a humidity chamber for 22 h at 37 °C in order to preform Aβ(1-42) aggregates. These preformed aggregates were coincubated with D-peptide in different concentrations (0.01, 0.05, 0.1, 0.5, 1, 5, 10, 50, 100 µM for DB3 or with half of the molar concentrations in case of DB3DB3) for additional 22 h at 37 °C. The content of Aβ aggregates was measured and evaluated in the same way as the aggregation inhibition ELISA.

Transmission electron microscopy (TEM)

10 µM of freshly dissolved monomeric Aβ(1-42) was incubated in 10 mM sodium phosphate buffer pH 7.4 with or without DB peptide in equal molar ratios for 24 h at 37 °C. Afterwards, 20 µl of the samples were absorbed on formval/carbon coated copper grids (S162, Plano, Wetzlar, Germany) for 3 min, washed three times with water and negative stained with 1 % v/v

193 uranylacetate for 1 min. The images were acquired using a Libra 120 electron microscope
194 (Zeiss, Oberkochen, Germany) at 120 kV.

195 **Statistical analysis**

196 Statistical analysis was performed using the Origin 8.5 (OriginLab Cooperation, Northampton,
197 USA) software package.

7

198 Results

199 *Screening for optimized D3 derivatives using peptide microarrays*

200 Previously, we identified the Aβ oligomer eliminating D-enantiomeric peptide D3 via mirror image
201 phage display [10, 16]. One possible explanation of D3's efficiency is that it binds to Aβ
202 monomers and stabilizes them within the various equilibria with Aβ oligomers and other Aβ
203 assemblies. In order to identify more efficient derivatives, a systematic optimization of D3
204 regarding its binding affinity to monomeric Aβ(1-42) (Figure 1) was performed using a two-step
205 procedure. For the first step, every position of the original peptide D3 was replaced against each
206 of the 19 other proteinogenic amino acids residues in their D-enantiomeric form. These 20x12
207 different peptides were spotted on a Pepspot membrane (JPT, Berlin, Germany) and the binding
208 of monomeric Aβ(1-42) was measured according to the procedure described in the material and
209 method part. After washing, the amount of bound Aβ was determined by the Aβ-specific
210 antibody 6E10 and a secondary detection antibody (Figure 2A). The amino acid replacements
211 that yielded the highest Aβ binding activity, as measured by the dot staining density, were
212 chosen for further combinations in the second round (Figure 2B and C). In particular, the
213 replacements r3i, r5t, h9d, r10q, r10e, n11q and n11d were found to be of possible benefit for Aβ
214 monomer binding. The residue h7 seemed to have the highest potential for further improvement,
215 because most replacements suggested additional benefit. h7p, h7q, h7r and h7s have been
216 picked as the most promising replacements for h7. Replacements of r12 were excluded because
217 we anticipated a minimum number of arginines in D3 to be responsible for D3's superior
218 pharmacokinetic properties as reported recently [20]. Interestingly, nine of the eleven
219 replacements were located in the C-terminal half of D3 at positions 7, 9, 10 and 11.

220 For the second round of optimization every possible combination of the eleven single residue
221 replacements r3i, r5t, h7p, h7q, h7r, h7s, h9d, r10q, h10e, n11q and n11d, were combined
222 yielding in 360 different peptides, which were spotted on a glass chip (Pepscan, Lelystad,
223 Netherlands) (Figure 2C). To compare their binding activities to monomeric Aβ, the peptide
224 microarrays were incubated with freshly dissolved monomeric FITC-Aβ(1-42) and fluorescence
225 intensities of the Aβ-peptide interactions were measured. Five peptides, which showed tight
226 binding to Aβ monomers as deduced from high FITC fluorescence intensities, were chosen for
227 further *in vitro* characterization (Figure 2D and Table 1). The fluorescence intensities of these D3
228 derivatives, termed DB1 to DB5, were up to six times higher as compared to the fluorescence
229 intensity obtained with D3 (Figure 2D). As shown in Table 1, the sequences of DB1 to DB5 had
230 two to four amino acid residue exchanges as compared to D3.

8

The influence of DB3 and DB3DB3 on Aβ fibril formation

To investigate the influence of DB1 to DB5 on Aβ fibril formation, a Thioflavin T (ThT) assay was performed. In aqueous environment the benzothiazole dye has a low fluorescence. Upon interaction with regularly formed amyloid fibrils the fluorescence signal is greatly enhanced and excitation and emission maxima shift from 385 and 445 nm to 450 and 490 nm, respectively. The emission at 490 nm is directly proportional to the quantity of amyloid fibrils. Fibril formation of Aβ can be followed in real time by measuring the ThT fluorescence [21-23].

Therefore, the inhibitory effects of the D-peptides DB1 to DB5 and the original D-peptide D3 were investigated by ThT assays of coincubations of Aβ(1-42) with each of the DB peptides. Fluorescence emission data were compared at the time point of 5 h, at which the Aβ(1-42) control (without added peptide) reached its fluorescence maximum. As shown in Figure 3, D3 inhibited the Aβ(1-42) fibril formation by 30 %. DB3 inhibited the Aβ(1-42) fibril formation by 80 %, DB5 by 76 %, DB1 by 63 %, and DB2 by 49 % compared to the control with Aβ(1-42) only (Figure 3). Surprisingly, DB4 had no effect on the fibril formation of Aβ.

Considering the results of the ThT assay, DB3 seems to be the most promising peptide according to the inhibitory effect of fibril formation. Therefore, we selected DB3 for further *in vitro* studies. As a further potential optimization step of the DB peptides, we wanted to investigate the impact of avidity. As the simplest divalent DB peptide, we designed a head-to-tail tandem peptide of DB3, named DB3DB3. As shown in Figure 3, 10 µM DB3DB3 inhibited the formation of ThT-positive aggregates equally efficient as 20 µM DB3.

Binding affinities of DB3 and DB3DB3 to Aβ(1-42) monomers

For further characterization of DB3 and DB3DB3, the equilibrium dissociation constants (K_D) of the D-peptides were determined for their interaction with Aβ(1-42) monomers using biolayer interferometry (BLI) (Figure 4). For DB3, a K_D value of 75 µM was determined, whereas for the designed dimer peptide DB3DB3 a K_D value of 1 µM was obtained. Therefore, the binding affinity to Aβ(1-42) monomers was 75-fold enhanced for the dimeric version of DB3.

Aβ aggregation inhibition by DB3 and DB3DB3

To confirm and further investigate the efficiency of DB3 and DB3DB3 activity on Aβ aggregation, an aggregation inhibition ELISA was performed. Therefore, initially monomeric Aβ(1-42) was incubated with different concentrations of DB3 or DB3DB3 and the Aβ(1-42) aggregates were specifically detected via ELISA.

DB3 inhibits Aβ aggregate formation with an EC_{50} of 6 µM whereas DB3DB3 inhibits Aβ aggregate formation with an EC_{50} of 8 nM (Figure 5A). Thereby, DB3DB3 is 1000-fold more efficient in Aβ aggregation inhibition compared to DB3. Furthermore, the aggregation inhibition ELISA showed that the fibrillization of Aβ(1-42) was almost completely inhibited at a peptide concentration of 20 µM DB3 and 10 µM DB3DB3.

Aβ aggregates disassembly ability of DB3 and DB3DB3

With an Aβ aggregate disassembly ELISA the effect of DB3 and DB3DB3 on preformed Aβ aggregates was analyzed (Figure 5B). Preformed Aβ(1-42) aggregates were coincubated with different concentrations of DB3 or DB3DB3 for 24 h. By using an Aβ aggregates specific ELISA, Aβ aggregates were quantified. The raw data were normalized to Aβ aggregates without peptide. The results of measured Aβ aggregates normalized to the Aβ control were plotted against the peptide concentration. The EC_{50} was calculated by using a logistic dose response function.

For DB3 the EC_{50} of the Aβ aggregates disassembly ability is 2.5 µM. For DB3DB3 the EC_{50} could not be determined since the Aβ aggregates were already disassembled at very low peptide concentrations, i.e. by adding 10 nM DB3DB3 to 400 nM Aβ, 80 % of Aβ aggregates were disassembled compared to Aβ without peptides.

Elimination of Aβ oligomers

Aβ oligomers are the main toxic species and are discussed to be responsible for development and progression of AD [7]. A promising therapeutic approach is the elimination of Aβ oligomers. In previous studies, we established an assay that determines quantitatively the Aβ oligomer elimination efficiency of a given substance (QIAD assay) [14]. Applying this assay, we determined the Aβ(1-42) oligomer elimination efficacy of DB3 and DB3DB3 (Figure 6).

Incubation of 80 µM monomeric Aβ(1-42) for 4.5 h led to the formation of a mixture of Aβ monomers (fraction 1-2), oligomers (fractions 4-6), and larger aggregates (other fractions) (Figure 6A). By adding DB3 in different concentrations, Aβ oligomers were eliminated in a concentration-dependent manner. By adding 40 µM DB3, Aβ oligomers were nearly completely eliminated. In comparison, by adding 20 µM DB3DB3 to 80 µM Aβ, Aβ oligomers were totally eliminated. Here, the content of Aβ oligomers was already strongly eliminated at applying 10 µM DB3DB3.

RP-HPLC was used to quantify the Aβ oligomer elimination efficiency (Figure 6B). DB3 slightly eliminated Aβ oligomers at 20 µM by around 27 % compared to the Aβ only control. DB3DB3 at

a concentration of 10 µM, which is half of the molar ratio of DB3, eliminated significantly the content of Aβ oligomers by 82 %. The content of large coprecipitates was increased and represented the content of Aβ oligomers which was eliminated. The content of monomeric Aβ was not affected by DB3 and DB3DB3.

Thus, DB3 and DB3DB3 eliminate Aβ oligomers without affecting the monomers and shifted the equilibrium from oligomeric Aβ to larger Aβ aggregates.

Reduction of Aβ toxicity

To analyze the influence of DB3 and DB3DB3 to Aβ-induced cytotoxicity an MTT assay with rat PC12 cells was performed (Figure 7). For that, monomeric Aβ(1-42) was preincubated for 4.5 h to yield Aβ oligomers. After additional coincubation with DB3 or DB3DB3 for 40 min, the mixture was added to PC12 cells and cell viability was analyzed after 24 h using the MTT assay.

Without added peptides, 1 µM Aβ reduced the cell viability to 44 % (Figure 7). In contrast, neither DB3 (5 µM) nor DB3DB3 (5 µM) exhibt any effect on the cell viability when added to PC12 cells, which indicate that both peptides are not toxic at the applied concentration. Addition of DB3 in the concentration range from 0.2 to 5 µM to 1 µM preincubated Aβ did not significantly increase the cell viability. However, a significant increase of cell viability was observed in the presence of 0.1 to 2.5 µM DB3DB3 in a concentration dependent manner up to 80 % (Figure 7). Thus, DB3DB3 was able to inhibit Aβ-induced cytotoxicity.

Morphology of coincubated Aβ

To analyze the morphology of Aβ co-complexes with DB3 and DB3DB3, initial monomeric Aβ(1-42) was incubated with DB3 and DB3DB3 for 24 h. For TEM analysis, the samples were absorbed onto formval/copper grids and negatively stained using uranyl acetate.

Aβ formed large meshes of fibrils after 24 h incubation (

Figure 8A). Coincubation of Aβ with DB3 in an equal molar ratio resulted in the formation of substantially fewer and shorter fibrils (

Figure 8B). Coincubation of Aβ with DB3DB3 yielded huge amorphous coprecipitates, which did not contain any fibrillar structures (

Figure 8C).

Discussion

At the moment, there is no causal therapy for Alzheimer's disease (AD) available. *In vitro* and *in vivo* studies showed, that Aβ oligomers play an important role in the progression of AD [7]. Therefore, elimination of these most toxic Aβ oligomers is obviously a promising strategy. Using peptide microarrays, we optimized the amino acid sequence of the well characterized D-enantiomeric Aβ oligomer-eliminating peptide D3. The most promising D3 derivatives, named DB1 to DB5, exhibit two to four different amino acids compared to D3. Except of DB4, all DB peptides have a lower net charge than D3, due to the replacements of r3, r5 and r10 and the introduction of negative charged amino acids. The replacement r10q at DB4 were compensated through the replacement h7r. Additional replacements with no effect to the net charge are h7q and n11q.

DB1 to DB5 were further investigated regarding to their inhibition efficacy of Aβ aggregation. Here, DB3 was the most promising D3 derivative which inhibited the Aβ aggregation by up to 80 %. In contrast, D3 inhibited Aβ aggregation by only 30 %. Considering the results of the ThT assay, DB3 was chosen for further *in vitro* characterizations.

BLI analysis revealed that DB3 interacts with Aβ monomers with a binding affinity of 75 µM. Via ELISA it was shown that DB3 inhibits the formation of Aβ aggregates with an EC_{50} of 6 µM.

The D-enantiomeric peptides D3 and DB1 to DB5 were developed for elimination of Aβ oligomers. This was tested by the QIAD assay [14]. By adding DB3 to Aβ, DB3 reduced 28 % of the Aβ oligomers. Aβ monomers, which are assumed to have neuroprotective functions [24], were not affected. The reduction of oligomeric Aβ resulted in an increase of large amorphous Aβ coprecipitates. TEM images showed that these aggregates possess a higher density. Typical Aβ fibrils, which are linear, unbranched and 5 to 10 nm wide [25], were not visible. Additionally, DB3 was able to disassemble preformed Aβ aggregates.

Because the target, Aβ oligomers, is a multivalent target, the divalent tandem peptide DB3DB3 was expected to be significantly more effective. Indeed DB3DB3 showed a 75-times higher affinity for Aβ monomers. This increased affinity resulted in increased inhibition of Aβ fibrillization and increased reduction of Aβ-induced cytotoxicity. Also in the Aβ aggregation inhibition ELISA, DB3DB3 showed an EC_{50}, which was 1000-fold lower as compared to DB3.

DB3DB3 was also able to efficiently eliminate Aβ oligomers as shown in the QIAD assay. Interestingly, DB3 and DB3DB3 did not significantly affect the Aβ monomer content. TEM images showed that these aggregates were not fibrillary structured.

In summary, our *in vitro* data show that the D3 derivative DB3 and its tandem version DB3DB3 show highly efficient properties according to the applied experiments. Especially designing the tandem peptide DB3DB3 resulted in a high grade of optimization compared to the original peptide DB3. *In vivo* studies will show whether the new compounds' *in vitro* properties can be translated into enhanced therapeutic activity in AD animal models.

Author Contributions

A.N.K, D.B., S.A.F., J.K. and D.W. designed the peptide combinations for the microarrays. A.N.K. carried out all experiments with the peptide microarrays, as well as the QIAD, TEM and the ThT assays. O.B. and L.G. designed the QIAD. T.Z. designed and performed the binding studies. J.K. designed and M.T. performed the cell toxicity assays. A.B., T.W. and E.W. designed and A.B. and T.W. performed the ELISA studies. D.W. designed the overall study. A.N.K., T.Z., J.K., and D.W. wrote most of the manuscript. All other authors contributed to the manuscript.

Acknowledgments

D. W. was supported by grants from the "Portfolio Technology and Medicine", the "Portfolio Drug Research" and the Helmholtz-Validierungsfonds of the Impuls- und Vernetzungs-Fonds der Helmholtzgemeinschaft. D.W. was also supported by the TT-Fonds of the Technology Transfer Department of the Forschungszentrum Jülich.

373 **References**

374 1. Ferri CP, Prince M, Brayne C, Brodaty H, Fratiglioni L, Ganguli M, et al. Global
375 prevalence of dementia: a Delphi consensus study. Lancet. 2005;366(9503):2112-7.
376 2. Sperling RA, Jack CR, Aisen PS. Testing the Right Target and Right Drug at the Right
377 Stage. Science Translational Medicine. 2011;3(111):111cm33.
378 3. Hardy J, Selkoe DJ. The Amyloid Hypothesis of Alzheimer's Disease: Progress and
379 Problems on the Road to Therapeutics. Science. 2002;297(5580):353-6.
380 4. Selkoe DJ. Alzheimer's Disease: Genes, Proteins, and Therapy. 2001;81(2):741-66.
381 5. Finder VH, Glockshuber R. Amyloid-β Aggregation. Neurodegenerative Diseases.
382 2007;4(1):13-27.
383 6. McLean CA, Cherny RA, Fraser FW, Fuller SJ, Smith MJ, Konrad V, et al. Soluble pool of
384 Aβ amyloid as a determinant of severity of neurodegeneration in Alzheimer's disease.
385 Annals of Neurology. 1999;46(6):860-6.
386 7. Shankar GM, Li S, Mehta TH, Garcia-Munoz A, Shepardson NE, Smith I, et al. Amyloid-β
387 protein dimers isolated directly from Alzheimer's brains impair synaptic plasticity and
388 memory. Nature medicine. 2008;14(8):837-42.
389 8. Schumacher TN, Mayr LM, Minor DL, Jr., Milhollen MA, Burgess MW, Kim PS.
390 Identification of D-peptide ligands through mirror-image phage display. Science.
391 1996;271(5257):1854-7.
392 9. Wiesehan K, Buder K, Linke RP, Patt S, Stoldt M, Unger E, et al. Selection of D-Amino-
393 Acid Peptides That Bind to Alzheimer's Disease Amyloid Peptide Aβ1–42 by Mirror
394 Image Phage Display. ChemBioChem. 2003;4(8):748-53.
395 10. Funke SA, van Groen T, Kadish I, Bartnik D, Nagel-Steger L, Brener O, et al. Oral
396 Treatment with the d-Enantiomeric Peptide D3 Improves the Pathology and Behavior of
397 Alzheimer's Disease Transgenic Mice. ACS Chemical Neuroscience. 2010;1(9):639-48.
398 11. Bartnik D, Funke SA, Andrei-Selmer L-C, Bacher M, Dodel R, Willbold D. Differently
399 Selected d-Enantiomeric Peptides Act on Different Aβ Species. Rejuvenation Research.
400 2009;13(2-3):202-5.
401 12. van Groen T, Kadish I, Wiesehan K, Funke SA, Willbold D. In vitro and in vivo Staining
402 Characteristics of Small, Fluorescent, Aβ42-Binding D-Enantiomeric Peptides in
403 Transgenic AD Mouse Models. ChemMedChem. 2009;4(2):276-82.
404 13. Wiesehan K, Stöhr J, Nagel-Steger L, van Groen T, Riesner D, Willbold D. Inhibition of
405 cytotoxicity and amyloid fibril formation by a d-amino acid peptide that specifically binds

406 to Alzheimer's disease amyloid peptide. Protein Engineering Design and Selection.
407 2008;21(4):241-6.
408 14. Brener O, Dunkelmann T, Gremer L, van Groen T, Mirecka EA, Kadish I, et al. QIAD
409 assay for quantitating a compound's efficacy in elimination of toxic Aβ oligomers.
410 Scientific Reports. 2015;5:13222.
411 15. van Groen T, Kadish I, Funke SA, Bartnik D, Willbold D. Treatment with D3 Removes
412 Amyloid Deposits, Reduces Inflammation, and Improves Cognition in Aged AβPP/PS1
413 Double Transgenic Mice. Journal of Alzheimer's Disease. 2013;34(3):609-20.
414 16. van Groen T, Wiesehan K, Funke SA, Kadish I, Nagel-Steger L, Willbold D. Reduction of
415 Alzheimer's Disease Amyloid Plaque Load in Transgenic Mice by D3, a D-Enantiomeric
416 Peptide Identified by Mirror Image Phage Display. ChemMedChem. 2008;3(12):1848-52.
417 17. Uttamchandani M, Yao SQ. Peptide Microarrays: Next Generation Biochips for Detection,
418 Diagnostics and High-Throughput Screening. Current Pharmaceutical Design.
419 2008;14(24):2428-38.
420 18. Foong YM, Fu J, Yao SQ, Uttamchandani M. Current advances in peptide and small
421 molecule microarray technologies. Current Opinion in Chemical Biology. 2012;16(1–
422 2):234-42.
423 19. Schagger H. Tricine-SDS-PAGE. Nat Protocols. 2006;1(1):16-22.
424 20. Jiang N, Leithold LHE, Post J, Ziehm T, Mauler J, Gremer L, et al. Preclinical
425 Pharmacokinetic Studies of the Tritium Labelled D-Enantiomeric Peptide D3 Developed
426 for the Treatment of Alzheimer´s Disease. PloS one. 2015;10(6):e0128553.
427 21. LeVine H. Thioflavine T interaction with amyloid β-sheet structures. Amyloid. 1995;2(1):1-
428 6.
429 22. Levine H. Thioflavine T interaction with synthetic Alzheimer's disease β-amyloid peptides:
430 Detection of amyloid aggregation in solution. Protein Science. 1993;2(3):404-10.
431 23. Naiki H, Higuchi K, Hosokawa M, Takeda T. Fluorometric determination of amyloid fibrils
432 in vitro using the fluorescent dye, thioflavine T. Analytical Biochemistry. 1989;177(2):244-
433 9.
434 24. Giuffrida ML, Caraci F, Pignataro B, Cataldo S, De Bona P, Bruno V, et al. β-Amyloid
435 Monomers Are Neuroprotective. The Journal of Neuroscience. 2009;29(34):10582-7.
436 25. Fändrich M, Schmidt M, Grigorieff N. Recent progress in understanding Alzheimer's β-
437 amyloid structures. Trends in Biochemical Sciences. 2011;36(6):338-45.

438

439 **Figure legends**

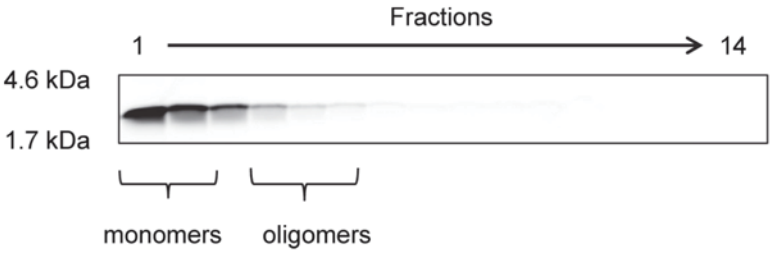

440

441 **Figure 1 Aggregation state of monomeric Aβ(1-42) after 1 h incubation.** For optimization of D3 with peptide
442 microarrays, the peptide microarrays were incubated with 5 µM initial monomeric Aβ(1-42) for 1 h at room
443 temperature. The aggregation state of this Aβ preparation was analyzed by density gradient centrifugation with
444 subsequently 16 % Tricine-SDS-PAGE. FITC-Aβ(1-42) was detected via FITC fluorescence and was only detectable
445 at the first four lanes, which represent mainly monomeric and oligomeric FITC-Aβ [14].

446

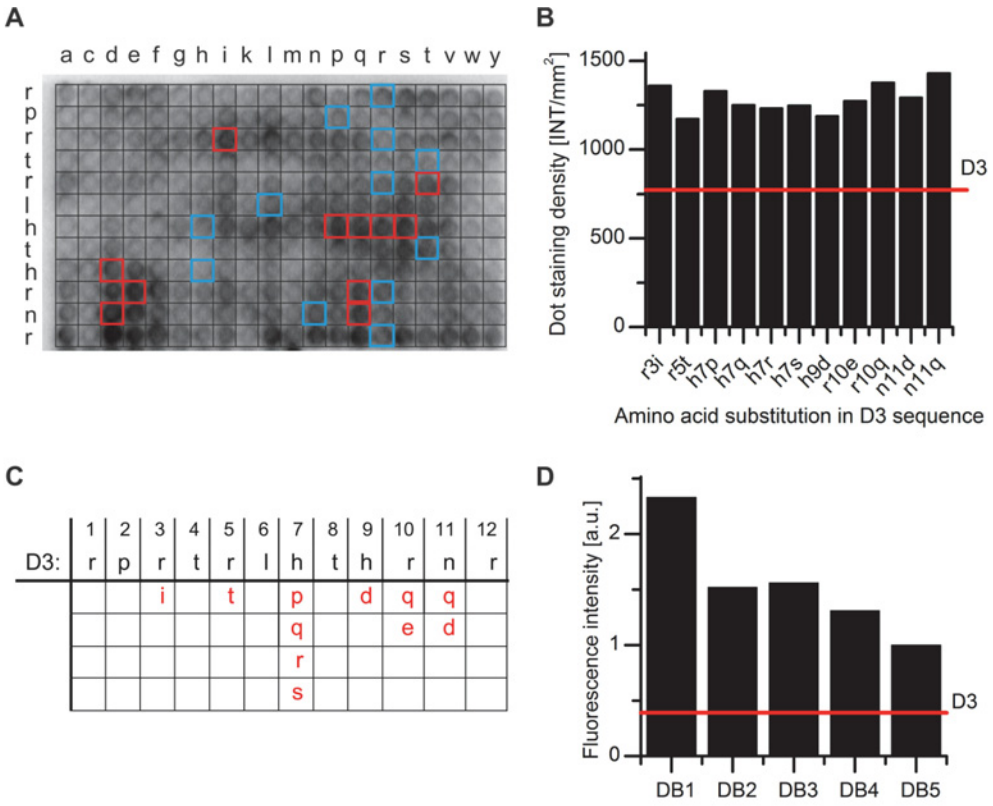

Figure 2 Selection of DB1 to DB5 based on two cycles of peptide microarray based screenings. A) Promising replacements in the sequence of D3 were selected via PepSpots peptide array. Binding of monomeric Aβ(1-42) to spotted D3 derivatives was detected using the Aβ antibody 6E10 and a HRP -labeled secondary antibody. Several of the highest dot staining density, representing the most promising single replacements, are marked in red, the original D3 controls in blue. B) The HRP -intensity was evaluated by the staining density of the peptide dots, plotted against the amino acid replacements. Eleven promising replacements, which showed up to 1.5 times increased binding to monomeric Aβ(1-42) compared to D3, were chosen for a second generation peptide microarray. The red line represents the mean dot staining intensity of D3. C) Schematic overview of the first generation microarray output. D) Binding of FITC-Aβ(1-42) to the peptides DB1 to DB5. The binding of FITC-Aβ(1-42) to the spotted peptides was analyzed by measuring the FITC-fluorescence intensity. All intensities were background corrected. The signal intensities of the top five peptides were plotted. The red line represents the mean fluorescence intensity of D3.

460 **Table 1 Amino acid sequences of D3 and DB1 to DB5.**

name	sequence
D3	rprtrlhthrnr
DB1	rpitrlht**d**rnr
DB2	rp**itt**l**q**th**q**nr
DB3	rpitrl**r**th**q**nr
DB4	rprtrl**r**th**q**nr
DB5	rpitrl**q**th**eq**r

461

462 All amino acids of the peptides are in D-enantiomeric conformation and their C-termini are amidated. The amino acid
463 replacements to D3 are marked in bold.

464

18

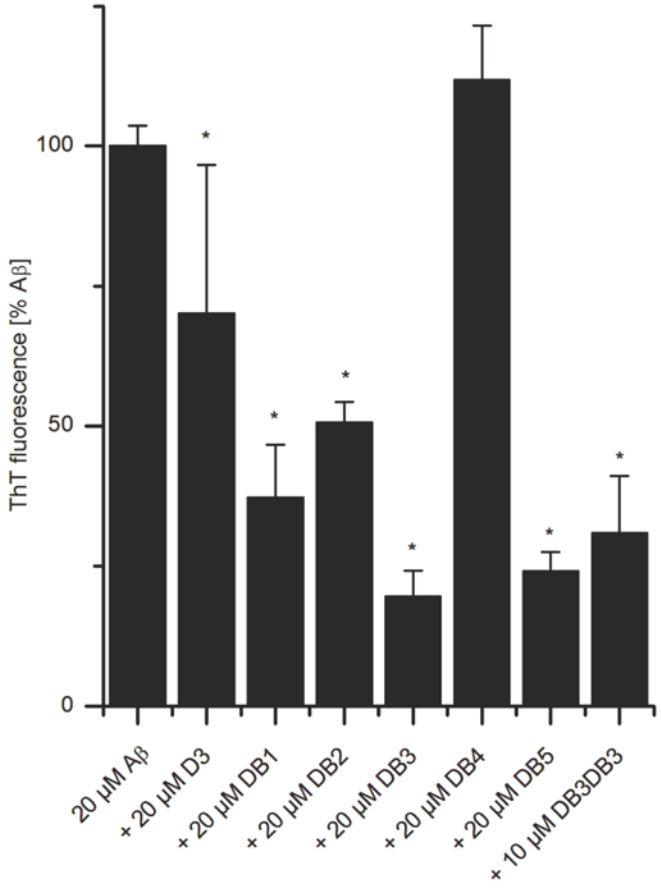

Figure 3 Thioflavin T fibril formation assay. 20 µM Aβ(1-42) was mixed with 20 µM DB1 to DB5 or 10 µM DB3DB3 and the ThT fluorescence was monitored. Aβ(1-42) without peptide addition was taken as control. The ThT fluorescence of all samples were compared after 5 h, where the control, Aβ(1-42) only, reached its maximum in fluorescence emission. Mann-Whitney-U-test was used for statistical analysis. * $p < 0.05$; ** $p < 0.01$; *** $p < 0.001$.

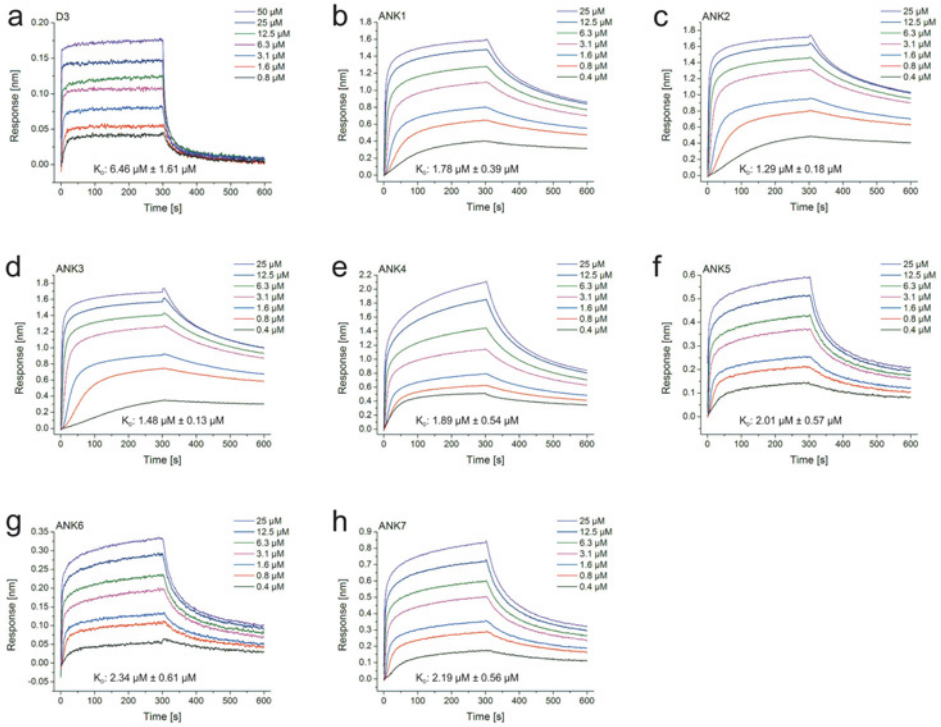

Figure 4 K_D determination of DB3 and DB3DB3 to monomeric Aβ using biolayer interferometry (BLI). N-terminally biotinylated Aβ(1-42) monomers were immobilized on streptavidin biosensors and the binding of DB3 and DB3DB3 was detected. Representative double referenced sensorgrams of a dilution series of DB3 (A) and DB3DB3 (B) are shown including equilibrium dissociation constants (K_D) as means ± SD of a triplicate. For steady state analysis Langmuir´s 1:1 binding model was applied. Representative fit curves of DB3 (C) and DB3DB3 (D) are depicted with the corresponding corrected R^2.

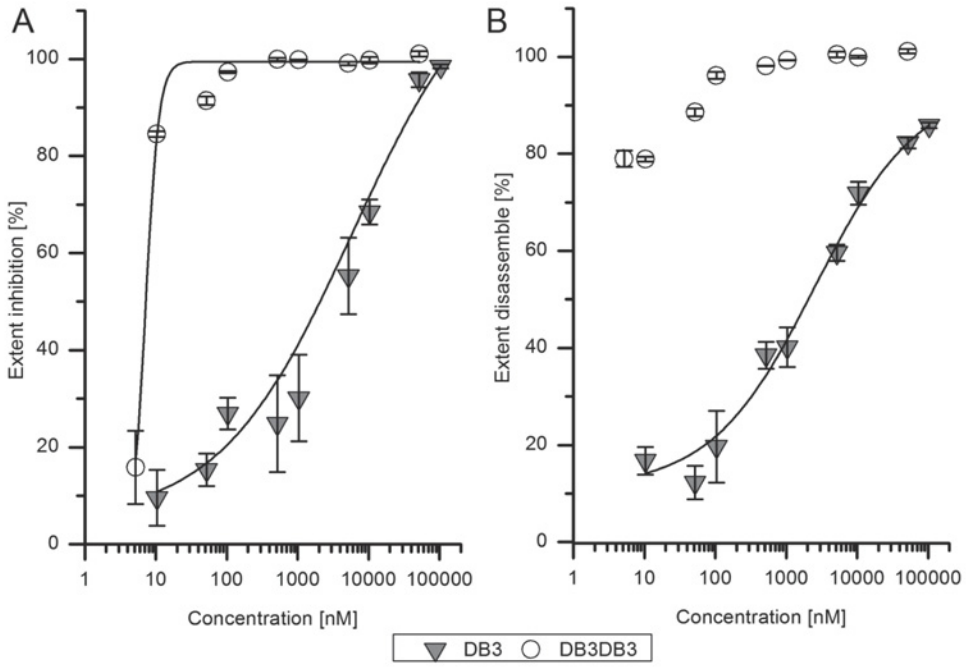

Figure 5 Inhibition of Aβ fibril formation and Aβ aggregation disassemble by DB3 and DB3DB3. A) Monomeric Aβ(1-42) (400 nM) was mixed with different concentrations of DB3 (0.01, 0.05, 0.1, 0.5, 1, 5, 10, 50, 100 µM) and the aggregation state of Aβ was analyzed using an Aβ aggregate specific ELISA. For DB3DB3 half of the molar concentrations compared to DB3 were used. Aβ without DB3 and DB3DB3 addition was taken as control. For DB3 an EC_{50} of 6 µM was calculated using a logistic fit model. DB3DB3 inhibited the formation of Aβ fibrils more efficiently with an EC_{50} of 7 nM. B) The disassembly properties of DB3 and DB3DB3 were measured using an Aβ aggregation specific ELISA. Monomeric Aβ(1-42) (400 nM) was preincubated in order to form fibrils and mixed with nine different concentrations of DB3 (0.01, 0.05, 0.1, 0.5, 1, 5, 10, 50, 100 µM). For DB3DB3 half of the molar concentrations compared to DB3 were used. For DB3 an EC_{50} of 2.5 µM was determined. DB3DB3 disassembled Aβ aggregates already at the lowest concentration (10 nM). Thus, EC_{50} could not be determined, but is lower than 10 nM. All data were determined in triplicate. Mann-Whitney-U-test was performed for statistical analysis. * $p < 0.05$; ** $p < 0.01$; *** $p < 0.001$

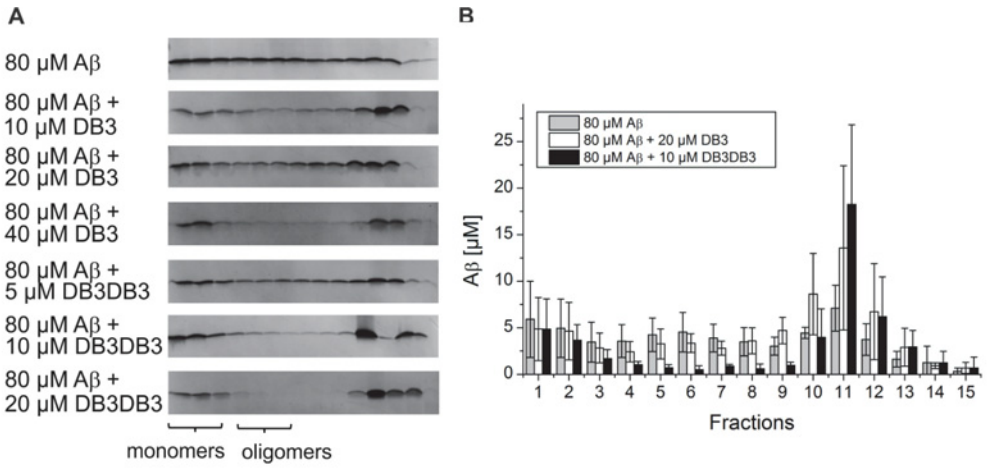

492

493 **Figure 6 Effect of DB3 and DB3DB3 on different Aβ aggregation species.** A) Analysis of Aβ(1-42) aggregation
494 species with density gradient centrifugation and following analysis via silver-stained tricine-SDS-PAGE in order to
495 analyze the influence of DB3 and DB3DB3 to the distribution of Aβ assemblies. B) Quantification of Aβ(1-42) by use of
496 RP-HPLC. All data consisted of triplicates.

22

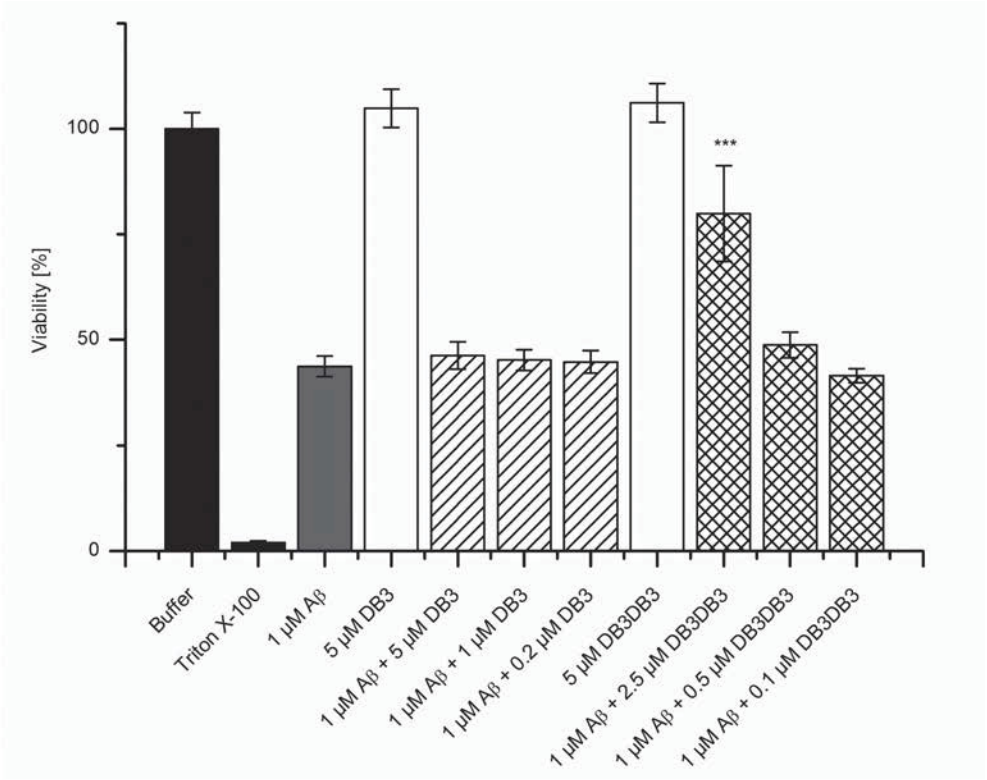

Figure 7 Influence of DB3 and DB3DB3 on Aβ-introduced cytotoxicity. Cell viability assay was performed by using PC12 cells in a MTT test. Therefore, Aβ(1-42) was preincubated for 4.5 h and further coincubated with DB3 or DB3DB3 for 40 min. The cells were incubated for 24 h with the Aβ(1-42)- peptide mixture or Aβ(1-42) alone as a control. The absorption of buffer treated cells was set to 100 % cell viability. The cell viability of cells treated with Aβ and DB3 or DB3DB3 were compared with cells treated with Aβ only. Mann-Whitney-U-test was used for statistical analysis. * $p < 0.05$; ** $p < 0.01$; *** $p < 0.001$.

23

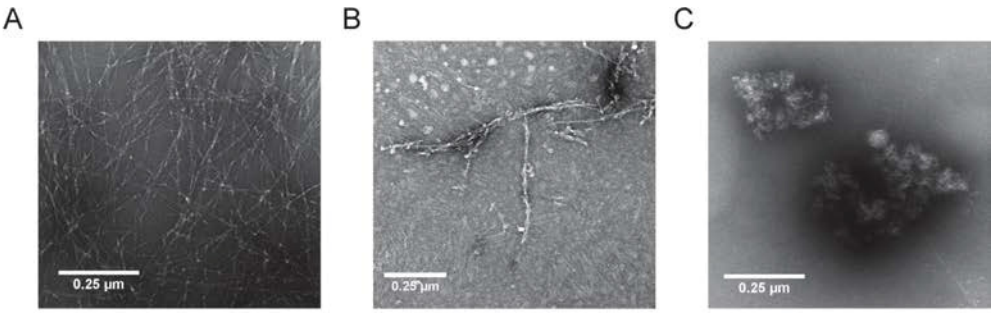

Figure 8 TEM of Aβ-DB3 and -DB3DB3 co-complexes. 10 µM initial monomeric Aβ(1-42) without (A) and with 10 µM DB3 (B) or 5 µM DB3DB3 (C) were coincubated for 24 h. Afterwards, the samples were absorbed on formval/carbon coated copper grids and negative stained with 1 % uranyl acetate. The pictures were obtained using a transmission electron microscope (TEM). Scale bar: 0.25 µm.

24

3.1.2. Optimization of D-peptides for Aβ monomer binding specificity enhances their potential to eliminate toxic Aβ oligomers

Eingereicht bei: Journal of the American Chemical Society (JACS)

Impact Factor (2015): 11.444

Eigener Anteil: 70 %

Entwicklung und Durchführung der -Mikroarray-Studien, Thioflavin T- Assay, QIAD, transmissionselektronenmikroskopischen Aufnahmen, Auswertung der in vivo-Studien, Schreiben des Manuskripts

Optimization of D-peptides for Aβ monomer binding specificity enhances their potential to eliminate toxic Aβ oligomers

Antonia Nicole Klein[†], Tamar Ziehm[†], Thomas van Groen[‡], Inga Kadish[‡], Anne Elfgen[†], Markus Tusche[†], Maren Thomaier[†], Kerstin Reiss[†], Oleksandr Brener[†,#], Lothar Gremer[†,#], Janine Kutzsche[†], Dieter Willbold[†,#]

† Institute of Complex Systems, Structural Biochemistry (ICS-6), Research Center Jülich, 52425 Jülich, Germany

‡ Department of Cell, Developmental and Integrative Biology, University of Alabama at Birmingham, Birmingham, AL, USA

Institut für Physikalische Biologie, Heinrich-Heine-Universität Düsseldorf, 40225 Düsseldorf, Germany

ABSTRACT: Amyloid-beta (Aβ) oligomers are thought to be decisive in the development and progression of Alzheimer's disease (AD). Here, we selected new peptides, which bind to Aβ(1-42) monomers, stabilize them and shift the equilibrium between Aβ monomers and Aβ aggregates towards monomers and non-toxic co-aggregates while eliminating toxic Aβ oligomers. Starting from the Aβ oligomer eliminating D-enantiomeric peptide D3, we developed and applied a two-step procedure to identify D3 derivatives with increased binding specificity for monomeric Aβ(1-42). The first step consisted of a variation of each amino acid residue within D3 with all other proteinogenic amino acid residues, except cysteine, but in their D-enantiomeric form and 13 non-proteinogenic amino acid residues resulting in a total of 384 different D3 derivatives with single replacements. These 384 different D3 derivatives were then assayed for increased binding specificity to Aβ(1-42) monomers. In a second step, the most promising single replacements were combined with each other and the resulting about 1.000 combination peptides were again screened for increased Aβ(1-42) monomer binding specificity. We selected seven novel D3 derivatives, named ANK1 to ANK7, and characterized them *in vitro*. All of them bind to monomeric Aβ(1-42), eliminate Aβ(1-42) oligomers, inhibit Aβ(1-42) aggregation into fibrils, and reduce Aβ(1-42)-induced cell toxicity more efficiently than D3. Finally, ANK6 was chosen as the most efficiently performing D3 derivative *in vitro* and characterized in more detail. ANK6 inhibits the prion-like propagation of pre-formed Aβ(1-42) seeds and improves memory performance of tg-APPSwDI mice after i.p. application for 4 weeks.

INTRODUCTION

Alzheimer's disease (AD) is the major type of dementia affecting more than 36 million people worldwide[1]. Loss of memory and other severe cognitive deficits are the key symptoms of AD[2]. According to the modified amyloid cascade hypothesis, the aggregation of amyloid-beta (Aβ) is responsible for the development and progression of this neurodegenerative disease[3]. Aβ is a product of the proteolytic cleavage of the amyloid precursor protein (APP) by β-secretase and γ-secretase. Aβ aggregates from its monomeric state into fibrils and various oligomeric Aβ species, although to date it is not clear, whether they are on- or off-pathway intermediates towards fibrils. Nonetheless, oligomers are thought to be the most toxic species[4]. The level of cognitive defects in AD correlates with the level of Aβ oligomers in the brain[5]. Thus, the elimination of the oligomeric Aβ is, from the current point of view, the most promising objective for causal therapy of AD.

Previously, we selected the D-enantiomeric peptide D3 by mirror image phage display[6,7]. D3 consists of twelve amino acid residues, inhibits the formation of Aβ(1-42) fibrils, eliminates Aβ(1-42) oligomers, and reduces the Aβ(1-42)-induced cell toxicity. *In vivo*, D3 improves cognitive performance of transgenic AD mice and reduces plaque load and inflammation of transgenic AD mice after oral application[8-12].

In this study, we present the selection and identification of D3 derivatives, which are more efficient in their *in vitro* performance compared to the original peptide D3.

RESULTS and DISCUSSION

Development of a two-step procedure to identify D3 derivatives with increased binding specificity to monomeric Aβ(1-42). Peptide microarrays (Pepscan, Lelystad, Netherlands) were used for amino acid replacement analysis and optimization of D3 with respect to specific binding to monomeric Aβ(1-42). By increasing the specific binding of the D-peptide to Aβ monomers, we intended to stabilize Aβ monomers and consequently to shift the equilibrium away from toxic Aβ oligomers to Aβ monomers. In a first step, a complete replacement set of

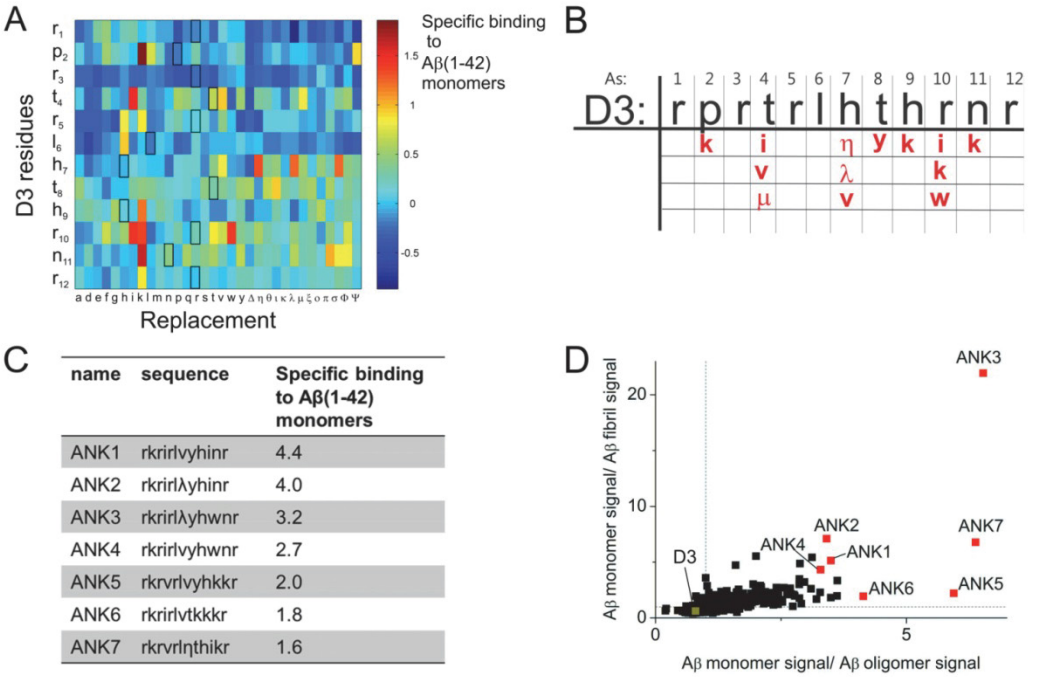

name	sequence	Specific binding to Aβ(1-42) monomers
ANK1	rkrirlvyhinr	4.4
ANK2	rkrirlλyhinr	4.0
ANK3	rkrirlλyhwnr	3.2
ANK4	rkrirlvyhwnr	2.7
ANK5	rkrvrlvyhkkr	2.0
ANK6	rkrirlvtkkkr	1.8
ANK7	rkrvrlηthikr	1.6

Figure 1| A) Interaction of Aβ(1-42) monomers with immobilized D3 derivatives. Peptide microarrays with immobilized D3 derivatives were incubated with monomeric, oligomeric or fibrillar FITC-Aβ(1-42) for 1 h at room temperature. The FITC fluorescence intensities of the peptide to FITC-Aβ(1-42) interaction were measured and the signal of oligomeric and fibrillary FITC-Aβ(1-42) was subtracted pro rata from the signal derived from monomeric FITC-Aβ(1-42) to identify specific Aβ(1-42) monomer binder. High interactions between D3 derivatives and FITC-Aβ(1-42) monomers were colored in red. Low values, corresponding to poor interactions, were colored in dark blue. The positions of original D3 samples on the microarray are framed. B) Layout of the second generation peptide microarray. All promising replacements of the first generation peptide microarray were combined for a second generation peptide microarray. Some promising replacements were not considered due to high SD of fluorescence intensities of the triplicates. C) Sequences and spezific binding to Aβ(1-42) monomers of novel D3 derivatives. All amino acid residues were in the D-enantiomeric conformation. D) Binding specificities of the novel D3 derivatives ANK1 to ANK7. The signal intensities of monomeric Aβ-peptide-interaction of the second generation microarray were set in relation to oligomeric and fibrillar Aβ. A specific binding to monomeric Aβ binding was achieved since the quotient of the signals was above 1 (dashed lines). The original peptide D3 is marked in yellow and the novel ANK peptides in red. The remaining peptides are presented in black.

Δ: trans-4-L-fluoro-proline; η: 4-fluoro-D-phenylalanine; θ: 4-benzyl-D-phenylalanine; ι: 1-naphthyl-D-alanine; κ: 3,5-diiodo-D-tyrosin; λ: D-phenylglycine; μ: D-homoarginine; ξ: D-homocitrulline; ο: β-homoarginine; π: β-cyclohexyl-D-alanine; σ: cyclovaline; Φ: β-alanine; Ψ: γ-aminobutyric acid.

D3 derivatives in which each amino acid residue of D3 was successively substituted by all other proteinogenic amino acids, except cysteine, in their D-enantiomeric conformation, and 13 non-proteinogenic amino acids, were spotted on the peptide microarray (Figure 1A, Figure S1). For peptide interaction analysis with different Aβ conformers, the peptide microarrays were incubated with fluorescein isothiocyanate (FITC) labelled Aβ(1-42) monomers, oligomers and fibrils (see Methods section). Different FITC-Aβ(1-42) species were verified by density gradient centrifugation (DGC) with subsequently SDS-PAGE (Figure S2), based on a protocol published by Ward et al[13].

The incubation of the peptide microarrays with different Aβ(1-42) aggregation species was performed in triplicate and fluorescence intensities were median-based normalized in order to compare the triplicate. To obtain specific binding of the D3 derivatives to Aβ(1-42) monomers, FITC-background signal, Aβ oligomer binding signal and fibril binding signal were subtracted pro rata.

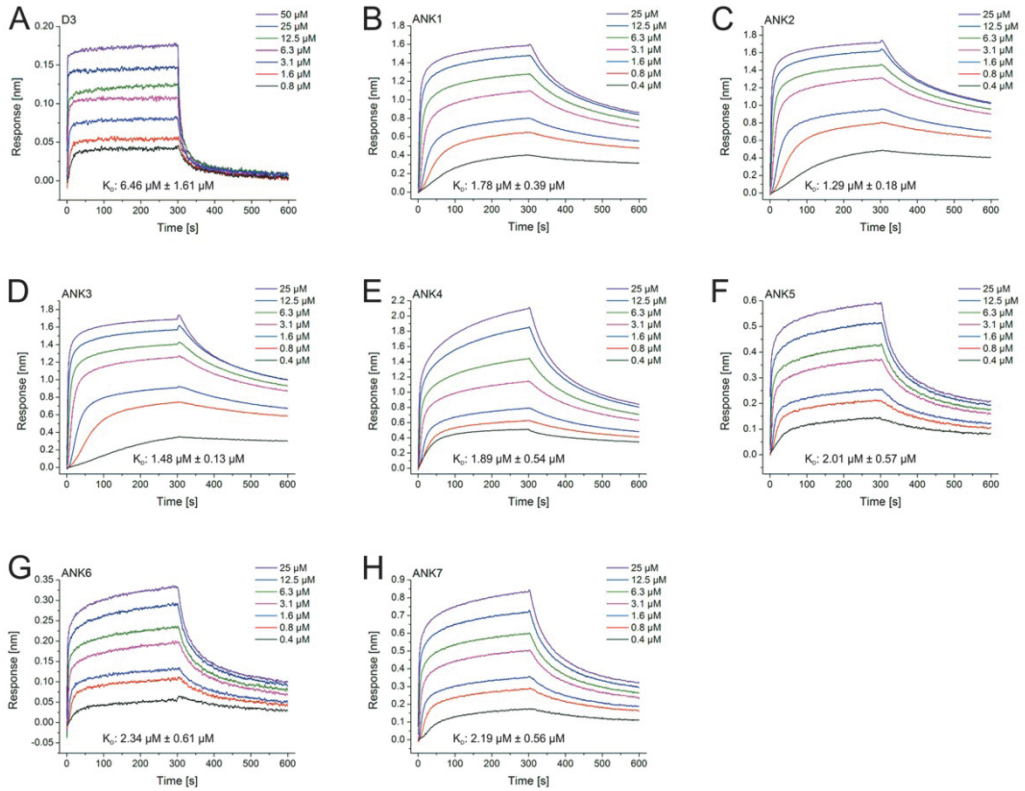

Figure 2| Sensorgrams and apparent equilibration dissociation constants (KD) of ANK–Aβ(1-42) interactions. KD values of D3 and ANK1 to ANK7 interactions with monomeric Aβ(1-42) were determined using biolayer interferometry (BLI). Biotinylated Aβ(1-42) was coupled to streptavidin sensor surfaces and the peptides were used as analytes. By plotting the equilibrium response signals of each cycle against the applied peptide concentrations overall KD values were determined. Data were fitted according to Langmuir´s 1:1 binding model. The sensorgrams show one representative experiment and KD values represent means ± SD of three independent experiments. A) D3; B) ANK1; C) ANK2; D) ANK3; E) ANK4; F) ANK5; G) ANK6; H) ANK7.

High FITC readout corresponded to a high specific binding to Aβ monomer binding, which is illustrated in Figure 1A. As shown in Figure 1A, the original D3 peptide interacted moderately with Aβ monomers with a slight variation of the specific binding to Aβ monomers between different D3 spots. Replacement of D3 residues 1 to 3 did not enhance the interaction between peptide and Aβ monomers, except for the replacement p2k. Replacement of the original C-terminus of D3 (amino acid residues 7 to 11) frequently resulted in enhanced Aβ monomer-peptide interaction. Replacement of residues r11, r13 and l16 had no effect on the interaction of D3 derivatives to Aβ monomers, whereas replacement of residues h17, t18, r110 and n111 showed the greatest scope of improvement.

Selection of new D3 derivatives with increased binding specificity to monomeric Aβ. For further increase of Aβ monomer binding specificity the 13 most promising single replacements were combined and the resulting peptides were tested for enhanced specificity in a second generation peptide microarray analog to the first generation array (Figure 1B). Selection criterium for the optimized D3 derivatives was a high specific binding to Aβ monomers (Figure 1A). For D3, the specific monomeric Aβ binding at the second generation array was -0.6, which indicates that D3 did not bind specific to Aβ monomers. The most promising D3 derivatives with the highest specific binding to FITC-Aβ(1-42) monomers were selected for *in vitro* characterization and named ANK1 to ANK7.

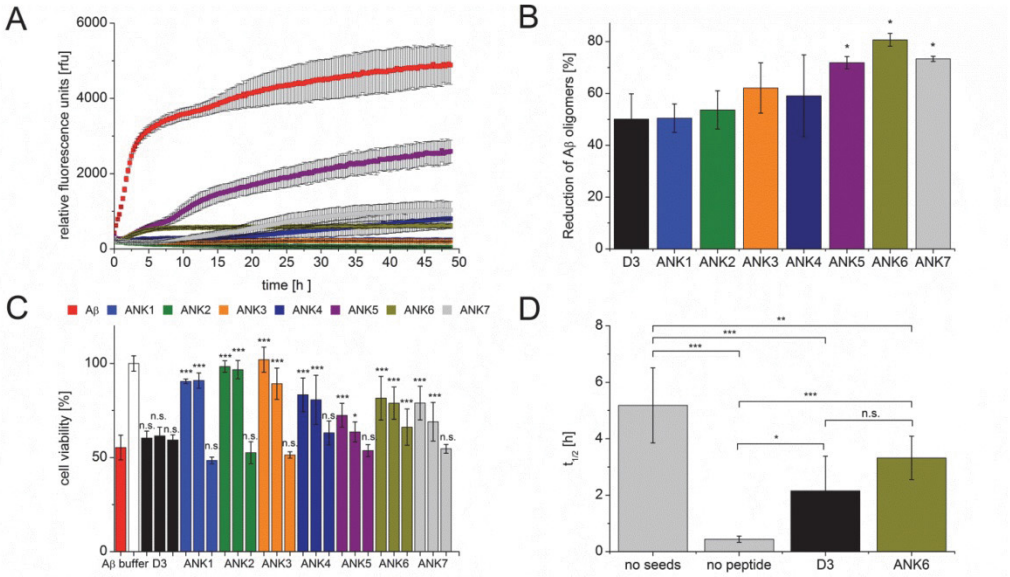

Figure 3| *In vitro* characterization of ANK1 to ANK7. A) A Thioflavin T (ThT) assay was performed using 20 µM Aβ(1-42), 20 µM peptide and 10 µM ThT. The ThT fluorescence was measured at λ_{ex} = 440 nm and λ_{em} = 490 nm for 48 h at 37 °C. B) Elimination of Aβ(1-42) oligomers was analyzed via QIAD assay. The mean values ± SD of four measurements are illustrated. C) MTT cytotoxicity assay for ANK1 to ANK7 in comparison to D3. ANK1 to ANK7 were co incubated in three different ratios (Aβ(1-42):peptide; 1:5, 1:1 and 1:0.2) with pre-incubated Aβ(1-42) for 40 min at 21 °C and 600 rpm. Significant differences are in relation to the Aβ(1-42) control (red bar) and were tested by using one way ANOVA with Bonferroni post-hoc test. D) Analysis of the seeding potential of Aβ(1-42) fibrils on monomeric Aβ(1-42) influenced by D3 or ANK6. 4.5 h pre-incubated Aβ(1-42) further incubated over 24 h with and without D3 or ANK6 were used as seeds. The Aβ(1-42) fibril formation was monitored using ThT fluorescence. * $p \leq 0.05$; ** $p \leq 0.01$; *** $p \leq 0.001$; n.s. not significant.

The identified peptides ANK1 to ANK7 and their amino acid sequences are shown in Figure 1C. The specific binding to Aβ monomers was up to two times higher compared to the single replacements in the first generation microarray (Figure 1C). Additionally, the ratio of Aβ monomer binding to oligomer binding and fibril binding was always above one, i.e. for ANK3 the respective ratios were 6.5 and 22, indicating an increased binding specificity to Aβ(1-42) monomers (Figure 1D). In comparison, the ratios for D3 were below one (0.8 and 0.6), indicating that D3 binds with a slightly higher affinity to Aβ(1-42) oligomers and fibrils than to Aβ(1-42) monomers.

ANK1 to ANK7 bind to Aβ monomers with increased affinity. After selection of the D3 derivatives ANK1 to ANK7, their *in vitro* performance was investigated and compared to D3. First, the interaction between the peptides and monomeric Aβ(1-42) was examined using biolayer interferometry (BLI) (Figure 2). The sensorgrams of D3 binding to monomeric Aβ(1-42) showed a homogeneous 1:1 interaction composed of a fast on-rate and off-rate (Figure 2A). ANK1 to ANK7 exhibited a heterogeneous binding behavior consisting of two kinetics with a slow final off-rate (Figure 2B-H). Nevertheless, monovalent steady state analyses were applied resulting in a robust determination of the overall apparent equilibration dissociation constants (in the following named K_D). The fitting curves of one representative experiment are shown in Figure S3.

D3 binds to Aβ(1-42) monomers with a K_D value of 6.5 µM under the given assay conditions (Figure 2A). The BLI sensorgrams of the optimized D3 derivatives ANK1 to ANK7 were similarly shaped (Figure 2B-H) resulting in K_D values ranging from 1.3 µM to 2.3 µM. Thus, ANK1 to ANK7 showed 3- to 5-fold increased binding affinities to monomeric Aβ(1-42) compared to the original peptide D3 and the binding mode changed from a homogeneous 1:1 interaction to a heterogeneous interaction.

ANK1 to ANK7 inhibit Aβ fibril formation highly efficient. To study the influence of ANK1 to ANK7 on the Aβ(1-42) fibril formation a Thioflavin T (ThT) assay was performed. As shown in Figure 3A, all novel D3 derivatives inhibited the formation of ThT positive Aβ(1-42) fibrils within 48 h. Co-incubation of Aβ(1-42) with ANK1, ANK2 and ANK3 showed only 5 %, 1 %, and 4 % of the fluorescence signal of Aβ(1-42) alone, indicating that Aβ(1-42) fibril formation was almost completely suppressed by the respective peptides. The D-peptides ANK4, ANK6 and ANK7 significantly inhibited the Aβ(1-42) fibril

formation, which is shown by a decreased ThT fluorescence signal to 16 %, 13 % and 21 %. ANK5 co-incubated with Aβ(1-42) resulted in a ThT fluorescence signal of 53 % normalized to the control, indicating that it inhibits fibril formation by 47 %.

ANK1 to ANK7 eliminate Aβ oligomers. A suitable method to assess a compound's efficacy to eliminate toxic Aβ oligomers is the QIAD assay, an assay for the quantitative determination of interference with Aβ(1-42) aggregate size distribution[14]. ANK1 to ANK7 were compared to each other and to D3 according to their ability to eliminate Aβ(1-42) oligomers which are located in fractions 4 to 6 of the used density gradient. As shown in Figure 3B, ANK5, ANK6, and ANK7 eliminated those Aβ(1-42) oligomers significantly more efficient than D3: D3 eliminated the content of Aβ(1-42) oligomers to 50 %, while ANK6, ANK7 and ANK5 removed 81 %, 73 % and 72 % of the Aβ(1-42) oligomers, respectively. The concentration of Aβ monomers, present in fractions 1 and 2, was affected by all tested D-peptides, but not significantly (Figure S4). This finding indicates that the peptides have no influence on Aβ monomers, whose potential physiological effect might be neuroprotective[15]. The amount of Aβ(1-42) in fractions 10 to 13 was increased in samples of Aβ(1 42) co-incubated with D3 or ANK peptides (Figure S4). Thus, Aβ(1-42) oligomers were precipitated and converted into high-molecular-weight Aβ species.

ANK1 to ANK7 reduce the Aβ-induced cytotoxicity in a concentration dependent manner. Aβ has a toxic effect on neuronal cells[16]. To study the influence of ANK peptides on the Aβ-induced cytotoxicity, a cell viability assay was performed by using MTT. Treatment of SH-SY5Y cells with pre-incubated Aβ(1-42) significantly reduced cell viability up to 55 % (Figure 3C). Co-incubation of Aβ(1-42) with D3 or ANK1 to ANK7 was performed in Aβ(1-42):peptide ratios of 1:5, 1:1 and 1:0.2. D3 did not show any significant effects on the Aβ(1-42)-induced toxicity within all peptide ratios (Figure 3C). ANK1, ANK2 and ANK3 had the highest effect on the toxicity of Aβ at Aβ(1-42):peptide ratios of 1:5 and 1:1 compared to all other tested peptides and conditions. The Aβ-induced cytotoxicity was completely rescued at these ratios for ANK2 and ANK3. ANK4 and ANK6 increased the cell viability over the whole tested concentration range up to 83 %. Within this assay, the addition of ANK6 showed the highest rescue effect on Aβ(1-42) cytotoxicity when tested in a Aβ(1-42):peptide ratio of 1:0.2. The peptides alone had no influence on the viability of SH-SY5Y cells (Figure S5).

These results correlate to results obtained by the QIAD assay described above. There, the most efficiently optimized D3 derivative was ANK6 as well (Figure 3B). ANK6 eliminated Aβ(1-42) oligomers by 81 % and, thus, most likely, strongly reduced the Aβ (1-42)-induced toxicity on SH-SY5Y cells. Additionally, ANK6 binds to Aβ(1-42) with a K_D value of 2.3 µM (Figure 2G) and decreases the Aβ(1-42) fibril formation to 13 % (Figure 3A). Therefore, ANK6 was picked for following *in vitro* and *in vivo* characterizations.

ANK6 inhibits the prion-like propagation of pre-formed Aβ seeds. Aβ amyloidogenesis was described *in vitro* as a nucleated polymerization mechanism[17-19]. The surface of high-molecular-weight fibrillar Aβ can catalyze the generation of Aβ oligomers and aggregates. A catalytic cycle lowers the kinetic barrier of the formation of Aβ oligomers. The aggregation process can be characterized by three phases: the lag phase, a fast growing phase and a stationary phase. The lag phase is associated with the formation of an oligomeric nucleus. The duration of the lag phase is inverse proportional to the quantity of pre-formed amyloid fibrils or seeds[20]. To investigate the ability of D3 and ANK6 to inhibit the prion-like propagation of pre-formed Aβ seeds, a seeding assay was performed (Figure 3D). We examined the seeding potential of pre-formed Aβ(1-42) fibrils co-incubated with D3 or ANK6 on monomeric Aβ(1-42). For semiquantitative detection of seeding-competent Aβ aggregates, we calculated the half-life of the growth phase ($t_{1/2}$). For Aβ(1-42) monomers co-incubated with seeds, a $t_{1/2}$ of 0.44 h was calculated, without seeds 5.18 h (Figure 3D). The generated Aβ(1-42) seeds accelerated the Aβ aggregation. Both peptides, the original D3 and its derivative ANK6, reduced the seeding potential of Aβ(1-42) seeds *in vitro* (Figure 4D). Seeds of pre-formed Aβ fibrils co-incubated with D3 shifted $t_{1/2}$ to 2.15 h, co-incubation with ANK6 shifted $t_{1/2}$ to 3.32 h. These results suggest that the formed co-aggregates have reduced fibrillar or amyloidic structures, which could act as seeds for Aβ fibril formation. The saturation level of the ThT intensity within 24 h was affected by the addition of D3 or ANK6 to Aβ(1-42) seeds, but not significant, suggesting that the 8-fold lower concentration of ANK6 compared to freshly prepared monomeric Aβ(1-42) was too low to inhibit Aβ aggregation (Figure S6). Therefore, both peptides inhibit the catalytic effect of pre-formed fibrillar structures on Aβ aggregation but ANK6 showed a higher efficacy compared to D3 within this assay as well.

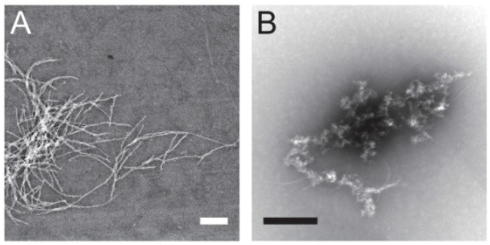

Figure 4| TEM images of A) initially 4.5 h aggregated Aβ(1-42) without and B) co-incubated with ANK6 (molar ratio 1:1) for further 24 h at 21 °C. Scale bars: 0.25 µm

ANK6 converts Aβ oligomers into amorphous aggregates. Previous studies showed that D3 converts Aβ into amorphous aggregates[11]. Since ANK6 is a derivative of D3, we hypothesized that ANK6 has a similar effect on Aβ(1-42). To investigate this, Aβ(1-42) was pre-incubated for 4.5 h to enrich oligomers and co-incubated with ANK6 afterwards. Transmission electron microscope (TEM) images confirmed this hypothesis. Aβ(1-42) incubated for

28.5 h contained fibrillary structures, as shown in Figure 4A. Aβ(1-42) co-incubated with ANK6 in the same molar ratio resulted in the formation of amorphous Aβ(1-42) aggregates (Figure 4B). These results correlate with the observation, that ANK6 inhibits the formation of ThT positive Aβ(1-42) fibrils.

***In vivo* study of ANK6.** The therapeutic effect of ANK6 was investigated in the transgenic mouse model tg-APPSwDI[21]. Two groups of tg-APPSwDI mice (see Table 1) were treated either with saline or ANK6 (0.13 mg per mouse per day, i.p., for 4 weeks using Alzet minipumps). Their cognition was assessed using the open field, zero maze, Morris water maze, and object recognition tests.

The open field test provides data for the assessment of novel environment exploration and for the effects of drugs on anxiety-related behavior of mice, which can also be evaluated by zero maze. Changes in the behavior are hints for hypo- or hyperactivity[22-24]. ANK6 had no influence on the general behavior of tg-APPSwDI mice as demonstrated by no differences in time spend in the center or open arena between saline and ANK6 treated animals in the open field and the zero maze experiments (Figure S7). Therefore, tg-APPSwDI mice show no changes in general activity and fear upon ANK6 treatment.

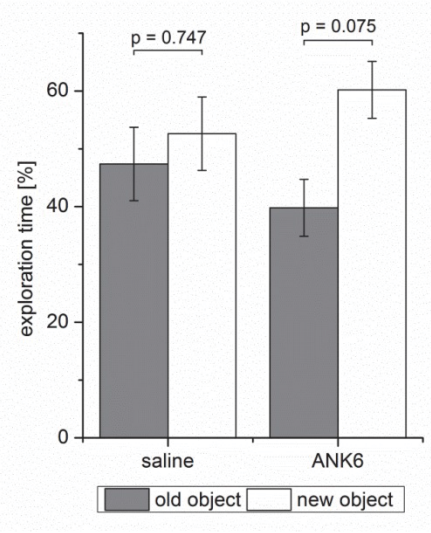

Figure 5| Object recognition test. Tg-APPSwDI mice were treated i.p. over four weeks with a total peptide amount of 3.7 mg ANK6 or saline as control. To investigate the cognitive abilities of the treated mice, an object recognition test was performed. The amount of time which the mice explored either the familiar or the new object are presented as mean values ± SEM. A two sample t-test was performed to compare the exploration times for both objects within one group.

Reversal of cognitive deficits in tg-APPSwDI mice treated with ANK6. After 3 weeks of treatment, a Morris water maze was performed to study spatial learning and memory (Figure S8)[25]. No significant differences in the swimming speed were observed (15.0 ± 0.6 for saline and 16.4 ± 0.9 for ANK6 treated mice) and both groups showed a significant improvement of learning during five days of training. Therefore, no treatment effect of ANK6 could be observed within the Morris water maze due to significant learning abilities of the control group.

Table 1| Summary of important quantities.

Group	control	ANK6
Infusion[a]	saline	ANK6 peptide
Number[b]	n = 11	n = 11
Body weight [g]		
before	35.4 ± 5.2	33.2 ± 4.6
after	31.8 ± 2.9	25.8 ± 3.7

[a] Intraperitoneal (i.p.) Alzet pumps, treatment with 3.696 mg / 4 weeks
[b] Number of animals per group

Furthermore, we studied the performance of both groups in the novel object recognition test. This test bases on the spontaneous behavior of rodents to interact more intensively with a novel object compared to a familiar one[26,27]. If a rodent interacts with a familiar object for the same time compared to a novel object, this is a hint for a lack of recall or loss of memory. Saline treated mice displayed deficits in episodic memory as demonstrated by lacking preference for any object in this test (p = 0.75). Surprisingly, ANK6 treated mice showed increased preference for the new object (Figure 5, p = 0.08) indicating that ANK6 improves the cognition of tg-APPSwDI mice. Borderline significance may be due to the short treatment period.

No significant changes in Aβ plaque load in ANK6 treated tg-APPSwDI mice measureable. Tg-APPSwDI mice are developing typical Aβ plaques, starting at the age of three month[21]. After finishing the behavior experiments, mice were sacrificed and the brains were assessed for Aβ plaque load (Figure S9). Although the tg-APPSwDI mice treated with ANK6 showed improved cognitive performance and the control group did not, no significant changes in the Aβ plaque load were measured.

CONCLUSION

Within this study, we successfully optimized D3 concerning the affinity to monomeric Aβ(1-42) by using a two-step procedure with peptide microarrays. The novel Aβ monomers-stabilizing D3 derivatives ANK1 to ANK7 bind with 3- to 5-fold higher affinity to monomeric Aβ compared to D3 and inhibit Aβ fibril formation, eliminate Aβ oligomers, and reduce the Aβ-induced cell toxicity more efficiently than D3. Additionally, the in more detail studied peptide ANK6 reduces the seeding potential of Aβ by converting Aβ fibrils into amorphous aggregates. *In vivo* studies show that ANK6 improves the cognition of tg-APPSwDI mice. Taken together, the optimized ANK peptides are promising drug candidates for the treatment of AD and will be further investigated *in vivo*.

EXPERIMENTAL SECTION

Peptides. Aβ(1-42), N-terminally biotinylated Aβ(1-42) and FITC-Aβ(1-42) were purchased from Bachem (Heidelberg, Germany). The D-enantiomeric peptides D3 and ANK1 to ANK7 were purchased with a purity of 95 % from peptides&elephants (Potsdam, Germany). The C-terminus of the D-peptides was amidated.

Preparation of seedless Aβ(1-42) stock solutions. In general, all Aβ preparations were carried out in Protein LowBinding tubes (Eppendorf AG, Hamburg, Germany). Lyophilized Aβ(1-42), N-terminally biotinylated Aβ(1-42) and FITC-Aβ(1-42) was dissolved in 1,1,1,3,3,3-Hexafluor-2-propanol (HFIP) to a final concentration of 1 mg/ml overnight at room temperature and stored at -20 °C until further use. For experiments, required amounts were aliquoted and HFIP was evaporated using a vacuum concentrator (Concentrator 5301, Eppendorf, Germany) for 20 min.

Preparation of different Aβ(1-42) species in solution. For incubation of the peptide microarrays with different Aβ(1-42) species, the preparation of monomeric and oligomeric FITC-Aβ(1-42) was carried out using size exclusion chromatography (SEC) as described before[28]. In brief, HFIP pre-treated FITC-Aβ(1-42) was freshly dissolved in 10 mM sodium phosphate buffer pH 7.4 containing 150 mM NaCl to a concentration of 0.1 mM FITC-Aβ(1-42), centrifuged and supplied on a Superdex 75 10/300 GL column (GE Healthcare, Uppsala, Sweden) connected to an Äkta purifier system (GE Healthcare, Uppsala, Sweden). The separation of monomeric and oligomeric FITC-Aβ(1-42) was performed with a flow rate of 0.6 ml/min and recorded by measuring the absorption at 490 nm and 260 nm. 500 µl fractions were collected and fractions, containing monomeric or oligomeric FITC-Aβ(1-42), were pooled.

For preparation of Aβ fibrils, FITC-Aβ(1-42) was dissolved in 10 mM sodium phosphate buffer pH 7.4 as described above and incubated for three days at 37 °C. Generated fibrils were centrifuged by 14,000 x g and washed three times with buffer to remove soluble monomeric and oligomeric Aβ species.

Peptide microarrays. The peptide microarray was produced by Pepscan (Lelystad, Netherlands). Each peptide was covalently coupled on glass slides in triplicate (spots with a diameter of 100 µm).

As a pre-treatment, the slides were shortly washed with bidest. water and 20 % ethanol. Three slides were incubated with 1-5 µM monomeric, oligomeric or fibrillar FITC-Aβ(1-42), respectively, in 10 mM sodium phosphate buffer pH 7.4 for 1 hour at room temperature with gentle agitation. After incubation, the slides were washed three times with TBS and 0.1 % v/v TWEEN20 (TBS-T) for 10 min and three times with water for 10 min, following by drying with nitrogen.

The fluorescence intensity of the FITC-Aβ(1-42) bound to the peptides on the slides was evaluated using a FLA800 fluorescence image system (Fujifilm Medical Systems USA Inc, Stamford, USA) with slide carrier employing a 473 nm laser for excitation. 5 µm resolution digital images were generated. The fluorescence intensity was analyzed by using the software AIDA array Metrix (Raytest, Staubenhardt, Germany). The integral of the fluorescence intensities (diameter 80 µm) was calculated. Background subtraction was carried out by local dot rings with inflate dots of 150 µm and background ring width of 30 µm.

To compare the different peptide microarrays, a median-based normalization was performed:

$$s = \frac{s_{spot}}{median(s_{all})} \quad (1)$$

with s_{spot}, fluorescence intensity of one spot and s_{all}, fluorescence intensity of all spots. Afterwards, the fluorescence intensities were FITC corrected and the mean value of three spots from three different slides was calculated. For predicting the optimization of the peptide-FITC-Aβ(1-42) binding to monomeric FITC-Aβ(1-42), the monomeric FITC-Aβ(1-42) signal intensities were subtracted pro rata using the following formula:

$$\text{specific binding to monomeric A}\beta = s_{monos} - 0.5 * s_{oligos} - 0.5 * s_{fib} \quad (2)$$

with s_{monos}, monomeric FITC-Aβ(1-42) bound to immobilized peptide; s_{oligos}, oligomeric FITC-Aβ(1-42) bound to immobilized peptide; s_{fib}, fibrillary FITC-Aβ(1-42) bound to immobilized peptide.

The results were displayed in heatmaps generated with MatLab (The MathWorks, Natick, USA).

The binding specificity was determined by calculating the quotient of the binding signal of monomeric Aβ-peptide-interaction to oligomeric or fibrillar Aβ-peptide-interaction.

Biolayer interferometry (BLI). The equilibration dissociation constants (K_D) determination of D3 and ANK1 to ANK7 to monomeric Aβ(1-42) was examined using biolayer interferometry (BLI) where biotinylated Aβ(1-42) was immobilized to the sensor surface via biotin-streptavidin coupling and the peptides were used as analytes in solution.

The purification and immobilization of Aβ(1-42) monomers was performed as described before with minor changes[29]. Briefly, HFIP pre-treated N-terminally biotinylated Aβ(1-42) was dissolved in 20 mM sodium phosphate buffer pH 7.2 to a final concentration of 80 µg/ml. Monomers were purified on a Superdex 75 10/300 GL column (GE Healthcare, Uppsala, Sweden) connected to an ÄKTA purifier system (GE Healthcare, Uppsala, Sweden). Purified monomers were directly immobilized on the sensor surface of Super Streptavidin biosensors (SSA) (fortéBIO, PALL Life Science, Menlo Park, USA) using an Octet RED96 instrument (fortéBIO, PALL Life Science, Menlo Park, USA) to a final level of 2 nm. Ligand and reference biosensors were quenched with 20 µg/ml biotin for 7 min.

The K_D determinations of D3 and ANK1 to ANK7 to monomeric Aβ(1-42) were performed in multi cycle kinetics at 26 °C. Association of 0.8 µM, 1.6 µM, 3.1 µM, 6.3 µM,

12.5 µM, 25 µM, 50 µM D3 and 0.4 µM, 0.8 µM, 1.6 µM, 3.1 µM, 6.3 µM, 12.5 µM, 25 µM ANK peptides diluted in running buffer (20 mM sodium phosphate, 50 mM sodium chloride, pH 7.4) was recorded for 300 sec. on ligand and reference biosensors, followed by a dissociation phase of 300 sec. After each cycle, a regeneration step using 2 M guanidine hydrochloride for 30 sec was implemented. After measurement, the sensorgrams were double referenced using the reference biosensors and a buffer cycle. Evaluation was performed by plotting the respective response levels against the applied peptide concentrations. The curves were fitted using Langmuir´s 1:1 binding model (Hill function with n = 1, OriginPro 8.5G, OriginLab, Northampton, USA).

Thioflavin T (ThT) assay. The thioflavin T (ThT) assay was performed as described before[28]. In brief, HFIP pretreated Aβ(1-42) was dissolved to 20 µM in 10 mM sodium phosphate buffer pH 7.4 were mixed with 20 µM ThT and 20 µM D-peptide. The ThT fluorescence was monitored over 48 h every 15 min at λ_{ex} = 440 nm and λ_{em} = 490 nm in a plate reader (Polarstar Optima, BMG, Ortenberg, Germany) at 37 °C. Each value was background corrected (ThT fluorescence signal of solution without Aβ(1-42) or with peptide only respectively).

Quantitative determination of interference with Aβ(1-42) aggregate size distribution (QIAD). The QIAD assay was performed according to Brener et al.[14] Briefly, after a pre-incubation of 4.5 h in 10 mM sodium phosphate buffer pH 7.4 at 21 °C and shaking at 600 rpm, 80 µM Aβ(1-42) was co-incubated with 10 µM D-peptide for 40 min at the same conditions. For separation of the different Aβ(1-42) species, a density gradient centrifugation with a discontinuous gradient ranging from 5 to 50 % iodixanol (Optiprep, Axis-shield, Oslo, Norway) was performed by using an ultracentrifuge (Optima MAX-XP) with an TLS-55 rotor (both Beckman Coulter, Brea, USA). 100 µl of the sample were loaded on the top of the gradient. After centrifugation at 259,000 x g for 3 h at 4 °C, 14 x 140 µl fractions were collected. To dissolve the pellet, representing the 15th fraction, 60 µl 6 M guanidinium hydrochloride was boiled for 5 min within the centrifuge tube. The samples were stored at -20 °C until further use.

For quantification of the content of the different Aβ(1-42) species, a reverse phase high performance liquid chromatography (RP-HPLC) was performed. 20 µl were supplied on a Zorbax SB-300 C8 column (Agilent, Böblingen, Germany) connected to an Agilent 1260 Infinity system. 30 % v/v acetonitrile with 0.1 % (v/v) trifluoroacetic acid (TFA) was used as mobile phase. The column was tempered at 80 °C and the UV absorption at 214 nm was detected. For quantification of the Aβ(1-42) amount, the area under the peak representing Aβ(1-42) was calculated and the molar concentration was determined using a calibration equation.

The recovery rate R was determined by using the following equation:

$$R = \frac{c_P V_P + \sum_{n=1}^{14} c_n \cdot V_F}{c_0 \cdot V_0} \qquad (3)$$

with c_P the Aβ(1-42) concentration in the last fraction (15th fraction), c_n the Aβ(1-42) concentration in fraction 1 to 14, c_0 the initial Aβ(1-42) concentration, V_F the volume of the fractions 1 to 14, V_P the volume of the last fraction and V_0 the volume of the initial sample. Total Aβ recovery rate within the quantification of Aβ(1-42) using RP-HPLC was about 94 % for Aβ without peptide and 92 % for Aβ(1-42) co-incubated with ANK1 to ANK7.

The elimination (E) of the oligomeric Aβ(1-42) by the D-peptides D3 and ANK1 to ANK7 were determined as followed:

$$E = 100 \cdot \left(1 - \frac{\sum_{n=4}^{6} c_n}{\sum_{n=4}^{6} c_{A\beta}}\right) \qquad (4)$$

with c_n the Aβ(1-42) concentration in fraction 4 to 6 of samples where Aβ was incubated with D-peptide, $c_{A\beta}$ the Aβ(1-42) concentration of the control.

The results were statistically analyzed with the paired Mann-Whitney U-test. Aβ(1-42) without ligand was measured eleven times, Aβ(1-42) with ANK1 to ANK7 four times.

Tricine-SDS-PAGE. 16 % Tricine-SDS-PAGE was performed according to Schagger[30]. In brief, all samples were mixed with 4x Tris-tricine gel loading buffer (4 % SDS (w/v), 12 % Glycerin (v/v), 50 mM Tris, 2 % β-mercaptoethanol (v/v), 0.01 % SERVA BlueG (w/v); pH 6.8), boiled for 5 min, and the proteins separated within a 16 % Tricine-SDS-PAGE at 100 V constantly. The ultra-low range Color Protein marker (C6210, Sigma-Aldrich, St. Louis, USA) with molecular weights between 1 and 26.6 kDa was use as a size standard. For visualization, the Chemidoc MP system (Biorad, Hercules, USA) was used.

MTT cell viability assay. The human neuroblastoma SH-SY5Y cells (Leibniz Institute DSMZ, Braunschweig, Germany) were cultivated in DMEM medium supplemented with 20 % fetal bovine serum. 10.000 cells per well were seeded on collagen-coated 96 well plates (Gibco, Carlsbad, USA) and incubated in a 95 % humidified atmosphere with 5 % CO_2 and 37 °C for 24 h. Aβ(1-42) was pre-incubated for 4.5 h in 10 mM sodium phosphate buffer pH 7.4 at 21 °C and 600 rpm and co-incubated with ANK4 to ANK7 and D3 for further 40 min with the same conditions. The SH-SY5Y cells were treated with 1 µM Aβ(1-42) and 0, 0.2, 1, or 5 µM peptide, finally. For quantitation of the cell viability, the Cell proliferation Kit I (MTT) (Roche, Germany) was used according to manufacturer's instructions. The absorbance of the formazan product was determined by measuring the absorption at 570 nm subtracted by the absorption at 660 nm in a plate reader (Polarstar Optima, BMG). The positive control, consisting of cells only, is normalized to 100 % cell viability. One Way ANOVA with Bonferroni post-hoc test were used for statistical analysis.

Seeding assay. Pre-treated 200 µM Aβ(1-42) was incubated in 10 mM sodium phosphate buffer pH 7.4 over three days at 37 °C and 600 rpm for seed preparation. The sample was centrifuged at 14,000 x g at 4 °C for 45 min and the pellet resuspended in 10 mM sodium phosphate buffer pH 7.4 and sonicated for 2 min. The concentration

of Aβ(1-42) seeds according to the monomers was determined with RP-HPLC. Seeds were mixed with D3 or ANK6 in a molar ratio of 1:1 (Aβ(1-42):peptide) and incubated for further 24 h at 37 °C and 600 rpm. Afterwards, seed mix, consisting of Aβ with or without peptide, were sonicated again for 2 min and 3.1 µM of this seeds were added to 25 µM freshly prepared monomeric Aβ(1-42) and 20 µM ThT (molar ratio of Aβ(1-42) monomers:Aβ(1-42) seeds 8:1). The ThT fluorescence was measured every 5 min for 24 h at 24 °C.

For evaluation of the seeding potential, curves were fitted by using a 5-parametrical logistic fit model and the $t_{1/2}$ value calculated. Additional, the plateau level of the ThT signal was analyzed. For statistical analysis, a one-way ANOVA was used. The measurements were performed in three independent experiments.

Transmission electron microscopy (TEM). The samples from the MTT assay with Aβ(1-42) and ANK6 in equal molar ratio were incubated 24 h and absorbed on formval/carbon coated copper grids (S162, Plano, Wetzlar, Germany) for 5 min. After three times washing with water, the samples were negative stained with 1 % (w/v) uranylacetat for 1 min. Images were taken using a Libra 120 transmission electron microscope (Zeiss, Oberkochen, Germany) operating at 120 kV.

Animals. In the present study 10 month (± 1 week) old female APPSwDI (human APP with Swedish K670N/M671L, Dutch E693Q and Iowa D694N mutations on a C57BL/6 background) mice were used. The animals were housed at controlled environments (temperature 22 °C, humidity 50 to 60 %, and light from 07:00 am to 07:00 pm), food and water were available ad libitum. Group sizes were decided on the basis of data from previous studies. The experiments were conducted in accordance with the local Institutional Animal Care and Use Committee (IACUC) guidelines.

ANK6 treatment. Tg-APPSwDI mice (11 animals per group) were treated over four weeks with a total peptide amount of 3.7 mg. The implantation of the Alzet minipumps was performed intraperitoneal (model #1004; delivery rate: 0.11 µl/h; duration: 4 weeks). The Alzet minipumps were filled with the appropriate solutions and implanted into the peritoneal cavity.

Behavior. During the last week of treatment, animals were tested in three different behavioral tests to assess cognition and to monitor side effects like changes in general activity and anxiety. Experimenters were not informed about group allocation.

First the open field test was conducted. The maze consisted of an arena of 42 x 42 cm^2 with clear Plexiglas walls (20 cm high). The animal was put into the arena and observed for 4 min, with a camera driven tracker system, Ethovision 8.5 (Noldus, Wageningen, The Netherlands). The arena was subdivided into two areas, the "open" center and the area by the walls. The system recorded the position of the animal in the arena at 5 frames/second and the data were analyzed regarding time spent in each area (center vs. wall). For disinfection and to avoid olfactory cues the apparatus was wiped down with chlorhexidine and 70 % ethanol and allowed to air-dry.

Next, the zero maze test was conducted. The maze consisted of a circular arena with a diameter of 70 cm and four areas of equal size, two with walls with the height of 0.5 cm, and two walls with the height of 15 cm walls of nontransparent material. The animal was put in the arena, and observed for 4 min, with a camera driven tracking system (Ethovision 8.5, Noldus, Wageningen, The Netherlands). The time spent in each area (open vs. closed) was recorded. After every trail, the box was cleaned with chlorhexidine and 70 % ethanol and allowed to air-dry to avoid olfactory cues.

The water maze procedure has been described in detail before[31]. Briefly, a pool, with 120 cm in diameter and a see-through round platform, 10 cm in diameter, located 0.5 cm below the water surface was used. During day 1 through day 5 of the testing period, the mice were trained to find a hidden platform that is kept in a constant position throughout these 5 days. Three trials a day were performed; each trial started at another starting position in random order. The mice had 60 s to find the platform and 10 s to stay on the platform. The inter-trial interval was 2 min. The swimming speed, latency to find the platform, and the path length of each animal to find the platform was determined.

The object recognition test (ORT) was carried out in a maze consisting of a rectangular polycarbonate box, with partitions separating the box into three chambers. The partitions had openings that allowed the animal to move freely from one chamber to another. The animal was monitored by the Noldus tracking system Ethovision 8.5. The Test consisted of two sessions: a training session and a testing session. In the training session two identical objects were placed on each side of the box. The mouse was placed in the box and allowed to move freely throughout the apparatus for a 10-minute training session. After 30 min, a new object replaced one of the "old" objects and the mouse was put in the box and allowed to move freely throughout the box over a 4-minute test session. The time spent with each object was recorded. All objects used in this study were different in size and shape. They were fixed in the box to avoid movement and cleaned with chlorhexidine and 70 % ethanol and allowed to air-dry to avoid olfactory cues. The apparatus was also wiped down with chlorhexidine followed by ethanol and water and dried with paper towels for each mouse tested.

Histochemistry. After the treatment period, mice were sacrificed for histochemical analysis. Therefore, the mice were anesthetized and transcardially perfused. The brain was removed and the right hemisphere was fixed with 4 % paraformaldehyde overnight. Afterwards, it was cryoprotected in 30 % sucrose for 24 h and antifreezed in 15 % sucrose and 30 % ethylene glycol in 0.05 M phosphate buffer, pH 7.4. The brain was cut into six sections (1 to 6) of coronal sections (30 µm). The first series of sections was mounted unstained; the second and third series were immunohistochemically stained, using the W0-2 antibody

for human Aβ, according to van Groen et al.[32] The other series were stored in antifreeze at -20 °C.

Plaque loads were determined as described before[32,33]. In brief, the appropriate areas (dorsal hippocampus and frontal cortex) of the brain were digitized using an Olympus DP73 digital camera. To avoid changes in light, which might affect the measurement, all images were acquired in one session. The measurements were performed on sections that were stained simultaneously, i.e. in the same staining tray (n=24), to avoid differences in staining density between sections. The percentage of area covered by the reaction product reflecting binding to Aβ was measured in the hippocampus using the ImageJ (NIH) program. Aβ plaques stained by Wo-2 antibody were counted in the same brain area on the adjacent sections that were stained with Congo red using digital images with overlays of defined measurement areas. These measurements were in triplicate per section (that had been stained simultaneously.

ASSOCIATED CONTENT

Supporting Information

This material is available free of charge via the Internet at http://pubs.acs.org.

AUTHOR INFORMATION

Corresponding Author

* d.willbold@fz-juelich.de

ACKNOWLEDGMENT

D.W. was supported by grants from the "Portfolio Technology and Medicine", the "Portfolio Drug Research" and the Helmholtz-Validierungsfonds of the "Impuls und Vernetzungs-Fonds der Helmholtzgemeinschaft". The study was supported by the TT-Fonds of the Technology Transfer Department of the Forschungszentrum Jülich.

REFERENCES

(1) Prince, M.; Bryce, R.; Albanese, E.; Wimo, A.; Ribeiro, W.; Ferri, C. P. Alzheimer's & Dementia 2013, 9, 63.
(2) Querfurth, H. W.; LaFerla, F. M. New England Journal of Medicine 2010, 362, 329.
(3) Hardy, J.; Selkoe, D. J. Science 2002, 297, 353.
(4) Finder, V. H.; Glockshuber, R. Neurodegenerative Diseases 2007, 4, 13.
(5) Lue, L.-F.; Kuo, Y.-M.; Roher, A. E.; Brachova, L.; Shen, Y.; Sue, L.; Beach, T.; Kurth, J. H.; Rydel, R. E.; Rogers, J. The American Journal of Pathology 1999, 155, 853.
(6) Schumacher, T. N.; Mayr, L. M.; Minor, D. L., Jr.; Milhollen, M. A.; Burgess, M. W.; Kim, P. S. Science 1996, 271, 1854.
(7) Wiesehan, K.; Buder, K.; Linke, R. P.; Patt, S.; Stoldt, M.; Unger, E.; Schmitt, B.; Bucci, E.; Willbold, D. ChemBioChem 2003, 4, 748.
(8) Funke, S. A.; van Groen, T.; Kadish, I.; Bartnik, D.; Nagel-Steger, L.; Brener, O.; Sehl, T.; Batra-Safferling, R.; Moriscot, C.; Schoehn, G.; Horn, A. H. C.; Müller-Schiffmann, A.; Korth, C.; Sticht, H.; Willbold, D. ACS Chemical Neuroscience 2010, 1, 639.
(9) Bartnik, D.; Funke, S. A.; Andrei-Selmer, L.-C.; Bacher, M.; Dodel, R.; Willbold, D. Rejuvenation Research 2009, 13, 202.
(10) van Groen, T.; Kadish, I.; Funke, S. A.; Bartnik, D.; Willbold, D. Journal of Alzheimer's Disease 2013, 34, 609.
(11) van Groen, T.; Wiesehan, K.; Funke, S. A.; Kadish, I.; Nagel-Steger, L.; Willbold, D. ChemMedChem 2008, 3, 1848.
(12) Wiesehan, K.; Stöhr, J.; Nagel-Steger, L.; van Groen, T.; Riesner, D.; Willbold, D. Protein Engineering Design and Selection 2008, 21, 241.
(13) Ward, R. V.; Jennings, K. H.; Jepras, R.; Neville, W.; Owen, D. E.; Hawkins, J.; Christie, G.; Davis, J. B.; George, A.; Karran, E. H.; Howlett, D. R. Biochemical Journal 2000, 348, 137.
(14) Brener, O.; Dunkelmann, T.; Gremer, L.; van Groen, T.; Mirecka, E. A.; Kadish, I.; Willuweit, A.; Kutzsche, J.; Jürgens, D.; Rudolph, S.; Tusche, M.; Bongen, P.; Pietruszka, J.; Oesterhelt, F.; Langen, K.-J.; Demuth, H.-U.; Janssen, A.; Hoyer, W.; Funke, S. A.; Nagel-Steger, L.; Willbold, D. Scientific Reports 2015, 5, 13222.
(15) Giuffrida, M. L.; Caraci, F.; Pignataro, B.; Cataldo, S.; De Bona, P.; Bruno, V.; Molinaro, G.; Pappalardo, G.; Messina, A.; Palmigiano, A.; Garozzo, D.; Nicoletti, F.; Rizzarelli, E.; Copani, A. The Journal of Neuroscience 2009, 29, 10582.
(16) Iversen, L. L.; Mortishire-Smith, R. J.; Pollack, S. J.; Shearman, M. S. Biochemical Journal 1995, 311, 1.
(17) Cohen, S. I. A.; Linse, S.; Luheshi, L. M.; Hellstrand, E.; White, D. A.; Rajah, L.; Otzen, D. E.; Vendruscolo, M.; Dobson, C. M.; Knowles, T. P. J. Proceedings of the National Academy of Sciences of the United States of America 2013, 110, 9758.
(18) Jarrett, J. T.; Berger, E. P.; Lansbury, P. T. Biochemistry 1993, 32, 4693.
(19) Petkova, A. T.; Leapman, R. D.; Guo, Z.; Yau, W.-M.; Mattson, M. P.; Tycko, R. Science 2005, 307, 262.
(20) Du, D.; Murray, A. N.; Cohen, E.; Kim, H.-E.; Simkovsky, R.; Dillin, A.; Kelly, J. W. Biochemistry 2011, 50, 1607.
(21) Davis, J.; Xu, F.; Deane, R.; Romanov, G.; Previti, M. L.; Zeigler, K.; Zlokovic, B. V.; Van Nostrand, W. E. Journal of Biological Chemistry 2004, 279, 20296.
(22) Lalonde, R.; Fukuchi, K.; Strazielle, C. Rev Neurosci 2012, 23, 363.
(23) Xu, F.; Grande, A. M.; Robinson, J. K.; Previti, M. L.; Vasek, M.; Davis, J.; Van Nostrand, W. E. Neuroscience 2007, 146, 98.
(24) Prut, L.; Belzung, C. European journal of pharmacology 2003, 463, 3.
(25) D'Hooge, R.; De Deyn, P. P. Brain Research Reviews 2001, 36, 60.
(26) Zhang, R.; Xue, G.; Wang, S.; Zhang, L.; Shi, C.; Xie, X. Journal of Alzheimer's Disease 2012, 31, 801.
(27) Ennaceur, A.; Delacour, J. Behav Brain Res 1988, 31, 47.
(28) Widera, M.; Klein, A.; Cinar, Y.; Funke, S.; Willbold, D.; Schaal, H. AIDS Research and Therapy 2014, 11, 1.
(29) Frenzel, D.; Glück, J. M.; Brener, O.; Oesterhelt, F.; Nagel-Steger, L.; Willbold, D. PloS one 2014, 9, e89490.
(30) Schagger, H. Nat. Protocols 2006, 1, 16.
(31) Liu, L.; Ikonen, S.; Heikkinen, T.; Heikkila, M.; Puolivali, J.; van Groen, T.; Tanila, H. Behav Brain Res 2002, 134, 433.
(32) van Groen, T.; Kiliaan, A. J.; Kadish, I. Neurobiology of Disease 2006, 23, 653.
(33) Kadish, I.; Pradier, L.; van Groen, T. Brain Research Bulletin 2002, 57, 587.

TOC graphic

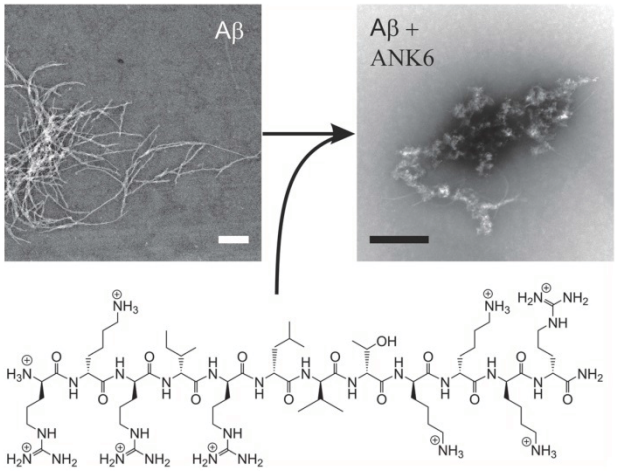

11

Supporting Information

Optimization of d-peptides for Aβ monomer binding specificity enhances their potential to eliminate toxic Aβ oligomers

Antonia Nicole Klein[1], Tamar Ziehm[1], Thomas van Groen[2], Inga Kadish[2], Anne Elfgen[1], Markus Tusche[1], Maren Thomaier[1], Kerstin Reiß[1], Oleksandr Brener[3], Lothar Gremer[1,3], Janine Kutzsche[1], Dieter Willbold[1,3,*]

[1] Institute of Complex Systems, Structural Biochemistry (ICS-6), Research Center Jülich, 52425 Jülich, Germany

[2] Department of Cell, Developmental and Integrative Biology, University of Alabama at Birmingham, Birmingham, AL, USA

[3] Institut für Physikalische Biologie, Heinrich-Heine-Universität Düsseldorf, 40225 Düsseldorf, Germany

*Correspondence: d.willbold@fz-juelich.de

Δ	trans-4-fluoro-L-proline	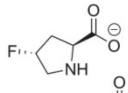
η	4-fluoro-D-phenylalanine	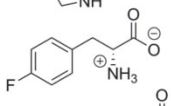
θ	4-benzyl-D-phenylalanine	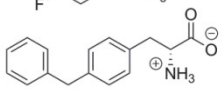
ι	1-naphthyl-D-alanine	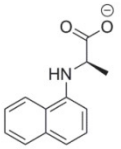
κ	3,5-diiodo-D-tyrosin	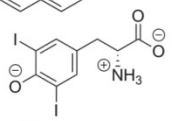
λ	D-phenylglycine	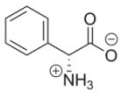
μ	D-homoarginine	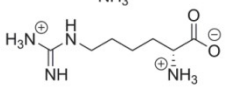
ξ	D-homocitrulline	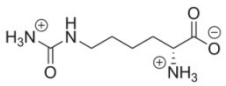
ο	β-homoarginine	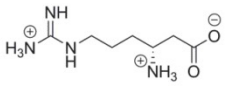
π	β-cyclohexyl-D-alanine	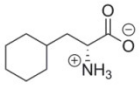
σ	cyclovalin	
Φ	β-alanine	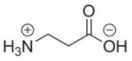
Ψ	γ-aminobutyric acid	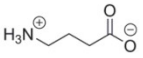

Figure S1| Non-proteinogenic amino acids. To increase the variability of D3 derivatives, non-proteinogenic amino acids were introduced. The amino acids were in d-enantiomeric conformation, if possible, except of trans-4-fluoro-L-proline.

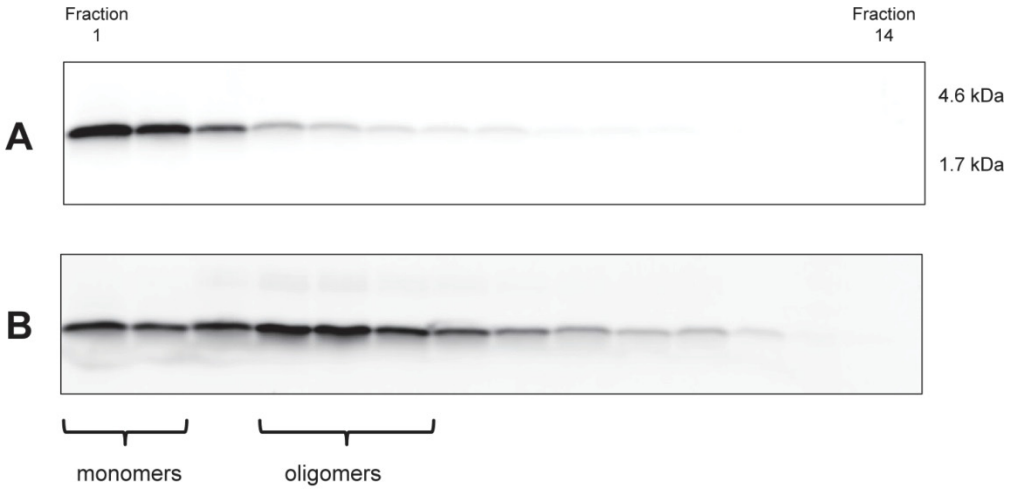

Figure S2| Size distribution of FITC-Aβ(1-42) monomers (A) and oligomers (B) after size exclusion chromatography and additional 1 h incubation at room temperature. Aβ species were verified by density gradient centrifugation (DGC), fractionated within 14 fractions, visualized by SDS-PAGE and detecting the FITC tag by fluorescence.

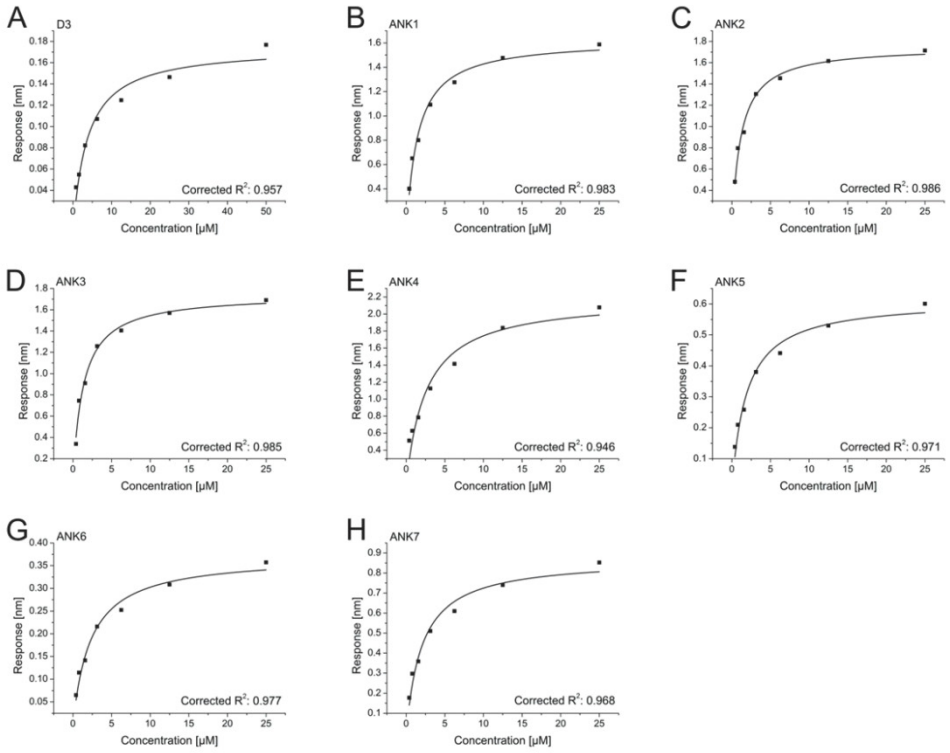

Figure S3| Steady state fit curves of one representative interaction study using biolayer interferometry (BLI). Apparent equilibration dissociation constants of peptide-Aβ(1-42) interactions were determined applying Langmuir´s 1:1 binding model. A) D3; B) ANK1; C) ANK2; D) ANK3; E) ANK4; F) ANK5; G) ANK6; H) ANK7. Corrected R2 values represent the goodness of the fit.

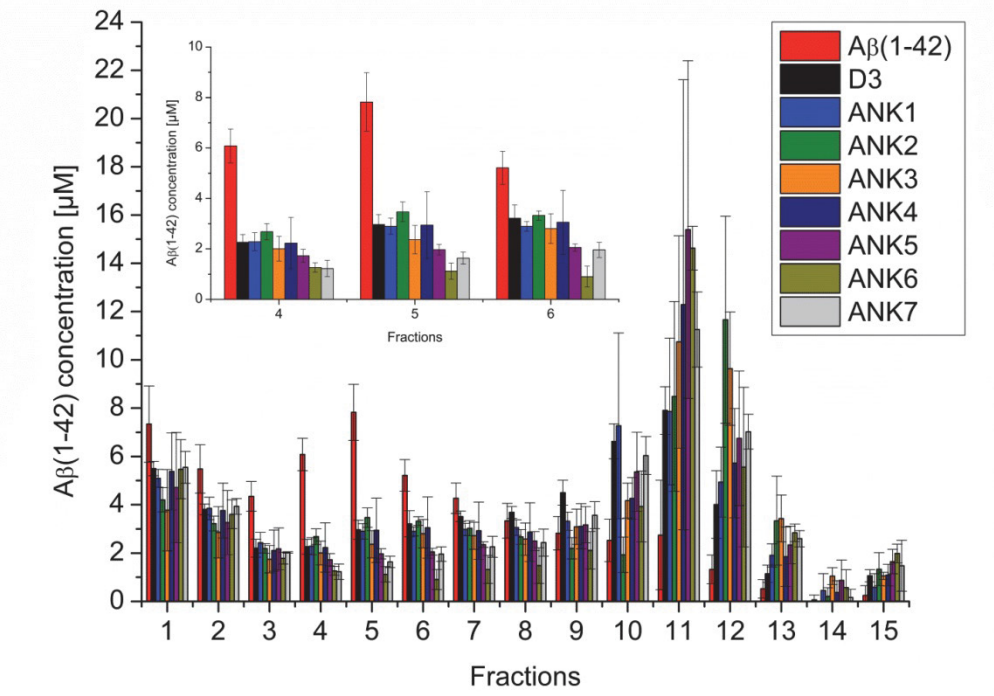

Figure S4| Effects of ANK1 to ANK7 on Aβ(1-42) assemblies. 80 µM pre-incubated Aβ(1-42) (4.5 h at 21 °C, 600 rpm) was co-incubated with 10 µM D3 or ANK1 to ANK7 (40 min, 21 °C, 600 rpm). Afterwards, the different Aβ(1-42) aggregates were separated via density gradient centrifugation, fractionated into 15 fractions and quantified via RP-HPLC according to their Aβ(1-42) content. Fractions 1 and 2 represented monomeric Aβ(1-42) and fractions 4 to 6 oligomeric Aβ(1-42). Aβ(1-42) oligomer concentrations present in fractions 4 to 6 are shown in the inlet.

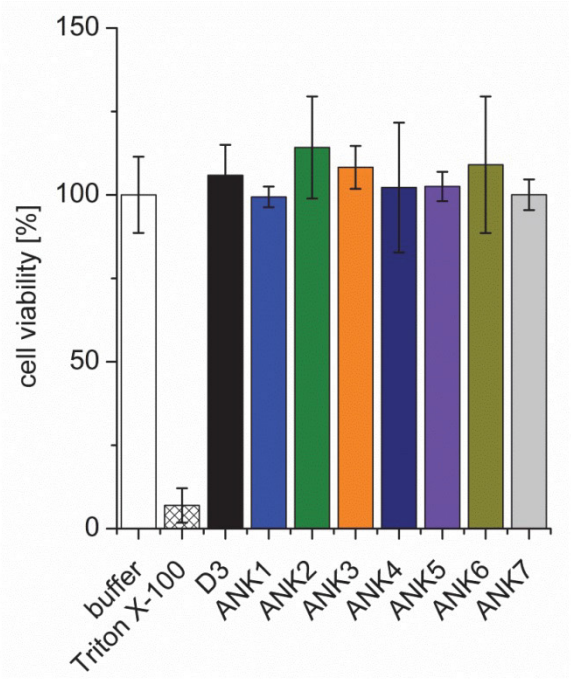

Figure S5| Investigation of the toxicity of D3 and ANK1 to ANK7 on SH-SY5Y cells. As a control for the MTT-based cytotoxicity assay, the influence of 5 µM D3 and 5 µM ANK1 to ANK7 without Aβ on the cell viability was determined. Cell viabilities were measured by measuring the absorption of MTT at 570 nm subtracted by the absorption at 660 nm and normalized to non-treated cells. As a negative control, the influence of 0.125 % Triton X-100 on the cell viability was measured.

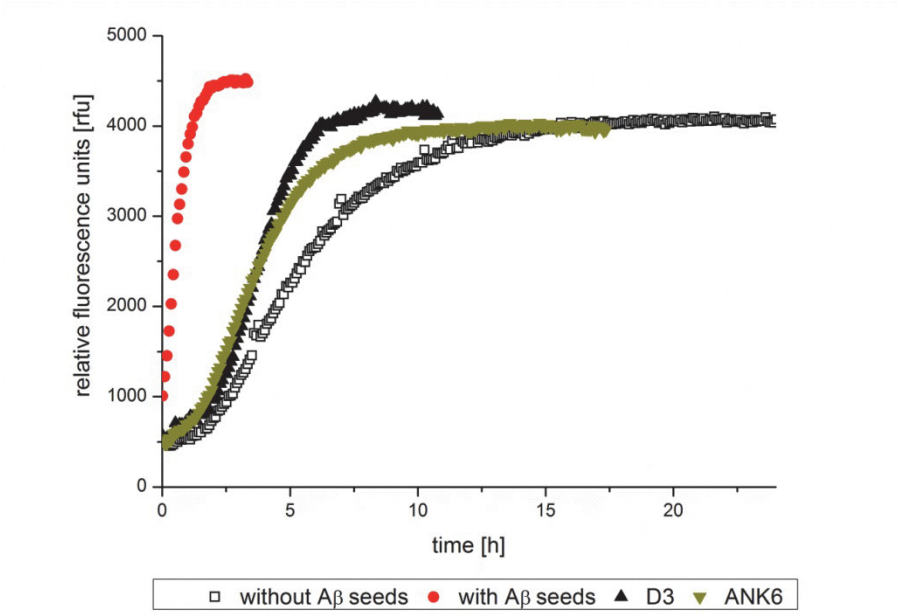

Figure S6| Effects of ANK6 on the Aβ seeding potential. To examine the seeding potential, Aβ(1-42) fibrils were co-incubated for 24 h with an equal molar ratio between Aβ monomer units and D3 or ANK6. 3.1 µM of these seeds were co-incubated with 25 µM monomeric Aβ and Aβ fibril formation was monitored for 24 h using ThT fluorescence. The ThT fluorescence decreased after reaching the saturation point, probably due to sedimentation. Thus, curves were cut after ThT fluorescence reached the saturation point.

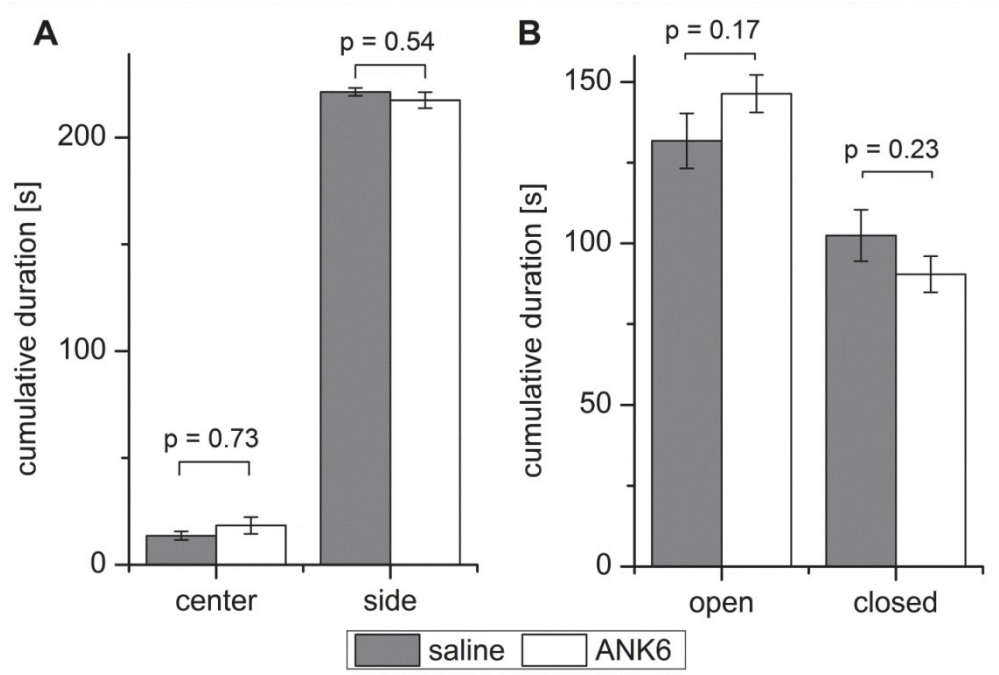

Figure S7| Effects of treatment on general activity or anxiety studied via A) open field test and B) zero maze test. A) A squared arena was divided into the "open" center and the "side" near the walls. B) A circular maze was divided into four parts with equal size. Two parts have nonvisible walls (closed) and two parts have open arms (open). For both tests, the time the mice spent in both parts was compared between both groups. For statistical analysis, Mann-Whitney-U-test was performed.

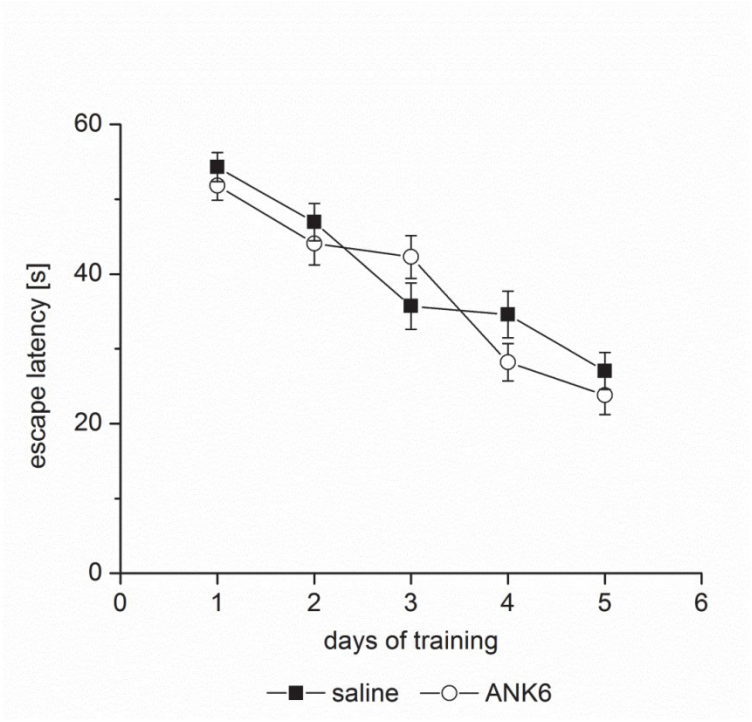

Figure S8| Morris water maze performance of non-treated and ANK6 treated tg-APPSwDI mice. The time spend in the water until they found the hidden platform was investigated daily over a period of five days. For experimental details, see the experimental section. The mean values ± SEM are shown. For statistical analysis, whether the mice learned within the training, a Friedman-ANOVA was performed. Both groups significantly learned within this training interval.

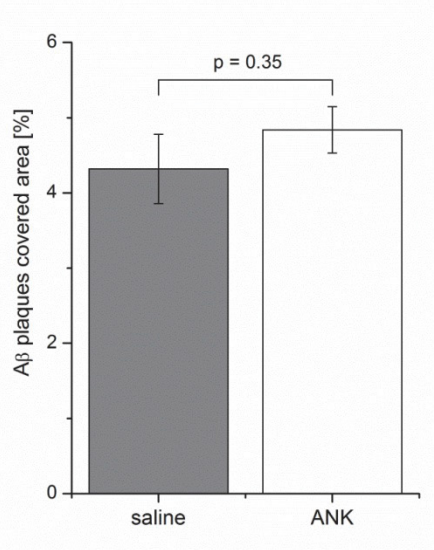

Figure S9| Aβ plaque loads of saline- and ANK-treated tg-APPSwDI mice. After behavioral studies, the mice were sacrificed and brain slices were analyzed according to the Aβ plaque load. For statistical analysis, a t-test was performed.

3.1.3. Competitive mirror image phage display derived peptide modulates amyloid beta aggregation and toxicity.

Einzureichen bei: PlosOne

Impact Factor (2013): 3.534

Eigener Anteil: 10 %

Durchführen von transmissionselektronenmikroskopischen Aufnahmen

Competitive mirror image phage display derived peptide modulates amyloid beta aggregation and toxicity.

Stephan Rudolph[1], Antonia Nicole Klein[1], Markus Tusche[1], Christine Schlosser[1], Anne Elfgen[1], Oleksandr Brener[1,3], Lothar Gremer[1,3], Susanne Aileen Funke [1,2], Janine Kutzsche[1] und Dieter Willbold[1,3,*]

[1] Institute of Complex Systems, Structural Biochemistry (ICS-6), Research Centre Jülich, 52425 Jülich, Germany

[2] Fakultät Angewandte Naturwissenschaften, Hochschule für angewandte Wissenschaften Coburg, 96450 Coburg

[3] Institut für Physikalische Biologie, Heinrich-Heine-Universität Düsseldorf, 40225 Düsseldorf, Germany

*Correspondence: d.willbold@fz-juelich.de

Abstract

Alzheimer´s disease is the most prominent type of dementia and currently no causative treatment is availabble. According to recent studies, oligomeric species of the amyloid beta (Aβ) peptide appear to be the most toxic Aβ assemblies. In contrast, Aβ monomers may be not toxic per se and may even have a neuroprotective role. Here we describe a competitive mirror image phage display procedure that allowed us to identify preferentially $Aβ_{1-42}$ monomer binding and thereby stabilizing peptides, which destabilize and thereby eliminate toxic oligomer species. One of the peptides, called Mosd1 (monomer specific d-peptide 1), was characterized in more detail. Mosd1 abolished oligomers from a mixture of $Aβ_{1-42}$ species, reduced $Aβ_{1-42}$ toxicity in cell culture, and restored the physiological phenotype in neuronal cells stably transfected with human amyloid precursor protein.

Keywords: Alzheimer´s disease; amyloid beta; mirror image phage display; D-enantiomeric peptides

Introduction

Dementia counts for more than 30 million patients worldwide. Alzheimer´s disease (AD) is the most frequent type of dementia and therefore largely contributes to this number [1, 2]. Because age is the most important risk factor for AD, the number of AD patients is expected to increase further.

AD is a progressive type of dementia with symptoms like memory loss, apathy, depression, anxiety and behavioral changes as well as neuropathological hallmarks including inflammation, neuronal cell death and loss of brain mass [2-6]. To date, AD can only be treated palliatively and symptomatically, although with only limited success. Throughout our life time, Aβ is constantly produced from the amyloid precursor protein (APP) by β- and γ-secretases [7, 8].

Currently, soluble Aβ oligomers are assumed to be the major toxic species in AD [9-11]. Aβ oligomers were shown to account for neuronal atrophy already at nanomolar concentrations, induction of synaptic dysfunction, formation of pores and thereby disturbance of cellular ion homeostasis and inhibition of long-term potentiation, altogether leading to impaired neuronal function, reduced cognition and a decline in memory [12-16]. The conversion between the different Aβ assembly states is dynamic and reversible [13, 14, 17-22]. Recent research gave rise to the fact that AD might be a prion-like disease with misfolded Aβ molecules acting as nucleation seeds and initiating aggregate formation by recruiting additional unfolded or oligomeric Aβ peptides and thereby accelerating amyloid growth [23, 24].

From the current point of view, elimination of Aβ oligomers may be the most promising therapeutic intervention to AD. Our approach was to select compounds, which modulate the dynamic equilibrium of $A\beta_{1-42}$ species towards decomposition of toxic oligomers by binding and stabilizing monomeric Aβ.

Phage display selection is suitable to identify small peptides, which bind to Aβ. The variation of phage display using the exact mirror image of the original target is called mirror image phage display. This method allows the identification of peptides that consist solely of D-enantiomeric amino acid residues [25, 26]. Such D-peptides are more protease-resistant than peptides consisting of L-enantiomeric amino acid residues and have a prolonged half-life in the body [27-30]. Additionally, D-peptides are

assumed to show lower immunogenicity even though immunogenicity levels may depend on the dose and frequency of administration [27-29, 31, 32].

Previously, we have shown that the D-peptide D3, which was derived from a mirror image phage display selection, is able to reduce the amyloid plaque load in transgenic mice and improve cognition and reduce inflammation after oral application [33, 34]. This has proven the suitability of mirror image phage display to identify highly active compounds that are stable enough for oral administration.

Here, we set out to repeat this successful strategy, but with an important modification to yield small, D-enantiomeric peptides that show increased specificity for Aβ monomers in order to stabilize them. Based on a previously described combination of selection and counterselection [35] we used D-enantiomeric $A\beta_{1-42}$ monomers as bait and added $A\beta_{1-42}$ oligomers and fibrils as counterselective agents to achieve our goal.

Materials and Methods

Peptides

Mosd1 (ysyltsyhmwvr-NH_2, all amino acids are D-enantiomers) with > 98 % purity was purchased from peptides & elephants (Potsdam, Germany). N-terminally biotinylated and non-biotinylated D-enantiomeric $A\beta_{1-42}$ was purchased from JPT (Berlin, Germany), N-terminal biotinylated L-enantiomeric $A\beta_{1-42}$ was purchased from AnaSpec (Fremont, CA, USA) and L-enantiomeric $A\beta_{1-42}$ was acquired from Bachem (Bubendorf, Switzerland).

Preparation of seedless $A\beta_{1-42}$ stock solutions

Generally, all $A\beta_{1-42}$ preparations were handled in siliconized reaction tubes with protein low binding features (Protein LoBind tubes, Eppendorf AG, Hamburg, Germany) and prepared as seedless stock

solutions as follows. $A\beta_{1-42}$ was dissolved in PTFE-filtered 1,1,1,3,3,3-Hexafluor-2-propanol (HFIP) and incubated at room temperature (RT) overnight. The HFIP was evaporated in a vacuum centrifuge at RT and additionally overnight in the open reaction tube covered with a lint-free wipe. The $A\beta_{1-42}$ film was dissolved in filtered HFIP to 1 mM, aliquoted, sealed with parafilm and frozen at -20 °C. Prior to use, HFIP was evaporated.

Separation of $A\beta_{1-42}$ species via size exclusion chromatography (SEC)

In order to obtain monomeric and oligomeric $A\beta_{1-42}$ fractions, size exclusion gel filtration chromatography was executed following an optimized protocol of Johansson *et al.* [36]. Seedless $A\beta_{1-42}$ in HFIP was dried in a vacuum centrifuge and solved in elution buffer (50 mM sodium phosphate, 150 mM NaCl, pH 7.4) to a concentration of 250 µM. After one minute vortexing, the sample was sonicated for one minute and centrifuged for 60 seconds at 16,000 x g to precipitate eventually undissolved remains. The supernatant was transferred in a syringe to a Superdex 75 10/300 GL column connected to an ÄKTA purifier FPLC chromatography system (both GE Healthcare Europe GmbH, Freiburg, Germany). Size exclusion was executed at a flow rate of 0.6 ml per minute and detection took place at 214 nm. The desired fractions were collected and pooled. $A\beta_{1-42}$ oligomers elute at about 8 ml and $A\beta_{1-42}$ monomers at approximately 14 ml.

Preparation of $A\beta_{1-42}$ samples with a broad range of different sized species

In order to gain a solution of $A\beta_{1-42}$ which resembles several toxic and nontoxic Aβ species over a broad size range, 80 µM seedless $A\beta_{1-42}$ was incubated in 10 mM sodium phosphate buffer (pH 7.4) for 4.5 hours at RT and shaking at 600 rpm.

Preparation of $A\beta_{1-42}$ fibrils

In order to gain $A\beta_{1-42}$ fibrils, seedless $A\beta_{1-42}$ was incubated at 80 µM in 10 mM sodium phosphate buffer (pH 7.4) at RT for at least 24 hours with shaking at 600 rpm. To separate the fibrils from other species, the sample was loaded onto an iodixanol density gradient as described below. Fractions containing fibrils and high molecular weight (HMW) aggregates (fractions 12-14) were used for further experiments.

Density gradient centrifugation (DGC)

In order to separate differently sized $A\beta_{1-42}$ assemblies, 100 µl of the sample were added on the top of a discontinuous gradient of iodixanol (OptiPrep, AXIS-SHIELD, Oslo, Norway) preformed by layering 260 µl of 50 % iodixanol at the bottom of a 11 x 34 mm polyallomer centrifuge tube, overlaid by 260 µl of 40 %, 260 µl of 30 %, 780 µl of 20 %, 260 µl of 10 % and 100 µl of 5 % iodixanol. The samples were spun at 260,000 x g for three hours at 4 °C in an Optima MAX-XP ultracentrifuge with a TLS-55 rotor (both Beckman Instruments, Brea, USA). After centrifugation, 14 fractions of 140 µl each were harvested with a pipette from top to bottom.

Competitive mirror image phage display

In order to obtain specifically $A\beta_{1-42}$ monomer binding species, a mirror image phage display with six panning rounds was performed. To reduce binding of phages to larger $A\beta_{1-42}$ species, $A\beta_{1-42}$ oligomers and fibrils were added, starting from round two, as counter-selective agents. Phages binding to $A\beta_{1-42}$ oligomers and fibrils were subsequently removed from the solution leading to an enrichment of phages, which exclusively bind monomeric $A\beta_{1-42}$.

The target peptide, SEC-derived monomeric, D-enantiomeric, N-terminally biotinylated $A\beta_{1-42}$, was immobilized to plates with alternating surface properties. In order to avoid selection of plastic binding

phages, different plastic surfaces were used in each subsequent round of panning (Nunc 96-well Immobilizer Streptavidin microwell plate, polystyrene (Thermo Fisher Scientific Inc., Waltham, MA, USA), polypropylene and polycarbonate microwell plates 96-well (BioTeZ Berlin Buch GmbH, Berlin, Germany)). According to the manufacturer, the polystyrene plates were pretreated by washing three times with 300 µl of 1x TBS containing 0.05 % (v/v) Tween-20 per well. Additionally, in every second round, the surface was blocked with 150 µl of 1x TBS / 0.1 % (v/v) Tween-20 / 1 % BSA (w/v) per well with gentle shaking for one hour at RT prior to the addition of the target peptide to reduce unspecific binding. Thus, no combination of plate surface and blocking was used twice during the six panning rounds performed.

One-hundred microliters of a 63 nM solution of target peptide diluted in 1x TBS per well was immobilized to the well for five minutes at RT, followed by three washing steps with 150 µl of 1x TBS.

In the first panning round 90 µl of 1x TBS were mixed with 10 µl of the Ph.D.-12 Phage Display Peptide Library (New England Biolabs GmbH, Frankfurt/M, Germany) and added to the well for five minutes of incubation at RT. The solution was removed and 100 µl of 10 µM biotin in 1x TBS / 0.1 % (v/v) Tween-20 (TBS-T) were added for five minutes incubation at RT to reduce streptavidin-binding phages. Subsequently, the well was washed four times with TBS-T.

Elution of bound phages was conducted by adding 100 µl of 0.2 M glycine-HCl (pH 2.2) for ten minutes at RT. The solution was removed and subsequently added to a fresh reaction tube with 25 µl of 1 M Tris-HCl (pH 9.1) in order to neutralize the solution. Twenty microliters of the solution were then used for phage titer determination after elution (output titer). The remaining volume was used for amplification of the eluted phages.

Determination of the output titer and phage amplification was conducted according to the distributor´s manual. Shortly, 100 µl of phage dilutions ranging from 10^{-2} to 10^{-7} were mixed with 100 µl *E. coli* K12 ER2738 cells at an optical density of 0.6. The mixture was plated together with 800 µl top agar per dilution on LB / Tet / IPTG / XGal Petri dishes (40 x 10 mm) and incubated overnight at 37 °C. The next day, plaques were counted and the titer was determined.

For phage amplification, 20 ml *E. coli* K12 ER2738 cell solution were grown to an optical density of 0.1 and incubated with the remaining volume of eluted phages (105 µl) for 4.5 hours at 37 °C and

6

160 160 rpm. After incubation, the culture was centrifuged for 20 minutes at 2,300 x g at 4 °C and 1 ml of
161 the supernatant was removed and stored at 4 °C. The remaining volume was precipitated overnight at
162 4 °C with 7 ml PEG-8000 / 2.5 M NaCl. Subsequently, the solution was centrifuged for 60 minutes at
163 3,000 x g and 4 °C whereupon the supernatant was discarded. After dissolving the pellet in 1 ml of
164 1x TBS, the sample was centrifuged for five minutes at 9,300 x g at 4 °C. The supernatant was mixed
165 with 200 µl PEG-8000 / 2.5 M NaCl, followed by 60 minutes incubation on ice and a final centrifugation
166 step for 20 minutes at 16,000 x g and 4 °C. The supernatant was removed and the pellet was
167 resuspended in 100 µl of 1x TBS. The input titer was measured analogically to the output titration with
168 dilutions ranging from 10^{-8} to 10^{-13}.

169 While the concentration of the target peptide remained stable, D-enantiomeric $A\beta_{1-42}$ oligomers and
170 high molecular weight (HMW) aggregates / fibrils without an N-terminal biotin tag were added, starting
171 from panning round two in increasing concentrations (round 2: 1 nM – round 3: 5 nM – round 4: 10 nM
172 – round 5: 50 nM – round 6: 500 nM) as explained later. $A\beta_{1-42}$ oligomers and HMW aggregates and
173 fibrils were obtained from SEC and DGC, respectively, as described above. In order to obtain $A\beta_{1-42}$
174 HMW aggregates and fibrils fractions 12, 13 and 14 from the DGC were combined. Due to the addition
175 of the competition step with $A\beta_{1-42}$ oligomers and HMW aggregates / fibrils, the protocol was adjusted
176 starting from the second panning round as follows.
177 The amplified phages from the previous round were diluted to $1x10^{11}$ phages in 60 µl of 1x TBS and
178 added to the well previously coated with SEC-derived, D-enantiomeric, N-terminally biotinylated $A\beta_{1-42}$
179 monomers. Twenty microliters of SEC-derived $A\beta_{1-42}$ oligomers and 20 µl of DGC-separated $A\beta_{1-42}$
180 HMW / fibrils, each diluted in 1x TBS to the above mentioned concentration (e.g. for the second
181 panning round 1 nM and 5 nM for panning round 3), were additionally added to the sample. After five
182 minutes of incubation at RT, the solution was removed and the procedure went on with the
183 aforementioned biotin competition step. The amount of washing steps increased with every panning
184 round (4 – 6 – 8 – 10 – 12 – 15).

185
186
187

Single phage amplification

Single plaque forming units, each representing phages grown from one single clone, were picked from the output titer plates from round three to six and added to 5 ml of a *E. coli* K12 ER2738 culture at an optical density of 0.1 grown in LB / tetracycline medium and were then amplified for 4.5 h hours at 37 °C at 160 rpm. Cultures were centrifuged for 20 minutes at 3,000 x g and 4 °C and the supernatant was removed. Two milliliters were used for DNA extraction and kept at 4 °C until usage, one milliliter was aliquoted for single phage ELISA and 0.5 ml were mixed with 0.5 ml 80 % sterile glycerin as backup and stored at -80 °C.

Single phage ELISA

The specificity and affinity of single phage clones towards the target peptide and the counterselective agents $A\beta_{1-42}$ oligomers and HMW aggregates / fibrils was analyzed by ELISA.
320 nM of SEC-derived N-terminally biotinylated D-$A\beta_{1-42}$ monomers or 320 nM SEC-derived N-terminally biotinylated D-$A\beta_{1-42}$ oligomers mixed with DGC-derived N-terminally biotinylated $A\beta_{1-42}$ HMW aggregates / fibrils were immobilized in duplicates for each single phage clone. Therefore, the total amount of $A\beta_{1-42}$ in each well was 150 ng. Amplified single phage clones from panning rounds three to six were analyzed. Additionally, the different species were immobilized to two wells each in order to check the immobilization efficiency by the Aβ-specific antibody 6E10 (Beta Amyloid 1-16 (6E10) monoclonal antibody, BioLegend, Dedham, MA, USA). Also tested were non-coated wells for each phage. Additionally, buffer was analyzed as control for cross reactivity of the anti M13:HRP conjugated antibody to the well surface and the immobilized target in duplicate.

The microtiter plates (Nunc 96-well Immobilizer Streptavidin microwell plate, Thermo Fisher Scientific Inc., Waltham, MA, USA) were pretreated as recommended by the manufacturer. The aforementioned $A\beta_{1-42}$ species were diluted in 1x TBS to 320 nM each and 100 µl per well were incubated for 15 minutes at RT with gentle shaking. After washing the wells twice with 150 µl of 1x TBS and blocking for one hour at RT with 1 % (w/v) BSA in TBS-T, the plates were washed again three times with 150 µl of TBS-T. During the blocking step, the amplified phages and the buffer control (LB

medium) were mixed with 1 % (w/v) BSA in TBS-T in a ratio of 1:1 and incubated on a shaker at RT for 20 minutes. Afterwards 100 µl of the phage suspensions, the buffer control and the first antibody solution (6E10 1:1,000 in TBS-T) were given to the wells for one hour with gentle shaking at RT. After washing the plates for five times with 150 µl of TBS-T, 200 µl of TBS-T were added to each well and the plates were incubated at RT for another hour.

The supernatant was removed and 100 µl of the antibody dilutions were added to the adequate wells for one hour at RT (mouse anti bacteriophage M13 major coat protein (p8) HRP conjugated, GE Healthcare Europe GmbH, Freiburg, Germany and goat anti mouse IgG (H+L) HRP conjugated, Thermo Fisher Scientific Inc., Rockford, IL, USA, respectively). The anti-M13 antibody was diluted 1:5,000 in TBS-T and the goat anti mouse IgG antibody was diluted 1:1,000 in the same buffer. Subsequently, the plates were washed ten times with 150 µl of TBS-T and detection was conducted by measuring the conversion of the substrate 3,3',5,5'-tetramethylbenzidine (TMB) by HRP accompanied with a color change. Therefore, 50 µl of a TMB solution (one pill TMB was dissolved in 1 ml DMSO and diluted with 9 ml sterile filtered 0.05 M phosphate citrate buffer) was added to each well and color change was stopped by adding 50 µl of 2 M H_2SO_4 when the solution in the wells started getting turquoise. The absorption at 450 nm was measured in a microplate reader. After subtraction of the buffer control, the absorption at 450 nmfor the wells coated with $A\beta_{1-42}$ oligomers and fibrils were normalized to the $A\beta_{1-42}$ content of the $A\beta_{1-42}$ monomer-coated wells as determined by 6E10.

DNA extraction for sequencing

The single stranded phage DNA was purified as described in the NEB phage display manual (Instruction manual, version 2.7) with the exception that the iodide buffer was exchanged by a 10:1 mixture of 3 M sodium acetate (pH 5.2) and TE buffer. Sequencing was conducted by GATC Biotech AG (Konstanz, Germany).

Transmission electron microscopy (TEM)

In order to analyze which $A\beta_{1-42}$ species have formed after incubation with the peptide Mosd1, TEM images were taken. Ten micromolar seedless $A\beta_{1-42}$ was incubated with or without 10 µM Mosd1 for 24 hours at RT. Twenty microliters of each sample were spotted on a formvar/carbon coated copper grid (Plano GmbH, Wetzlar, Germany) for three minutes. Afterwards the solution was detached with filter paper and the grids were washed three times with 20 µl of ddH_2O and once with 5 µl 1 % aqueous uranyl acetate. Then, 5 µl of the 1 % uranyl acetate solution was applied to the grid for one minute for negative staining. The solution was removed and grids were dried overnight. The samples were analyzed with a Libra 120 transmission electron microscope (Carl Zeiss AG, Oberkochen, Germany) operating at 120 kV.

Quantitative determination of interference with $A\beta_{1-42}$ aggregate size distribution

The density gradient centrifugation method allows matrix-free separation and fractionation of different $A\beta_{1-42}$ species according to their sedimentation coefficients which depend on size and shape.

$A\beta_{1-42}$ was incubated as mentioned above (250 µl 80 µM seedless $A\beta_{1-42}$ in 10 mM sodium phosphate buffer at pH7.4, 4.5 hours, 600 rpm, RT) in order to gain a mixture of differently sized species. In order to analyze the influence of Mosd1, co-incubation for 40 minutes at RT with different concentrations of the peptide (0 - 10 - 20 - 40 - 80 µM) followed.

One-hundredmicroliters were given on the top of a discontinuous iodixanol gradient and spun in an ultracentrifuge as described above. Fourteen fractions of 140 µl each were harvested from top to bottom after centrifugation and the residual pellet (60 µl) was mixed with 60 µl of 6 M guanidine hydrochloride and boiled for ten minutes. This sample represents the 15^{th} fraction. The samples were analyzed by RP-HPLC and Tris-tricine SDS-PAGE followed by silver staining.

Peptides were quantified via isocratic reversed-phase high performance liquid chromatography (RP-HPLC). The column used was a Zorbax SB-300-C8 on a 1260 Infinity system (both Agilent Technologies Deutschland GmbH, Böblingen, Germany). Twenty microliters of each sample were injected and run with 1 ml per minute in an aqueous 30 % (v/v) acetonitrile / 0.1 % (v/v) trifluoric acid buffer as mobile phase and 80 °C column temperature to denature Aβ species and separate them

from other components, especially iodixanol. The signal was detected at an absorbance of 214 nm. The data were recorded and peaks were integrated using the ChemStation software (Agilent Technologies). In order to calibrate the column, $A\beta_{1-42}$ solutions of known concentration were used to plot peak area versus $A\beta_{1-42}$ concentration. The plot equation then allowed calculation of $A\beta_{1-42}$ concentration within the samples.

Seeding assay (ThT)

In order to analyze the influence of Mosd1 on seeded growth of $A\beta_{1-42}$, the seeding potential of fibrillary $A\beta_{1-42}$ seeds on seedless $A\beta_{1-42}$ was monitored via Thioflavine T (ThT) fluorescence.

Seedless $A\beta_{1-42}$ (200 µM in 10 mM sodium phosphate buffer) were incubated at 37 °C and 600 rpm for three days in order to gain seeding-competent $A\beta_{1-42}$ fibrils. The sample was centrifuged at 14,000 x g for 45 minutes at 4 °C in order to sediment fibrillary $A\beta_{1-42}$ content. The supernatant was removed and the remaining $A\beta_{1-42}$ fibrils were diluted in 100 µl 10 mM sodium phosphate buffer. After sonication for two minutes, concentration was determined by RP-HPLC. $A\beta_{1-42}$ seeds were incubated with or without a fivefold molar excess of Mosd1 for additional 24 hours. The final concentrations were 1.88 µM $A\beta_{1-42}$ seeds and 9.4 µM Mosd1. The mixture of $A\beta_{1-42}$ seeds and Mosd1 was again sonicated for two minutes and added to freshly prepared seedless $A\beta_{1-42}$ (15 µM) and 20 µM ThT. Each sample was added to a 96-well microtiter plate in triplicate and progression of fluorescence values was monitored over time. The experiment was conducted independently for three times.

For each sample an asymmetric five parameter fit was used in order to determine the amplitude of relative fluorescence units and EC_{50} serving as half maximal time $t_{1/2}$. After checking for Gaussian distribution by D´Agostino-Pearson omnibus normal test, significance was determined by one-way ANOVA.

Cell viability assay (MTT reduction)

PC-12 cells (DSMZ-Deutsche Sammlung von Mikroorganismen und Zellkulturen GmbH, Braunschweig, Germany) were cultured in DMEM medium supplemented with 10 % fetal calf serum,

1 % antibiotics (Penicillin / Streptomycin) (all Sigma-Aldrich Corp., St.Louis, MO, USA) and 5 % horse serum (PAA Laboratories GmbH, Pasching, Germany) on collagen A-coated (Biochrom GmbH, Berlin, Germany) tissue culture flasks (SPL Life Sciences Co., Korea) in a humidified incubator with 5 % CO_2 at 37 °C and grown for a maximum of 15 passages. Medium was changed every two days and cells were passaged, according to their confluence, every three to five days.

PC-12 cells were seeded in clear, collagen-coated 96-well flat bottom microwell plates (Life Technologies Inc., Carlsbad, CA, USA) at a density of $1x10^4$ cells in a volume of 100 µl per well and incubated for 24 hours. $A\beta_{1-42}$ / Mosd1 mixtures were incubated as already described in the above mentioned assay for quantitative determination of interference with $A\beta_{1-42}$ aggregate size distribution. Mosd1 concentrations of 0 / 40 / 80 µM were used. From each well that contained cells 1.25 µl medium were removed and replaced with 1.25 µl of the preparations in order to gain a final concentration of 1 µM $A\beta_{1-42}$ and 0 / 1 / 0.5 µM Mosd1 in every well, respectively. Every approach was tested three times at least in quintuplicates. The plates were incubated for 24 hours in the incubator with 5 % CO_2 at 37 °C. Subsequently, 10 µl of the supernatant were taken out of every well and 10 µl of MTT reagent (Cell proliferation kit 1, Roche Diagnostics GmbH, Mannheim, Germany) were added for four hours of incubation in the incubator. Afterwards, 100 µl of solubilization reagent (Roche Diagnostics GmbH, Mannheim, Germany) were added to all wells and the plate was incubated overnight. The plate was shaken on a table shaker for five minutes to distribute the purple colored solution equally within each well and absorbance was measured at 660 nm and 570 nm with a microplate reader (POLARstar OPTIMA, BMG Labtech GmbH, Ortenberg, Germany). Reference values at 660 nm were subtracted from values for formazan absorbance (570 nm). The mean value of cell-free wells was subtracted as background. The arithmetic mean of all measurements per approach was calculated. Results are represented as the percentage of MTT reduction, assuming that the absorbance of control cells was 100 %. Cells treated with 0.1 % TritonX-100 in 10 mM sodium phosphate buffer (pH 7.4) served as control for dead cells.
After analysis for Gaussian distribution by Shapiro-Wilk test, the values were tested for significance using the Mann-Whitney *U* test.

Western blot to investigate γ-secretase inhibition

Neuro-2a cells (DSMZ, Braunschweig, Germany) and Neuro-2a cells stably transfected with human APP695 were cultured in DMEM with 10 % fetal calf serum and 1x non-essential amino acids (both Sigma-Aldrich Corp., St.Louis, MO, USA) in tissue culture flasks in a humidified incubator with 5 % CO_2 at 37 °C. Fifty thousand cells per well were seeded in 500 µl in a 24 well microwell plate for 24 hours at 37 °C and 5 % CO_2 to assure attachment to the surface. A stock solution of 1 mM Mosd1 was prepared in sterile water and the γ-secretase inhibitor DAPT was diluted to 5 mM in DMSO, respectively. The dilutions were spun at 1,000 x g for one minute prior to use. Then 0/10/100 µM Mosd1 and 1 µM DAPT were added to the cell supernatant and DMSO as well as water were tested as control. The cells were incubated at 37 °C and 5 % CO_2 for 24 hours. The cells were analyzed with a laser scanning microscope LSM 710 (Carl Zeiss AG, Oberkochen, Germany). Afterwards, the cells were washed three times with 1x PBS and lysed with 60 µl of NP-40 lysis buffer for 15 minutes. The lysates were resuspended, transferred to reaction tubes and centrifuged for five minutes at 12,000 x g. Afterwards, the supernatants were transferred to new reaction tubes and protein concentration was determined via microBCA assay.

For gel electrophoresis the lysates were adjusted to the lowest measured protein concentration. All samples were mixed with 4x Tris-tricine gel loading buffer (4 % SDS (w/v), 12 % Glycerin (v/v), 50 mM Tris, 2 % β-mercaptoethanol (v/v), 0.01 % SERVA BlueG (w/v); pH 6.8) in a ratio of 1:3 and boiled for ten minutes. Gel electrophoresis was conducted with 10 % Tris-tricine gels at a constant voltage of 120 V. The PageRuler prestained protein ladder 10 – 170 kDa (Thermo Fisher Scientific, Inc., Rockford, IL, USA) served as marker.

After gel electrophoresis, the proteins were transferred via semi-dry blotting to a PVDF membrane. Protein transfer took place at 1 A and 25 V for 30 minutes. The membrane was blocked with 5 % non-fat dry milk powder in 1x TBS-T at 4 °C overnight with gentle shaking. Subsequently, the membrane was washed three times with TBS-T at RT and gentle shaking. The primary antibody for the detection of C-terminal fragment of APP (anti-amyloid precursor protein, C-terminal (751-770) rabbit pAb, Merck KGaA, Darmstadt, Germany) was diluted 1:5,000 in TBS-T. Simultaneously, the anti-β-actin antibody (β-actin (8H10D10) mouse mAb, Cell Signaling Technology, Inc., Danvers, MA, USA) was diluted 1:1,000 in TBS-T and both antibodies were given to the membrane, which was

366 incubated overnight at 4 °C on a roller mixer, subsequently. The membrane was washed three times
367 with TBS-T and incubated with the secondary antibodies goat anti-rabbit IgG:HRP diluted 1:5,000 in
368 TBS-T and goat anti-mouse IgG:HRP diluted 1:10,000 in TBS-T (both Santa Cruz Biotechnology, Inc.,
369 Dallas, Texas, USA) for three hours at RT on a roller mixer. After three washing steps with TBS-T, the
370 membrane was incubated with the substrate for enhanced chemoluminescence (SuperSignal West
371 Dura Chemoluminescent Substrate, Thermo Fisher Scientific, Inc., Rockford, IL, USA) for five minutes
372 at RT in the dark. The signal was detected with the ChemiDoc MP gel documentation system (Bio-Rad
373 Laboratories, Inc., Hercules, CA, USA).

374

375 # Results
376

377 N-terminally biotinylated, SEC-derived $A\beta_{1-42}$ monomers were immobilized to streptavidin-coated
378 microwell plates. To avoid selection of plastic binders, different plastic surfaces were used in each
379 round. In particular, polystyrene, polypropylene and polycarbonate served as surface, alternating
380 every round. Additionally, in every second round, the surface was blocked with BSA. Due to this
381 procedure, six different combinations of blocking and surface type were used during the panning
382 rounds and not a single combination occurred twice. This step was important, because only very low
383 concentrations of $A\beta_{1-42}$ were immobilized in order to assure its monomeric state. Thus, there was a
384 substantial risk that uncoated surface may have a strong bias during selection. In the first panning
385 round, only $A\beta_{1-42}$ monomers were offered to the naïve library of phages. For the next round, amplified
386 phages from the previous round were added together with increasing concentrations of
387 non-biotinylated counterselective $A\beta_{-42}$ species (SEC-derived oligomers and DGC-derived HMW
388 aggregates and fibrils). After panning, a biotin competition step was conducted to remove phages that
389 compete with biotin. Afterwards the well was washed every round with increasing rigorand still bound
390 phages were eluted and amplified.

391 We verified the state of all used Aβ conformers by DGC followed by Tris-tricine-SDS-PAGE and silver
392 staining. SEC-derived $A\beta_{1-42}$ monomers, SEC-derived oligomers, and fibrillary $A\beta_{1-42}$ were analyzed.
393 As shown in Fig. 1, prepared monomers are indeed free of any aggregates, as only fractions 1 and 2

394 contained Aβ. Oligomers can be found predominantly in fractions 4 to 6, and in smaller amounts also
395 in neighboring fractions. Fibrils can be found in the extreme high molecular weight fractions, but
396 obviously, during the DGC run, a substantial fraction of monomers dissociated from them and can be
397 found in fractions 1 and 2.

398 Single phage clones from round three to six were amplified and sequenced. Sixteen sequences
399 occurred more than once and were therefore tested for binding to monomeric $A\beta_{1-42}$, $A\beta_{1-42}$ oligomers
400 and HMW aggregates / fibrils as well as non-coated wells in a single phage ELISA. Additionally,
401 several clones with uniquely occurring sequences and four clones from a previously conducted mirror
402 image phage display were tested. This former mirror image phage display was conducted with almost
403 identical conditions. The experimental setup differed only in two details. Firstly, the counterselective
404 $A\beta_{1-42}$ HMW aggregates and fibrils were derived from an iodixanol gradient with different iodixanol
405 concentrations (30 – 24 – 18 – 12 – 6 and 3 % iodixanol instead of 50 – 40 – 30 – 20 – 10 and 5 %).
406 Secondly, the neutralization of the eluate took place in the same well as the elution step.

407 Figure 2 shows the immobilization efficiency of different $A\beta_{1-42}$ species detected by $A\beta_{1-42}$ specific
408 antibody 6E10. On all plates used for single phage ELISA, $A\beta_{1-42}$ monomers and oligomers/fibrils were
409 immobilized in an amount which allowed normalization of the $A\beta_{1-42}$ oligomer/fibril content to the
410 content of $A\beta_{1-42}$ in $A\beta_{1-42}$ monomer-coated wells as determined by 6E10. As shown in Fig. 3, the
411 competitive mirror image phage display selection indeed yielded phages that display peptides that
412 specifically bind to $A\beta_{1-42}$ monomers as demonstrated by the strong binding to $A\beta_{1-42}$ monomer coated
413 wells and notably less binding to wells coated with $A\beta_{1-42}$ oligomers and HMW aggregates or fibrils.
414 We picked the clone with the highest signal intensity for monomeric $A\beta_{1-42}$, but also the highest
415 specificity for monomeric $A\beta_{1-42}$ as deduced from the high ratio of binding to $A\beta_{1-42}$ monomers and
416 binding to oligomeric and fibrillary $A\beta_{1-42}$. The amino acid sequence of the chosen clone 5.60 was
417 YSYLTSYHMVWR. The corresponding D-enantiomeric peptide, named Mosd1 (monomer specific
418 d-peptide 1), was synthesized from purely D-amino acids with its C-terminus amidated, and was
419 further characterized.

420

421 In order to obtain information on how Mosd1 changes $A\beta_{1-42}$ aggregation, TEM pictures were taken
422 after 24 hours incubation of $A\beta_{1-42}$ with and without an equimolar ratio of Mosd1. The $A\beta_{1-42}$ sample

15

without Mosd1 contained a mesh of fibrils. Additionally, Aβ oligomers and large aggregates (dot-like structures) were present, displaying a broad range of aggregated $A\beta_{1-42}$ species. In the sample with $A\beta_{1-42}$ and Mosd1 neither fibrils nor oligomers were observed. Instead, amorphous, unstructured aggregates were the major species found on the grid (Fig. 4).

After incubation of 80 µM $A\beta_{1-42}$ followed by coincubation with different concentrations of Mosd1 (0/10/20/40/80 µM), samples were loaded on a discontinuous iodixanol gradient and centrifuged. Fifteen fractions were harvested from top to bottom, applied to Tris-tricine SDS-PAGE and silver stained. With this experiment we were able to show that Mosd1 abolishes different $A\beta_{1-42}$ species from the sample, which contains $A\beta_{1-42}$ species of different size, ranging from monomers to fibrils and HMW aggregates.

The distribution of 80 µM $A\beta_{1-42}$, incubated for 4.5 hours without addition of Mosd1, showed a broad range of species distributed from fraction 1 to 12, representing monomers, small and large oligomers, protofibrils, fibrils and HMW aggregates [37]. The amount of $A\beta_{1-42}$ as estimated from silver staining decreased with the fraction number, indicating substantial amounts of $A\beta_{1-42}$ in form of monomers and small oligomers. The most toxic oligomers can be expected in fractions four to six [38]. The addition of Mosd1 shifted the distribution of $A\beta_{1-42}$ towards large aggregates that are non-toxic [39]. The $A\beta_{1-42}$ contents in fractions one to ten were decreased with increasing Mosd1 concentrations. We therefore conclude that Mosd1 decreased the amount of toxic $A\beta_{1-42}$ oligomers and shifted the distribution equilibrium towards non-toxic aggregates in a concentration dependent manner (Fig. 5).

Silver staining does not allow a quantitative determination of the detected species. In order to gain quantitative information about $A\beta_{1-42}$ concentrations in every fraction, samples of each fraction were applied to RP-HPLC chromatography and analyzed for their $A\beta_{1-42}$ contents (Fig. 6). The QIAD assay (quantitative determination of interference with $A\beta_{1-42}$ aggregate size distribution) widely confirmed the above described behavior of Mosd1. Most importantly, Mosd1 is able to almost completely eliminate $A\beta_{1-42}$ oligomers.

The ability of fibrillar $A\beta_{1-42}$ to turn over monomeric $A\beta_{1-42}$ into aggregation prone Aβ assemblies is one driving force of $A\beta_{1-42}$ aggregation. We therefore analyzed the impact of Mosd1 on $A\beta_{1-42}$ seeded growth via Thioflavin T (ThT) assay. Fibrillar $A\beta_{1-42}$ seeds were grown and afterwards incubated with or without Mosd1. ThT was added and the mixture was added to freshly prepared seedless $A\beta_{1-42}$. The progression of ThT fluorescence was monitored over time. Compared to freshly prepared seedless $A\beta_{1-42}$ ($t_{1/2}$ = 19.69 h), addition of fibrillary $A\beta_{1-42}$ seeds significantly reduced the time needed to increase fibrillar content ($t_{1/2}$ = 0.57 h). When fibrillary $A\beta_{1-42}$ seeds were coincubated with Mosd1 prior to addition of freshly prepared seedless $A\beta_{1-42}$, the time for the increase of fibrillary content was significantly reduced as well, yet the time for the increase was significantly longer ($t_{1/2}$ = 3.36 h) compared to the sample without Mosd1 (Fig. 7A). Furthermore, the amount of fibrillar $A\beta_{1-42}$ content in the samples, displayed by the amplitude of relative fluorescence units (Fig. 7B), did differ significantly between seedless $A\beta_{1-42}$ (set to 100 % RFU) and seedless $A\beta_{1-42}$ incubated with fibrillary $A\beta_{1-42}$ seeds (83.83 %) and fibrillary $A\beta_{1-42}$ seeds coincubated with Mosd1 (73.56 %).

In order to confirm that Mosd1 yields $A\beta_{1-42}$ species that are not toxic to cells and Mosd1 can indeed abolish the cytotoxic effect of $A\beta_{1-42}$ and rescue cell viability, an MTT assay was performed. PC-12 cells were incubated with $A\beta_{1-42}$ with or without different concentrations of Mosd1, derived from the same incubation method as mentioned above. Mosd1 without $A\beta_{1-42}$ was tested to ensure that Mosd1 itself is not toxic to the cells. TritonX-100 was used as a control for cell death. Untreated cells were set 100 % viable and all other values were normalized to this value. Incubation with 0.1 % TritonX-100 resulted in 1.6 % viable cells. The $A\beta_{1-42}$ composition led to a significantly decreased cell viability of 45 % and was therefore proven to be toxic. Mosd1 in a concentration of 1 µM did not alter MTT reduction in this assay and showed no toxic effect in PC-12 cells. When coincubated with Mosd1, the toxic effect of $A\beta_{1-42}$ was significantly decreased with increasing concentrations of Mosd1. In an equimolar ratio, 86 % of the cells stayed viable and with half the concentration of Mosd1 still 66 % of the cells were viable. Mosd1 is therefore able to rescue PC-12 cells from $A\beta_{1-42}$ induced toxicity (Fig. 8).

Neuro-2a cells, stably transfected with human APP695, develop a pathologic phenotype when compared with wild type Neuro-2a cells. Wild type Neuro-2a cells accumulate and grow protrusions between each other and appear polygonal, whereas Neuro-2a cells, which are stably transfected with human APP, appear isolated, spindle shaped and show less protrusions and cell contacts. Applied to wild type Neuro-2a cells, Mosd1 did not alter their physiological phenotype. The cells clotted and developed protrusions and appeared polygonal (Fig. 9). Added to hAPP695-transfected Neuro-2a cells, Mosd1 compensated the pathological phenotype. The cells developed connections and protrusions, grew denser and did partially clot, resembling the phenotype of wild type Neuro-2a cells. This effect is dose dependent, since higher concentrations of Mosd1 (10 and 100 µM) increased the development of cellular connections (Fig. 10).

In order to analyze whether Mosd1 influences γ-secretase activity, Neuro-2a cells, stably transfected with human APP695 were incubated with 10 and 100 µM Mosd1, respectively. The cells were lysed, lysates were separated by SDS-PAGE, blotted and the APP C-terminal fragment β (APP CTFβ) was detected by enhanced chemoluminescence. Both concentrations of Mosd1 showed no signs of γ-secretase activity inhibition, i.e. the γ-secretase substrate APP CTFβ was not accumulated as it is the case for the treatment with the γ-secretase inhibitor DAPT (Fig. 11) [40, 41].

Discussion

The competitive mirror image phage display yielded $A\beta_{1-42}$ monomer specific ligands

Our competitive mirror image phage display led to single phage clones that preferentially bind to monomeric $A\beta_{1-42}$. Sequencing of single phage clones revealed several consensus sequences which occurred multiply. Additionally, ELISA results showed an overall specificity of most single phage clones for monomeric $A\beta_{1-42}$ compared to $A\beta_{1-42}$ oligomers and fibrils and non-coated wells. Several single phage clones exhibited a very strong difference in binding affinities between monomeric and

aggregated $A\beta_{1-42}$ and also the non-coated surface. We picked the most promising clone and investigated the respective D-peptide Mosd1 for further analysis.

Mosd1 modulates $A\beta_{1-42}$ aggregation

Via TEM and quantitative determination of $A\beta_{1-42}$ aggregate distribution, we were able to show that coincubation of $A\beta_{1-42}$ with Mosd1 leads to an altered aggregation pathway of $A\beta_{1-42}$. While incubation of $A\beta_{1-42}$ alone for 24 hours led to oligomers and fibrillar structures, coincubation with Mosd1 led to large amorphous aggregates that were shown to be non-toxic [30, 39] . By combining these results with the experiment regarding interference of Mosd1 with $A\beta_{1-42}$ aggregate size distribution mentioned above, we suggest the followingmode of action. Mosd1 stabilizes $A\beta_{1-42}$ monomers and thereby modulates the dynamic equilibrium of $A\beta_{1-42}$ species. Toxic $A\beta_{1-42}$ oligomers are decomposed and the resulting $A\beta_{1-42}$ species being precipitated and converted into amorphous non-toxic aggregates instead of fibrils. According to Ladiwala *et al.*, Mosd1 can be sorted into class I molecules, which convert soluble Aβ oligomers into large, non-toxic conformers [42]. In addition, Mosd1 with 33 % residues being aromatic shares the overall aromatic features of compounds, which belong to this class. Indeed, also polyphenols like resveratrol and derivatives or polyphenolic flavones like kaempferol-3-O-rhamnoside are able to cause the development of large, non-toxic, off-pathway Aβ aggregates as shown in TEM, AFM and SDS-PAGE studies by several research groups [43, 44]. Additionally, Mosd1 is able to reduce $A\beta_{1-42}$ seeded growth which seems to be the driving force of Aβ aggregation. Therefore, Mosd1 is able to reduce the impact of already formed $A\beta_{1-42}$ seeds on monomeric $A\beta_{1-42}$ and their conversion into toxic aggregates as shown by Seeding ThT Assay.

According to cell culture experiments, the generated aggregates are not toxic to PC-12 cells, whereas, the mixture of $A\beta_{1-42}$ species not treated with Mosd1 showed significant cellular toxicity. Other compounds, which consist of aromates or include aromatic side chains, were also reported to reduce Aβ induced cell toxicity [42, 44, 45]. This might be contributed to the binding to $A\beta_{1-42}$ monomers and prevention of their aggregation as well as to the conversion of toxic oligomeric $A\beta_{1-42}$ species into large non-toxic species as shown in the latter experiments.

534 Additionally, we were able to show that human APP695 transfected Neuro-2a cells, treated with
535 Mosd1, appear healthier compared to untreated cells, which develop a pathological phenotype. Mosd1
536 is able to reverse the effects of human APP695 expression and its cleavage products like reduced cell
537 contacts and a lack of cellular protrusions.

538 Despite the fact that Mosd1 reduces $A\beta_{1-42}$ toxicity by modulating the equilibrium of $A\beta_{1-42}$ species, it
539 needs to be assured, that the compound is safe and does not interfere with related but physiological
540 relevant pathways. For example, γ-secretases are involved in the cleavage of APP, leading
541 subsequently to Aβ. Moreover, γ-secretases are also involved in cleavage of transmembrane Notch
542 and therefore interfere with Notch signaling pathways. Alterations within the Notch pathway can lead
543 to severe side effects [46, 47]. According to our results Mosd1 has no effect on γ-secretase activity.

544

545 Conclusion

546

547 Taken together, we have established a novel competitive mirror image phage display for the selection
548 of D-enantiomeric peptides, which bind specifically to monomeric $A\beta_{1-42}$. Using non-biotinylated SEC-
549 derived oligomers and DGC-derived HMW aggregates and fibrils of $A\beta_{1-42}$ as counterselective agents,
550 we were able to enrich phages, which bind specifically to the immobilized biotinylated monomeric
551 $A\beta_{1-42}$.

552 One of our selected D-enantiomeric peptides, Mosd1, shows promising characteristics in several *in*
553 *vitro* experiments. This leads to the assumption that Mosd1 is able to stabilize $A\beta_{1-42}$ monomers,
554 interferes with seeded growth and modulates $A\beta_{1-42}$ aggregation towards non-toxic, amorphous
555 aggregates and therefore rescues cells from $A\beta_{1-42}$ derived toxicity and reverses pathological
556 phenotypes from hAPP-transfected neuronal cells.

557 Mosd1 also does not affect γ-secretase function which makes it safer and more precise than
558 γ-secretase modulating compounds. Its small size should facilitate blood-brain-barrier transfer and the
559 D-enantiomeric conformation enables high proteolytic stability. Further investigations including affinity

studies and epitope mapping should provide more information about the mechanism how Mosd1 modulates $A\beta_{1-42}$.

We were able to show that a competitive mirror image phage display is a straightforward method to select compounds, which are $A\beta_{1-42}$ monomer specific and able to modulate $A\beta_{1-42}$ aggregation towards non-toxic species and therefore exhibit high therapeutic potential.

Author contributions

Conceived and designed the experiments: SR JK SAF DW.

Performed the experiments: SR ANK CS MT AE

Analyzed the data: SR JK DW

Wrote the paper: SR JK DW

Acknowledgement

We gratefully thank Dr. Charlotte E. Teunissen from the Department of Clinical Chemistry, VU University Medical Center, Amsterdam, The Netherlands for providing us with huAPP695 transfected Neuro-2a cells.

Figures

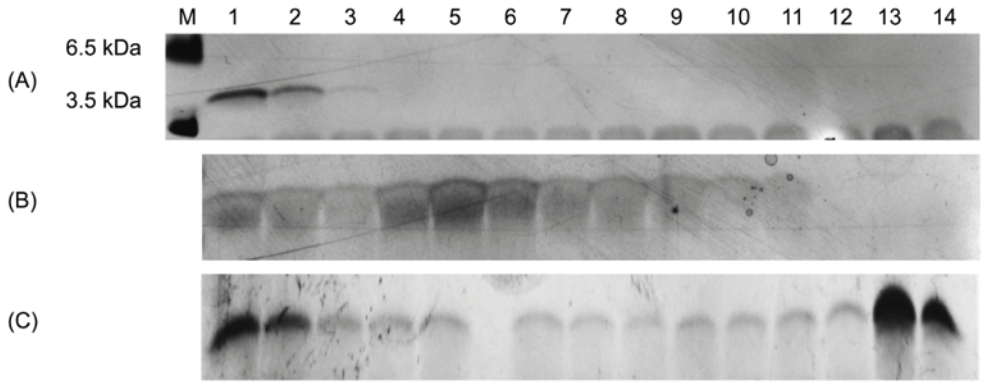

Fig 1. Silver stained Tris-Tricine-SDS-PAGE of different $A\beta_{1-42}$ species.

The $A\beta_{1-42}$ species used for panning and counter selection during mirror image phage display were analyzed via DGC followed by Tris-Tricine-SDS-PAGE and silver staining. The SEC peak corresponding with $A\beta_{1-42}$ monomers (A) presents $A\beta_{1-42}$ content only in fractions 1 to 2 of a DGC gradient and therefore represents exclusively monomeric $A\beta_{1-42}$. The SEC peak corresponding with $A\beta_{1-42}$ oligomers (B) presents mainly $A\beta_{1-42}$ in fractions 4 to 6, which is in accordance with oligomeric $A\beta_{1-42}$ species. The preparation of fibrillary $A\beta_{1-42}$ resulted in monomeric and fibrillary $A\beta_{1-42}$ content as seen in fractions 1 to 2 and 13 to 14 (C). Using only the pooled fractions 12 to 14 ensured that no monomeric $A\beta_{1-42}$ species were used as counterselective agent.

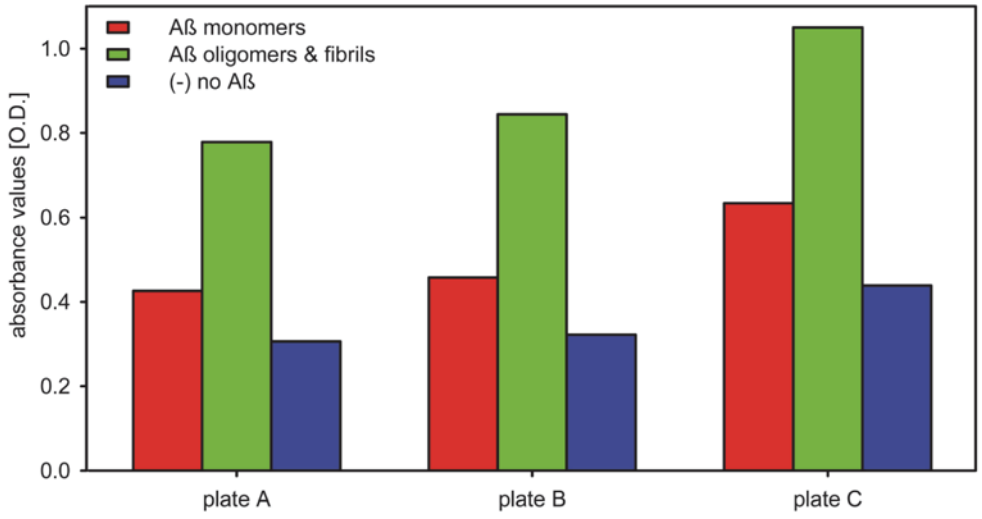

Fig 2. Single phage ELISA - immobilization control.

The immobilization efficiency of different $A\beta_{1-42}$ species was analyzed by the binding affinity of $A\beta_{1-42}$ specific antibody 6E10 to immobilized $A\beta_{1-42}$ on each plate used for single phage ELISA. The $A\beta_{1-42}$ specific antibody 6E10 was added to wells coated with 150 ng $A\beta_{1-42}$ monomers (red) or 150 ng $A\beta_{1-42}$ oligomers and fibrils (1:1; green) or to wells only coated with streptavidin (blue). Transformation of substrate by the secondary antibody-conjugated HRP was measured at 450 nm.

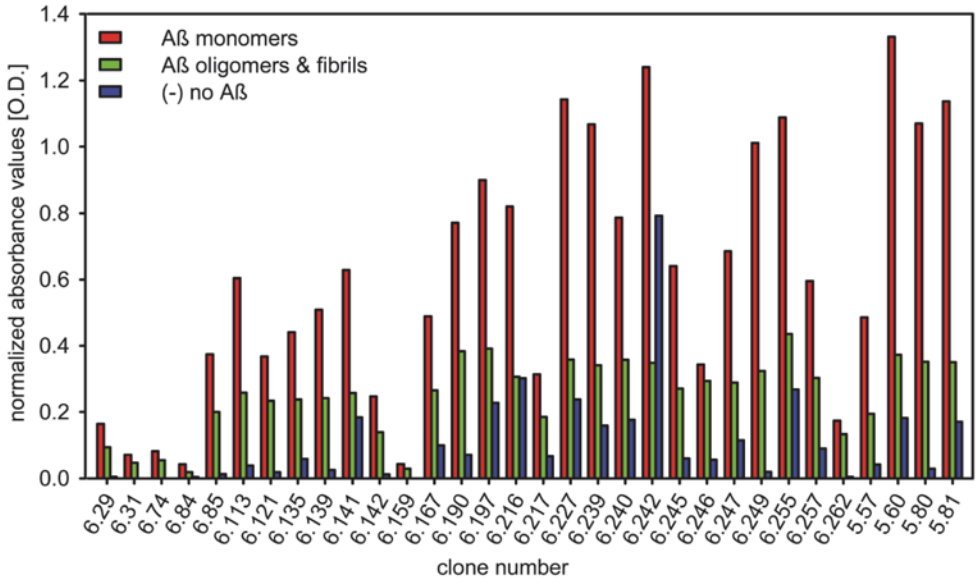

Fig 3. Single phage ELISA.

The relative binding affinity of single phage clones from mirror image phage display (clone numbers 6.xx) and a previously conducted mirror image phage display (clone numbers 5.xx) to SEC-derived biotinylated $A\beta_{1-42}$ monomers, oligomers and fibrils as well as the non-coated wells was analyzed. The M13 phage-specific antibody was used for detection. Transformation of substrate by the antibody-conjugated HRP was measured at 450 nm. Amplified single phage clones were added to wells coated with 150 ng $A\beta_{1-42}$ monomers (red) or 150 ng $A\beta_{1-42}$ oligomers and fibrils (1:1; green) or to wells only coated with streptavidin (blue). Cross reactivity of the M13 phage-specific antibody was tested in an approach without addition of phages. After background subtraction of the anti M13 antibody values, the values for phage to $A\beta_{1-42}$ oligomer/fibril binding were normalized to the values of phage to $A\beta_{1-42}$ monomer binding according to the outcome of coating efficiency controls with the Aβ specific antibody 6E10.

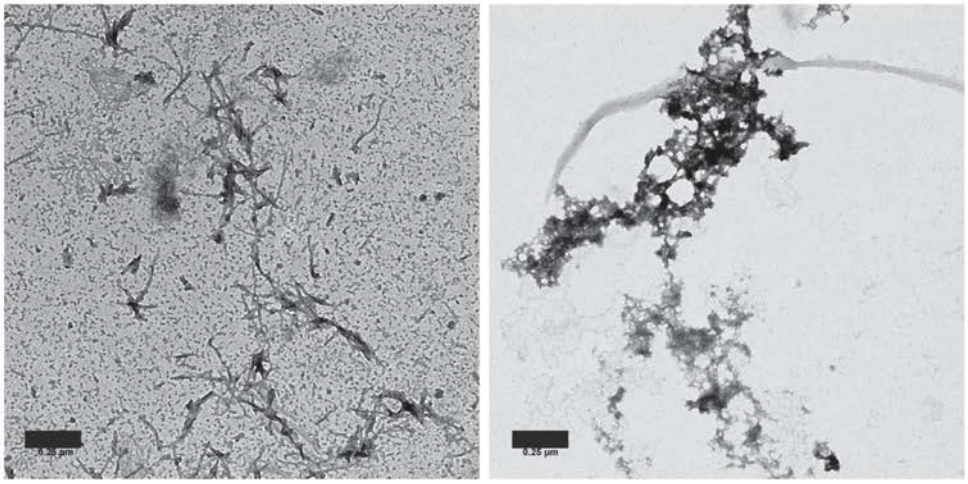

Fig 4. Transmission electron microscopy.

After incubation of 10 µM pretreated $A\beta_{1-42}$ without (left picture) and with 10 µM Mosd1 (right picture) for 24 hours at room temperature, samples were spotted onto a formvar/carbon coated copper grid and stained with 1 % aqueous uranyl acetate. Samples were analyzed with a Libra 120 TEM operating at 120 kV. Scale bar presents 0.25 µm.

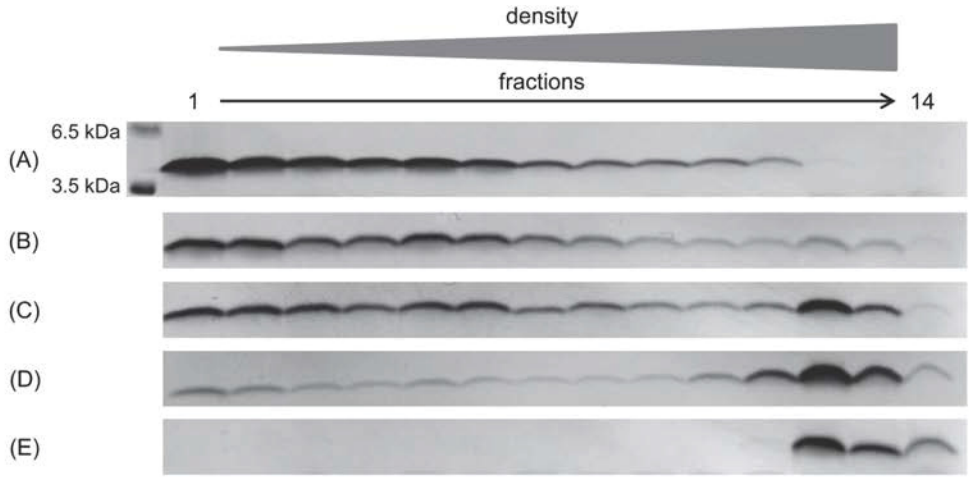

Fig 5. Qualitative $A\beta_{1-42}$ distribution alteration.

Silver staining of SDS gels after incubation of 80 µM $A\beta_{1-42}$ for 4.5 hours at RT and 600 rpm and additional coincubation for 40 minutes with 0 (A) / 10 (B) / 20 (C) / 40 (D) / 80 µM (E) Mosd1 followed by density gradient centrifugation for three hours at 4 °C at 259,000 x g. The bands display the signal for $A\beta_{1-42}$ (4.5 kDa).

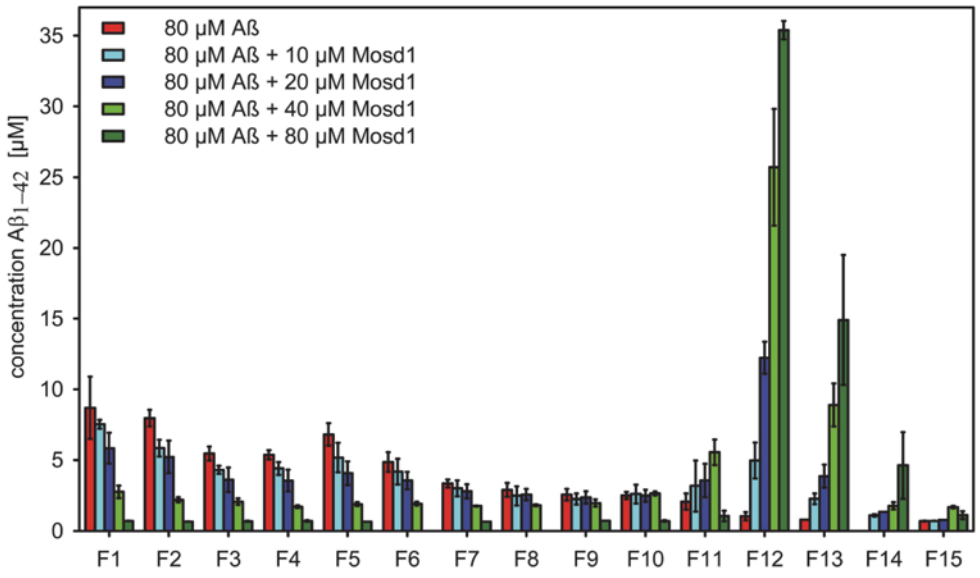

633

634 **Fig 6. Quantitative concentration determination (RP-HPLC) of $A\beta_{1-42}$ distribution.**

635 Concentrations of $A\beta_{1-42}$ in each DGC fraction were determined quantitatively via RP-HPLC. Samples
636 were loaded to a Zorbax 300SB-C8 column connected to a 1260 Infinity HPLC system. Separation of
637 the samples was achieved by elevated column temperature (80 °C) and an isocratic mobile phase of
638 30 % acetonitrile / 0.1 % TFA in water. The averaged concentration of $A\beta_{1-42}$ from three independent
639 experiments (with standard deviation) is plotted against the obtained fractions F1 to F15 of different
640 incubation approaches of $A\beta_{1-42}$ without or with Mosd1. Shown in red are the concentrations of
641 fractions from 80 µM $A\beta_{1-42}$ incubated without Mosd1. The following columns represent the $A\beta_{1-42}$
642 concentrations in the fractions from 80 µM $A\beta_{1-42}$ samples coincubated with increasing concentrations
643 of Mosd1 (10 µM = light blue; 20 µM = dark blue; 40 µM = light green; 80 µM = dark green).

644

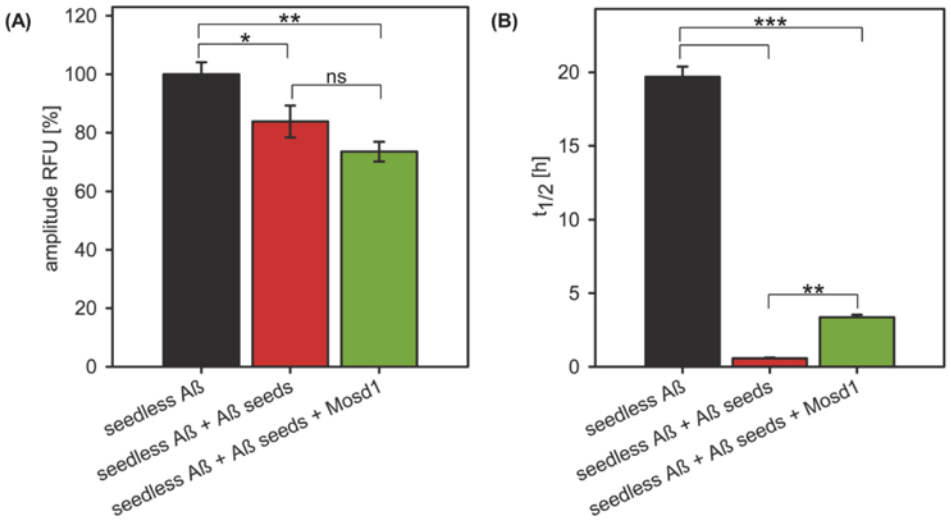

645

646 **Fig 7. Reduction of seeded $A\beta_{1-42}$ growth and fibrillar $A\beta_{1-42}$ content .**

647 Seedless $A\beta_{1-42}$ was incubated alone (black) or together with fibrillary $A\beta_{1-42}$ seeds previously
648 incubated with (green) or without (red) a fivefold molar excess of Mosd1. ThT (20 µM) was added to
649 each sample in order to measure fibrillar content. The data were fitted with an asymmetric five
650 parameter fit. The (A) amplitude of relative fluorescence (RFU) of fibrillated seedless $A\beta_{1-42}$ served as
651 100 % to which the other values were normalized. The (B) EC_{50} served as $t_{1/2}$, displaying the point in
652 time, when half of the maximum ThT signal (i.e. fibrillary content) was reached. Statistical significance
653 was determined by one-way ANOVA. Error bars display SEM. ns: $p > 0.05$; *: $p \leq 0.05$; **: $p \leq 0.01$;
654 ***: $p \leq 0.001$.

655

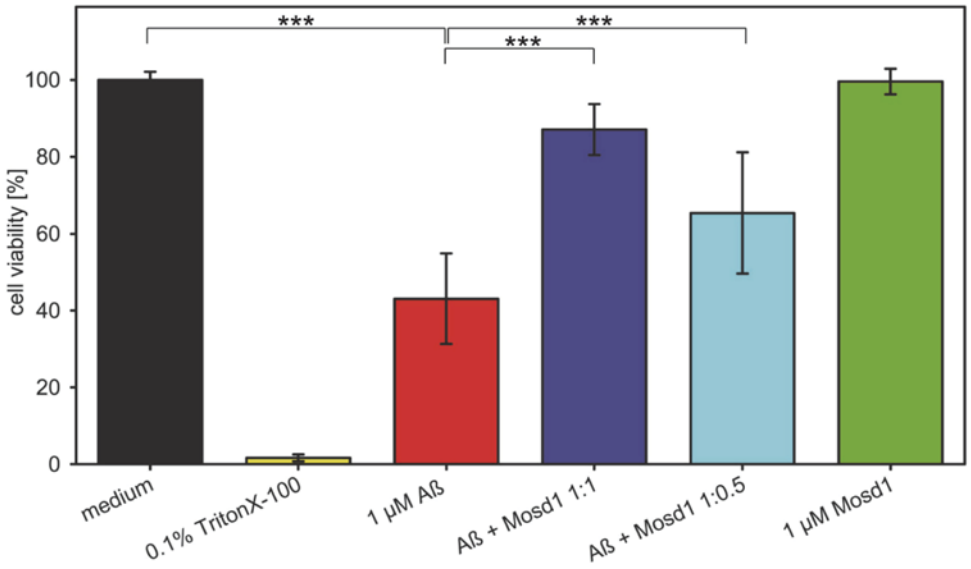

Fig 8. Effect of $A\beta_{1-42}$ and Mosd1 on cell viability.

$A\beta_{1-42}$ and Mosd1 were tested for their influence on PC-12 cell viability by MTT reduction assay. Cell viability (in percent) is plotted against different treatment conditions. Adherently grown PC-12 cells were incubated 24 hours with medium (black) or 0.1 % TritonX-100 (yellow) as controls for viable cells and cytotoxicity, respectively. Additionally, cells incubated for 24 hours with 1 µM $A\beta_{1-42}$ (red), $A\beta_{1-42}$ + Mosd1 1:1 (light blue) and 1:0.5 (dark blue), respectively. The green bar corresponds to cells incubated with 1 µM Mosd1 for 24 hours. Viability was analyzed by subsequent incubation with MTT substrate for four hours. After solubilization, absorbance was measured at 570 nm. The averages and standard deviations of absorbance values from five independently performed experiments were calculated and normalized to untreated cells (medium). Statistical significance was tested with Mann-Whitney *U* test. ***: $p \leq 0.001$.

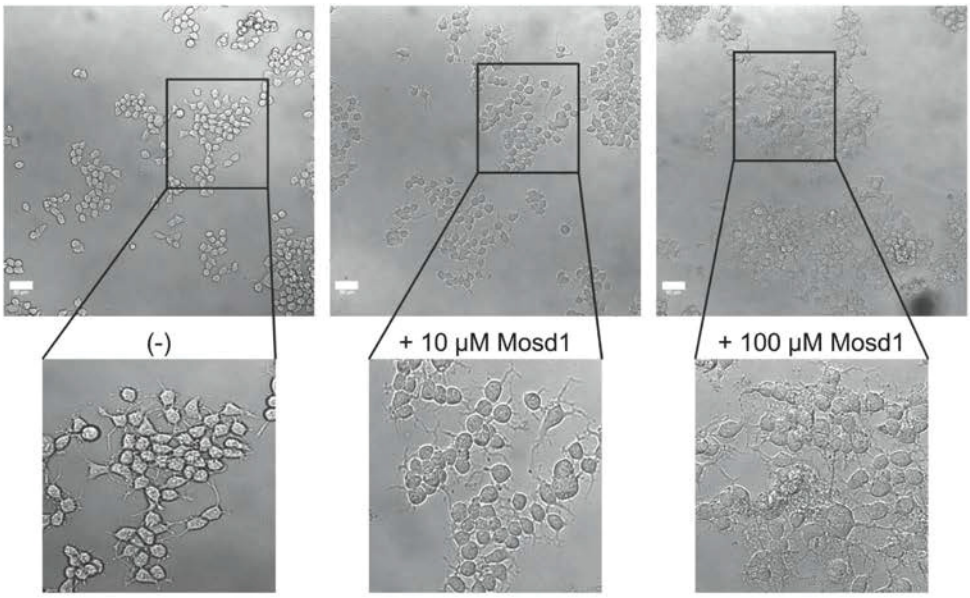

669

670 **Fig 9. Effect of Mosd1 on Neuro-2a cells.**

671 Overview and detailed pictures of wild type Neuro-2a cells are shown. Neuro-2a cells were treated
672 with 0, 10 and 100 µM of Mosd1, respectively. The left panel shows untreated wild type Neuro-2a
673 cells. In the middle and right panel, incubation of wild type Neuro-2a cells with 10 µM Mosd1 and
674 100 µM Mosd1 are shown. Cell viability and morphology were analyzed with a LSM 710 laser
675 scanning microscope. Scale bars equate 50 µm.

676

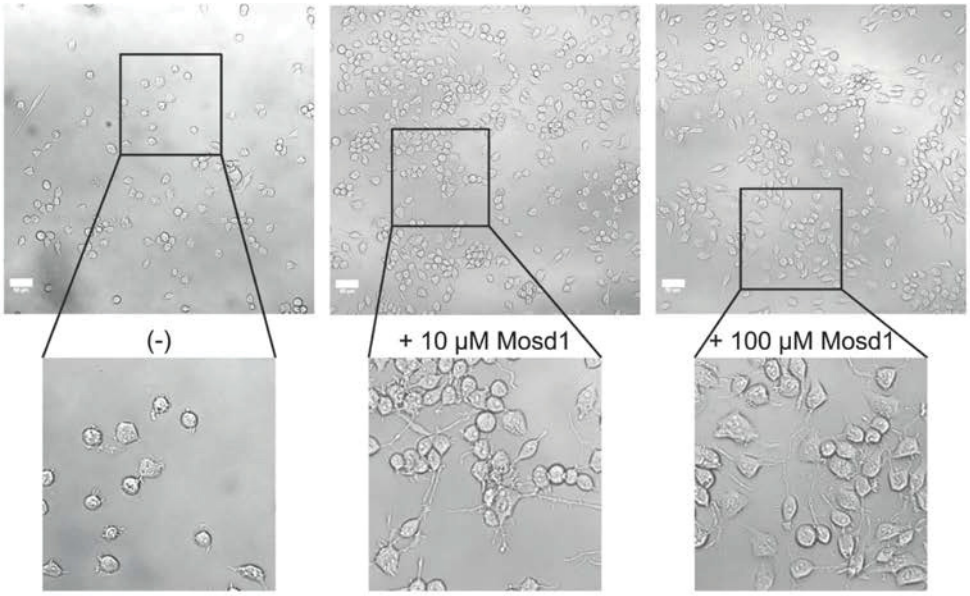

Fig 10. Effect of Mosd1 on Neuro-2a cells stably transfected with human APP695.

Overview and detailed pictures of Neuro-2a cells, stably transfected with human APP695, are shown. Cells were treated with 0, 10 and 100 µM of Mosd1, respectively. The left panel shows untreated hAPP695-transfected Neuro-2a cells. In the middle and right panel, incubation of hAPP695-transfected Neuro-2a cells with 10 µM Mosd1 and 100 µM Mosd1 are shown. Cell viability and morphology were analyzed with a LSM 710 laser scanning microscope. Scale bars equate 50 µm.

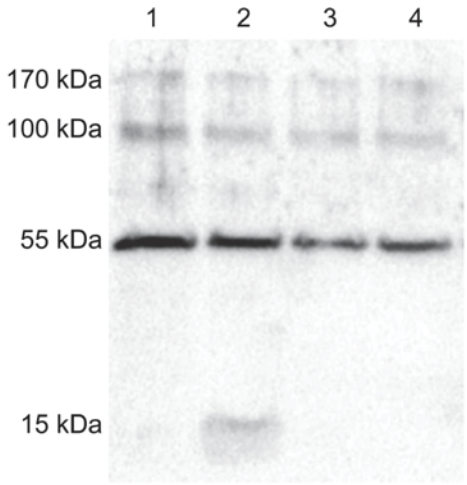

Fig 11. Analysis of potential γ-secretase activity alterations by Mosd1.

Detection of CTFβ and β-actin by enhanced chemoluminescence on a Western blot of lysed human APP695-transfected Neuro-2a cells. Human APP695-transfected Neuro-2a cells were grown in 24-well plates for 24 hours. Cells were incubated with DMSO (lane 1), DAPT (lane 2), 10 µM Mosd1 (lane 3) or 100 µM Mosd1 (lane 4) for additional 24 hours. The cells were harvested, lysed and proteins were separated by Tris-tricine SDS-PAGE. Proteins were blotted on a PVDF membrane and detected with an anti-APP-CTF antibody as well as an anti-β-actin antibody. Binding of HRP conjugated secondary antibodies was detected by transformation of enhanced chemoluminescence (ECL) substrate by HRP.

References

1. Organization, W.H., *Dementia: A Public Health Priority*. 2012: World Health Organization.
2. Querfurth, H.W. and F.M. LaFerla, *Alzheimer's disease.* N Engl J Med, 2010. **362**(4): p. 329-44.
3. Ritchie, K. and S. Lovestone, *The dementias.* Lancet, 2002. **360**(9347): p. 1759-66.
4. Bauer, J., *[Clinical diagnosis and therapeutic possibilities for dementia of the Alzheimer type].* Fortschr Neurol Psychiatr, 1994. **62**(11): p. 417-32.
5. Selkoe, D.J., *Translating cell biology into therapeutic advances in Alzheimer's disease.* Nature, 1999. **399**(6738 Suppl): p. A23-31.
6. Thal, D.R., et al., *Phases of A beta-deposition in the human brain and its relevance for the development of AD.* Neurology, 2002. **58**(12): p. 1791-800.
7. Kang, J., et al., *The precursor of Alzheimer's disease amyloid A4 protein resembles a cell-surface receptor.* Nature, 1987. **325**(6106): p. 733-6.
8. Selkoe, D.J., et al., *Beta-amyloid precursor protein of Alzheimer disease occurs as 110- to 135-kilodalton membrane-associated proteins in neural and nonneural tissues.* Proc Natl Acad Sci U S A, 1988. **85**(19): p. 7341-5.
9. McLean, C.A., et al., *Soluble pool of Abeta amyloid as a determinant of severity of neurodegeneration in Alzheimer's disease.* Ann Neurol, 1999. **46**(6): p. 860-6.
10. Haass, C. and D.J. Selkoe, *Soluble protein oligomers in neurodegeneration: lessons from the Alzheimer's amyloid beta-peptide.* Nat Rev Mol Cell Biol, 2007. **8**(2): p. 101-12.
11. Cizas, P., et al., *Size-dependent neurotoxicity of beta-amyloid oligomers.* Arch Biochem Biophys, 2010. **496**(2): p. 84-92.
12. Lambert, M.P., et al., *Diffusible, nonfibrillar ligands derived from Abeta1-42 are potent central nervous system neurotoxins.* Proc Natl Acad Sci U S A, 1998. **95**(11): p. 6448-53.
13. Zahs, K.R. and K.H. Ashe, *beta-Amyloid oligomers in aging and Alzheimer's disease.* Front Aging Neurosci, 2013. **5**: p. 28.
14. Connelly, L., et al., *Atomic force microscopy and MD simulations reveal pore-like structures of all-D-enantiomer of Alzheimer's beta-amyloid peptide: relevance to the ion channel mechanism of AD pathology.* J Phys Chem B, 2012. **116**(5): p. 1728-35.
15. Larson, M.E. and S.E. Lesne, *Soluble Abeta oligomer production and toxicity.* J Neurochem, 2012. **120 Suppl 1**: p. 125-39.
16. Wilcox, K.C., et al., *Abeta oligomer-induced synapse degeneration in Alzheimer's disease.* Cell Mol Neurobiol, 2011. **31**(6): p. 939-48.
17. Finder, V.H. and R. Glockshuber, *Amyloid-beta aggregation.* Neurodegener Dis, 2007. **4**(1): p. 13-27.
18. Shankar, G.M., et al., *Amyloid-beta protein dimers isolated directly from Alzheimer's brains impair synaptic plasticity and memory.* Nat Med, 2008. **14**(8): p. 837-42.
19. Jin, M., et al., *Soluble amyloid beta-protein dimers isolated from Alzheimer cortex directly induce Tau hyperphosphorylation and neuritic degeneration.* Proc Natl Acad Sci U S A, 2011. **108**(14): p. 5819-24.
20. Townsend, M., et al., *Effects of secreted oligomers of amyloid beta-protein on hippocampal synaptic plasticity: a potent role for trimers.* J Physiol, 2006. **572**(Pt 2): p. 477-92.
21. Lal, R., H. Lin, and A.P. Quist, *Amyloid beta ion channel: 3D structure and relevance to amyloid channel paradigm.* Biochim Biophys Acta, 2007. **1768**(8): p. 1966-75.
22. Paranjape, G.S., et al., *Amyloid-beta(1-42) protofibrils formed in modified artificial cerebrospinal fluid bind and activate microglia.* J Neuroimmune Pharmacol, 2013. **8**(1): p. 312-22.
23. Du, D., et al., *A kinetic aggregation assay allowing selective and sensitive amyloid-beta quantification in cells and tissues.* Biochemistry, 2011. **50**(10): p. 1607-17.

24. Yin, R.H., et al., *Prion-like Mechanisms in Alzheimer's Disease.* Curr Alzheimer Res, 2014. **11**(8): p. 755-64.
25. Schumacher, T.N., et al., *Identification of D-peptide ligands through mirror-image phage display.* Science, 1996. **271**(5257): p. 1854-7.
26. Wiesehan, K. and D. Willbold, *Mirror-image phage display: aiming at the mirror.* Chembiochem, 2003. **4**(9): p. 811-5.
27. Taylor, M., et al., *Development of a proteolytically stable retro-inverso peptide inhibitor of beta-amyloid oligomerization as a potential novel treatment for Alzheimer's disease.* Biochemistry, 2010. **49**(15): p. 3261-72.
28. Sela, M. and E. Zisman, *Different roles of D-amino acids in immune phenomena.* FASEB J, 1997. **11**(6): p. 449-56.
29. Tugyi, R., et al., *Partial D-amino acid substitution: Improved enzymatic stability and preserved Ab recognition of a MUC2 epitope peptide.* Proc Natl Acad Sci U S A, 2005. **102**(2): p. 413-8.
30. van Groen, T., et al., *In vitro and in vivo staining characteristics of small, fluorescent, Abeta42-binding D-enantiomeric peptides in transgenic AD mouse models.* ChemMedChem, 2009. **4**(2): p. 276-82.
31. Poduslo, J.F., et al., *Beta-sheet breaker peptide inhibitor of Alzheimer's amyloidogenesis with increased blood-brain barrier permeability and resistance to proteolytic degradation in plasma.* J Neurobiol, 1999. **39**(3): p. 371-82.
32. Van Regenmortel, M.H. and S. Muller, *D-peptides as immunogens and diagnostic reagents.* Curr Opin Biotechnol, 1998. **9**(4): p. 377-82.
33. van Groen, T., et al., *Reduction of Alzheimer's disease amyloid plaque load in transgenic mice by D3, A D-enantiomeric peptide identified by mirror image phage display.* ChemMedChem, 2008. **3**(12): p. 1848-52.
34. Funke, S.A. and D. Willbold, *Mirror image phage display--a method to generate D-peptide ligands for use in diagnostic or therapeutical applications.* Mol Biosyst, 2009. **5**(8): p. 783-6.
35. Hoffmann, S., et al., *Competitively selected protein ligands pay their increase in specificity by a decrease in affinity.* Mol Biosyst, 2010. **6**(1): p. 126-33.
36. Johansson, A.S., et al., *Physiochemical characterization of the Alzheimer's disease-related peptides A beta 1-42Arctic and A beta 1-42wt.* FEBS J, 2006. **273**(12): p. 2618-30.
37. Ward, R.V., et al., *Fractionation and characterization of oligomeric, protofibrillar and fibrillar forms of beta-amyloid peptide.* Biochem J, 2000. **348 Pt 1**: p. 137-44.
38. Rzepecki, P., et al., *Prevention of Alzheimer's disease-associated Abeta aggregation by rationally designed nonpeptidic beta-sheet ligands.* J Biol Chem, 2004. **279**(46): p. 47497-505.
39. Funke, S.A., et al., *Oral Treatment with the d-Enantiomeric Peptide D3 Improves the Pathology and Behavior of Alzheimer's Disease Transgenic Mice.* ACS Chemical Neuroscience, 2010. **1**(9): p. 639-648.
40. Zettl, H., et al., *Discovery of gamma-secretase modulators with a novel activity profile by text-based virtual screening.* ACS Chem Biol, 2012. **7**(9): p. 1488-95.
41. Sharples, R.A., et al., *Inhibition of gamma-secretase causes increased secretion of amyloid precursor protein C-terminal fragments in association with exosomes.* FASEB J, 2008. **22**(5): p. 1469-78.
42. Ladiwala, A.R., J.S. Dordick, and P.M. Tessier, *Aromatic small molecules remodel toxic soluble oligomers of amyloid beta through three independent pathways.* J Biol Chem, 2011. **286**(5): p. 3209-18.
43. Lu, C., et al., *Design, synthesis, and evaluation of resveratrol derivatives as Ass((1)-(4)(2)) aggregation inhibitors, antioxidants, and neuroprotective agents.* Bioorg Med Chem Lett, 2012. **22**(24): p. 7683-7.
44. Sharoar, M.G., et al., *Keampferol-3-O-rhamnoside abrogates amyloid beta toxicity by modulating monomers and remodeling oligomers and fibrils to non-toxic aggregates.* J Biomed Sci, 2012. **19**: p. 104.

796 45. Chemerovski-Glikman, M., M. Richman, and S. Rahimipour, *Structure-based study of*
797 *antiamyloidogenic cyclic d,l-α-peptides.* Tetrahedron, 2014. **70**(42): p. 7639-7644.
798 46. Mikulca, J.A., et al., *Potential novel targets for Alzheimer pharmacotherapy: II. Update on*
799 *secretase inhibitors and related approaches.* J Clin Pharm Ther, 2014. **39**(1): p. 25-37.
800 47. Olsauskas-Kuprys, R., A. Zlobin, and C. Osipo, *Gamma secretase inhibitors of Notch signaling.*
801 Onco Targets Ther, 2013. **6**: p. 943-55.

802

803

804

35

3.1.4. The D-amino acid peptide D3 reduces amyloid fibril boosted HIV-1 infectivity.

Publiziert in: AIDS research and therapy

Impact Factor (2015): 1.840

Eigener Anteil: 25 %

Durchführen von Größenausschlusschromatographie und Proteinkonzentrations-bestimmung. Mitverfassen der Publikation.

Widera *et al. AIDS Research and Therapy* 2014, **11**:1
http://www.aidsrestherapy.com/content/11/1/1

AIDS RESEARCH AND THERAPY

SHORT REPORT Open Access

The D-amino acid peptide D3 reduces amyloid fibril boosted HIV-1 infectivity

Marek Widera[1], Antonia Nicole Klein[2], Yeliz Cinar[2], Susanne Aileen Funke[2,4*], Dieter Willbold[2,3,5*] and Heiner Schaal[1,5*]

Abstract

Background: Amyloid fibrils such as Semen-Derived Enhancer of Viral Infection (SEVI) or amyloid-β-peptide (Aβ) enhance HIV-1 attachment and entry. Inhibitors destroying or converting those fibrils into non-amyloidogenic aggregates effectively reduce viral infectivity. Thus, they seem to be suitable as therapeutic drugs expanding the current HIV-intervening repertoire of antiretroviral compounds.

Findings: In this study, we demonstrate that the small D-amino acid peptide D3, which was investigated for therapeutic studies on Alzheimer's disease (AD), significantly reduces both SEVI and Aβ fibril boosted infectivity of HIV-1.

Conclusions: Since amyloids could play an important role in the progression of AIDS dementia complex (ADC), the treatment of HIV-1 infected individuals with D3, that inhibits Aβ fibril formation and converts preformed Aβ fibrils into non-amyloidogenic and non-fibrillar aggregates, may reduce the vulnerability of the central nervous system of HIV patients for HIV associated neurological disorders.

Keywords: HIV-1 infection, SEVI, D3, Amyloid-beta, Alzheimer's disease, D-enantiomeric peptide, Drugs, Monomers, Oligomers

Findings

Amyloid fibrils exhibiting a cationic surface [1], for example those of the Alzheimer's disease (AD) related amyloid-β peptide (Aβ) and the Semen derived Enhancer of Viral Infection (SEVI), promote HIV infection by facilitating viral attachment through neutralization of the electrostatic repulsion between the negatively charged surface of virions and target cells [2-4]. Experimental approaches to reduce SEVI-mediated enhancement of HIV-1 infection by amyloid binding agents have already been described [5-9]. However, except for epigallocatechin-3-gallate, the major active constituent of green tea, most of these compounds were shown to bind, but not to eliminate amyloids. Recently, it was demonstrated that the small D-amino acid peptide D3 converts Aβ oligomers and fibrils into non-amyloidogenic, non-fibrillar and non-toxic aggregates and reduces the cognitive deficits of the central nervous system in transgenic AD model mice [10]. Because many amyloid fibrils, despite their composition of different peptides or proteins, show significant structural similarities like a typical cross-beta sheet quaternary structure, we intended to analyze the inhibitory capacity of D3 to reduce other amyloid caused pathologic effects.

In order to utilize amyloidogenic inhibitors to reduce fibril boosted viral infectivity, we firstly wanted to unravel whether fibrils or even monomers or oligomers of Aβ are the causative agents for the infectivity enhancing effect. To achieve this, synthetic human Aβ(1–42) peptide (purity > 95%) was purchased from Bachem (Bubendorf, Switzerland). Lyophilizated Aβ(1–42) was dissolved to 1 mM with hexafluoroisopropanol (HFIP) overnight at room temperature (RT). Prior to use, HFIP was evaporated using a SpeedVac Concentrator 5301 (Eppendorf; Hamburg, Germany) at RT. For preparation of Aβ(1–42) fibrils, the Aβ pellet was dissolved in PBS (phosphate buffered saline: 140 mM NaCl, 2.7 mM KCl, 10 mM Na_2HPO_4, and 1.8 mM KH_2PO_4, pH 7.4) to 1 mM

* Correspondence: aileen.funke@hs-coburg.de; D.Willbold@fz-juelich.de; schaal@uni-duesseldorf.de
[2]Forschungszentrum Jülich, ICS-6, 52425 Jülich, Germany
[1]Institut für Virologie, Heinrich-Heine-Universität, D-40225 Düsseldorf, Germany
Full list of author information is available at the end of the article

Widera et al. AIDS Research and Therapy 2014, 11:1
http://www.aidsrestherapy.com/content/11/1/1

and incubated four days at 37°C without shaking. To remove all soluble Aβ, the samples were washed by centrifugation and redissolved in PBS. For preparation of Aβ(1–42) mono- and oligomers, the Aβ pellet was dissolved in SEC buffer (size exclusion chromatography buffer: 50 mM NaPi pH 7.4, 150 mM NaCl) and purified using size exclusion chromatography (Figure 1D). To test the different Aβ conformers for their infectivity

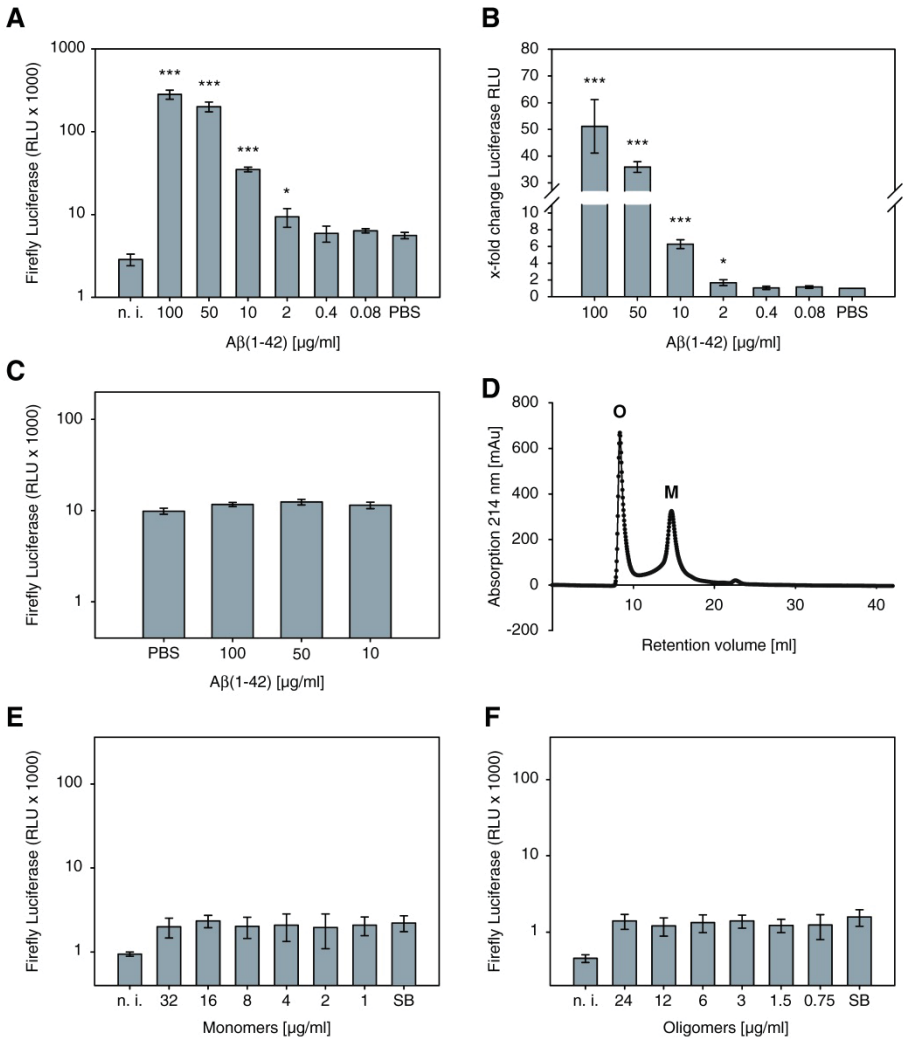

Figure 1 Aβ(1–42) fibrils but not mono- and oligomers enhance HIV-1 infection of TZM-bl cells. (A) Equal amounts (500 $TCID_{50}$ as determined with TZM-bl cells using supernatant of transfected HEK 293T cells) of the dual-tropic HIV-1 lab strain NL4-3 PI 952 [11] were pre-incubated for 5 min at RT with Aβ(1–42) fibrils. Subsequently, the pretreated viruses were used to infect TZM-bl reporter cells and infection-induced luciferase activity was assayed 48 h post infection. (*** $p < 0.001$, * $p < 0.05$ referred to PBS treated and infected cells). **(B)** X-fold change of luciferase enhancement was quantified relative to cells infected in the absence of Aβ(1–42) fibrils (PBS). **(C)** Luciferase RLUs of non-infected cells, which were treated with the indicated concentrations of Aβ(1–42). **(D)** Chromatogram of a size exclusion chromatography (SEC) showing the absorption profile of Aβ(1–42) monomers (M) and oligomers (O), which were used in the following analysis. **(E and F)** The same experiments as in **(A)** but viruses were pre-incubated with Aβ(1–42) mono- and oligomers obtained by SEC shown in **(D)**. milli-absorbance-units (mAu); non-infected (n.i.); relative light units (RLU); size exclusion chromatography buffer (SB).

enhancement potential, we used TZM-bl reporter cells that harbor a luciferase and a β-galactosidase expression cassette under the control of the HIV-1 LTR promoter, which are activated in infected cells due to expression of the HIV-1 trans-activator of transcription (Tat). These reporter cells were infected with equal amounts of the dual-tropic (R4 and R5) HIV-1 PI 952 [11] either in presence or absence of Aβ(1–42) monomers, oligomers or fibrils. For luciferase measurements, cells were rinsed in PBS and dispensed in passive lysis buffer (PLB) and shaken for 15 min at RT. Luciferase activity of cell lysates was measured by adding Beetle-Juice (p.j.k; Kleinblittersdorf, Germany) using an Infinite 200 PRO multimode reader (Tecan; Männedorf, Switzerland). We observed that Aβ(1–42) fibrils (Figure 1A and B) but not mono- or oligomers (Figure 1E and F) were able to enhance HIV-1 infection of TZM-bl cells. The enhancing effect of Aβ(1–42) fibrils on HIV-1 infectivity was observed at a concentration of 2 μg/ml and augments with increasing Aβ(1–42) fibril concentrations, whereas Aβ(1–42) fibrils alone had no effect on luciferase expression of TZM-bl cells (Figure 1C). In agreement with Münch et al. [3], but in contrast to Wojtowicz et al. [2], we did not observe any enhancing effect on HIV-1 infection when using Aβ(1–40) fibrils (Innovagen; Lund, Sweden) irrespective of whether these were incubated for four or six days of oligomerization under the same conditions as described above (Figure 2). The reason for this discrepancy was already discussed by Münch et al. arguing that amyloid fibrils composed of the same protein can show different conformations with distinct phenotypes [12].

To analyze whether the infectivity boosting effect of Aβ(1–42) but not Aβ(1–40) fibrils was cell type specific, we applied our approach also to the HIV-1 susceptible Molt-4 T cells [13,14]. Equal amounts of an R4 tropic HIV-1 NL4-3 derivate, which expresses a NEF-GFP fusion protein, were pre-incubated for 5 min at RT with Aβ(1–42) or Aβ(1–40) fibrils (10 μg/ml) and PBS as a control, respectively. Subsequently, the pre-treated viruses were used to infect Molt-4 T cells and the percentage of infected (GFP positive) cells was assayed by FACS analysis by using FACSCalibur (BD; Franklin Lakes, USA) 48 h post infection. As expected, treatment with Aβ(1–42) but not with Aβ(1–40) fibrils resulted in ~ six-fold higher percentage of GFP positive T cells when compared to PBS treated cells indicating that Aβ(1–42) specifically enhances viral infectivity also in T cells (Figure 3).

We further addressed the question of whether the boosted viral infectivity was also dependent on the membrane fusion activity of the gp41 N-terminus. Therefore, we transfected HEK 293T cells with pNL4-3 or the protease cleavage site mutant pNL Prot.Xa that prevents the Env glycoprotein mediated membrane fusion (kindly provided by Valerie Bosch) and performed immunoblot analysis of cellular as well as virion associated gp160/gp41 by using Chessie 8 antibody [15]. Virions were pelleted by using sucrose centrifugation as described before [16]. Next, we incubated TZM-bl cells with wild-type and mutant virus. By adding Aβ(1–42) fibrils, the defect in viral entry could not be restored indicating that the fibril-mediated enhancement was also dependent on the membrane fusion activity of gp41 (Figure 4).

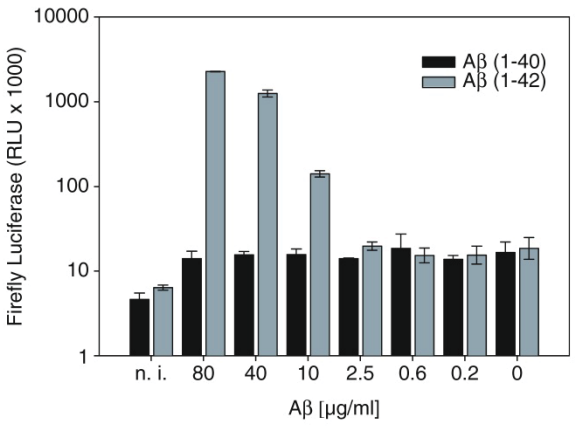

Figure 2 Aβ(1–42) but not Aβ(1–40) fibrils enhance HIV-1 infection of TZM-bl cells. Equal amounts of the dual-tropic HIV-1 lab strain NL4-3 PI 952 [11] were pre-incubated for 5 min at RT with the indicated concentrations of Aβ(1–42) or Aβ(1–40) fibrils, which were incubated for four and six days, respectively of oligomerization. Subsequently, the pretreated viruses were used to infect TZM-bl reporter cells and infection-induced luciferase activity was assayed 48 h post infection.

Widera *et al. AIDS Research and Therapy* 2014, **11**:1
http://www.aidsrestherapy.com/content/11/1/1

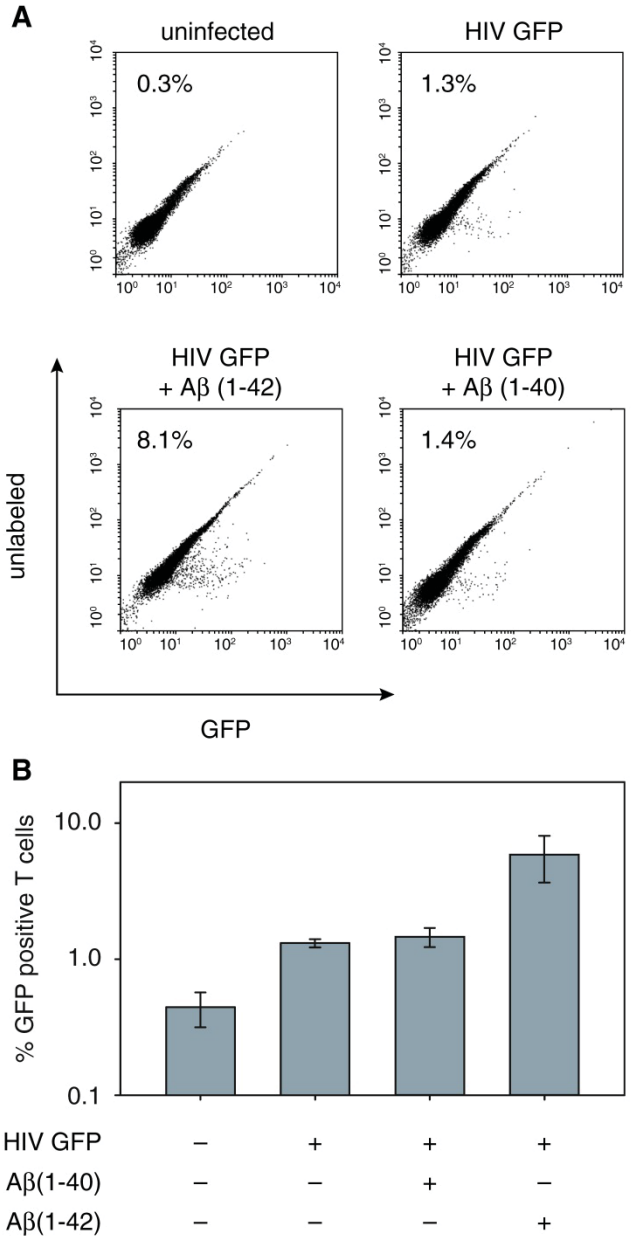

Figure 3 Aβ(1–42) peptide boosted infectivity of Molt-4 T cells. (A) Equal amounts of the R4 tropic HIV-1 NL4-3 lab strain expressing a NEF-GFP fusion protein were pre-incubated for 5 min at RT with PBS only, Aβ(1–40) or Aβ(1–42) fibrils [10 μg/ml]. Subsequently, Molt-4 T cells were infected with the pre-treated viruses and the percentage of HIV-1 infected (GFP positive) cells was assayed by FACS analysis 48 h post infection. **(B)** The percentage of HIV-1 infected (GFP positive) cells.

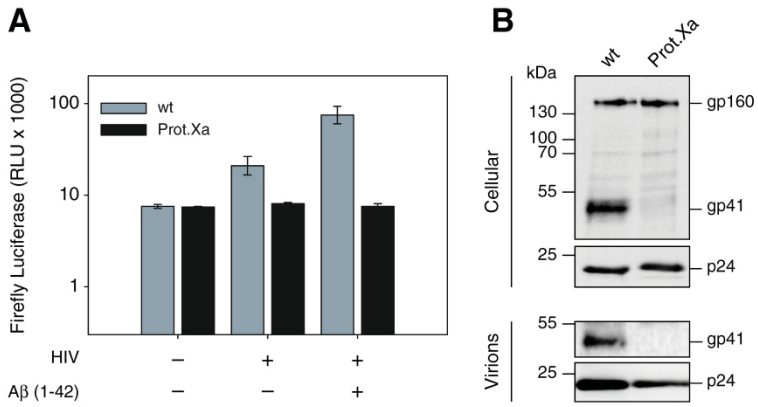

Figure 4 The fibril-mediated enhancement of HIV-1 infectivity is dependent on the membrane fusion activity of gp41. (A) TZM-bl cells were infected with R4 tropic HIV-1 strain NL4-3 (wt) or protease cleavage site mutant derivate (Prot.Xa), which were pre-incubated for 5 min at RT with Aβ(1–42) fibrils (50 μg/ml). Infection-induced luciferase activity was assayed 48 h post infection. **(B)** Immunoblot analysis of HEK 293T cells transfected with pNL4-3 or the protease cleavage site mutant pNL Prot.Xa by using Chessie 8 antibody (NIH) for gp160/gp41 analysis [15] and the p24 specific antibody (D7320, Aalto Bioreagents Ltd. Dublin, Ireland) for capsid protein detection. Virions were pelleted by using sucrose centrifugation as described before [16].

We next examined whether the peptide boosted enhancement can be reduced by pre-treatment with the non-cytotoxic Aβ fibril inhibitor D3 [17] (JPT; Berlin, Germany), which is a D-enantiomeric peptide (RPRTRLHTHRNR). SEVI and Aβ(1–42) fibrils (10 μg/ml) were pre-treated with D3 and the mixture was used to boost the infection of TZM-bl cells as described above. Following an incubation time of 48 h, the infectivity was determined by luciferase measurement and X-Gal staining (Figure 5). While SEVI and Aβ(1–42) fibrils were able to boost viral infection at similar amounts, already equimolar doses of D3 (10 μg/ml) were sufficient to significantly reduce the enhancing effect of SEVI (Figure 5A and 5C). By adding higher amounts of D3 (100 μg/ml), luciferase expression was further reduced to levels comparable with PBS treated control samples (Figure 5A, 5C and 5F). Similarly, the Aβ(1–42) boosted infection could be reduced. By adding ten-fold higher concentration of the inhibitor D3 (100 μg/ml), the infection rate of Aβ(1–42) boosted virions was significantly reduced to levels of PBS treated viruses (Figure 5B, 5D and 5F). To further control whether the reducing effect of D3 on fibril boosted infectivity was indeed due to the fibril-D3 interaction, we also pre-incubated virus containing supernatants with D3 in the absence of fibrils and then infected TZM-bl cells. As shown in Figure 5E, when infected in the absence of fibrils the cellular luciferase activity was not affected.

HIV-1 entry in female mucosa is restricted and requires overcoming at least three hurdles. These are to breach the mucosal barrier and get through the epithelium, infection and replication in sub-epithelial mononuclear cells and the initiation of a systemic infection in the lymph nodes [18]. Since genital mononuclear cells, including dendritic cells (DCs), macrophages and lymphocytes are susceptible to HIV-1 *in vivo* [18], amyloid fibrils might help HIV-1 to penetrate the mucosa and to reach these cells. Thus, treatment with D3 could inhibit the first sub-epithelial contact and prevent viral spreading.

In addition to its activity to enhance the infectivity of HIV-1 in semen, amyloids could play an important role in the progression of AIDS dementia complex (ADC) also known as HIV encephalopathy, which develops in between 20% and 30% of HIV patients in the course of infection. Interestingly, the formation of Aβ aggregates and fibrils is thought to precede the clinical symptoms of AD by three to four decades, and such fibrils may therefore be present in many mid-aged people. Since, the D-amino acid peptide D3 drastically reduces plaque load [17] and cognitive deficits even in orally D3 treated AD transgenic mice [10], it might be suitable to additionally reduce the fibril boosted HIV-1 infectivity *in vivo*.

In conclusion, the application of D3 may reduce SEVI-induced enhancement of viral infectivity of HIV-1 and the vulnerability of the central nervous system of HIV infected individuals. Thus, D3 seems to be suitable as therapeutic and prophylactic drug expanding the current HIV-intervening repertoire of antiretroviral compounds.

Widera et al. AIDS Research and Therapy 2014, 11:1
http://www.aidsrestherapy.com/content/11/1/1

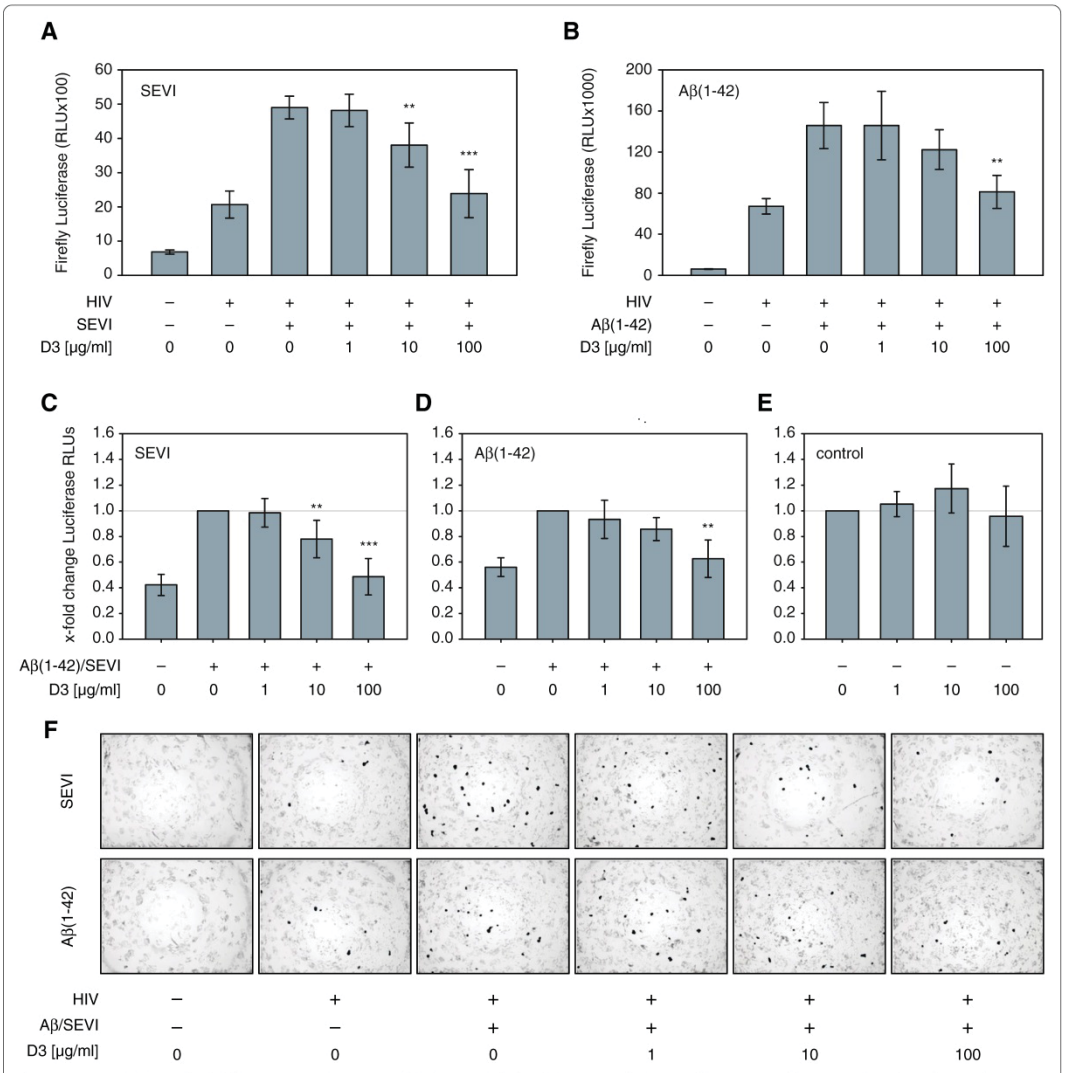

Figure 5 Amyloidogenic inhibitor D3 reduces peptide boosted infectivity. (A and B) TZM-bl reporter cells were infected with equal amounts of the dual-tropic HIV-1 lab strain NL4-3 PI 952 [11] in the presence of 10 μg/ml SEVI **(A)** or Aβ(1–42) fibrils **(B)**. As indicated, the fibrils were preincubated with D3 (0, 1, 10 or 100 μg/ml) prior to infection. Luciferase activity of infected cells was assayed 48 h post infection. **(C and D)** X-fold change Luciferase RLUs from **(A and B)**. **(E)** X-fold change Luciferase RLUs of infected TZM-bl cells, which were infected with viruses that were treated with D3 in the absence of fibrils at the indicated concentrations. **(F)** X-Gal staining of TZM-bl reporter cells that were infected as described above **(A and B)**. (*** $p < 0.001$, ** $p < 0.01$ referred to fibril treated and infected cells).

Abbreviations
Aβ: Amyloid-beta; CA: Capsid; ELISA: Enzyme-linked immunosorbent assay; FACS: Fluorescence activated cell sorting; GFP: Green fluorescent protein; HIV-1: Human immunodeficiency virus type 1; PBS: Phosphate buffered saline; PLB: Passive lysis buffer; RLU: Relative light units; SEC: Size exclusion chromatography; SEVI: Semen-derived enhancer of virus infection.

Competing interests
The authors declare that we have applied for a patent related to the content of this manuscript.

Authors' contributions
MW conceived, designed, and performed HIV-related infection and readout experiments, performed the statistical analysis and drafted the manuscript. AK carried out fibril preperations. YC carried out fibril preperations. AF conceived the study, and participated in its design and coordination and helped to draft the manuscript. DW conceived the study, and participated in its design and coordination and helped to draft the manuscript. HS conceived the study, and participated in its design and coordination and helped to draft the manuscript. All authors read and approved the final manuscript.

Acknowledgements
These studies were supported, in part, by the DFG (SCHA 909/3-1), the Stiftung für AIDS-Forschung, Düsseldorf (H.S.), BMBF-Kompetenznetz Degenerative Demenzen (KNDD FKZ 01GI1010A, D.W.), DFG Graduate School 1033 (S.F., D.W.) and Jürgen Manchot Stiftung (M.W., H.S., D.W.). The following reagents were obtained through the NIH AIDS Reagent Program, Division of AIDS, NIAID, NIH: TZM-bl cells from Drs. John C. Kappes, Dr. Xiaoyun Wu and Tranzyme Inc., Chessie 8 from Dr. George Lewis [17] and Molt-4 Clone 8 from Dr. Ronald Desrosiers. We thank Dr. Michael Schreiber for providing pNL4-3 PI 952 [11] and Dr. Valerie Bosch for pNL4-3-GFP. We also thank Dr. Jan Münch for providing SEVI-fibrils.

Author details
[1]Institut für Virologie, Heinrich-Heine-Universität, D-40225 Düsseldorf, Germany. [2]Forschungszentrum Jülich, ICS-6, 52425 Jülich, Germany. [3]Institut für Physikalische Biologie, Heinrich-Heine-Universität, 40225 Düsseldorf, Germany. [4]Bioanalytik, Fakultät für Angewandte Naturwissenschaften, Hochschule für Angewandte Wissenschaften Coburg, 96450 Coburg, Germany. [5]Biologisch und Medizinisches Forschungszentrum (BMFZ), Heinrich-Heine-Universität Düsseldorf, Düsseldorf, Germany.

Received: 24 July 2013 Accepted: 9 January 2014
Published: 14 January 2014

References

1. Luhrs T, Ritter C, Adrian M, Riek-Loher D, Bohrmann B, Dobeli H, Schubert D, Riek R: **3D structure of Alzheimer's amyloid-beta(1–42) fibrils.** *Proc Natl Acad Sci USA* 2005, **102:**17342–17347.
2. Wojtowicz WM, Farzan M, Joyal JL, Carter K, Babcock GJ, Israel DI, Sodroski J, Mirzabekov T: **Stimulation of enveloped virus infection by beta-amyloid fibrils.** *J Biol Chem* 2002, **277:**35019–35024.
3. Munch J, Rucker E, Standker L, Adermann K, Goffinet C, Schindler M, Wildum S, Chinnadurai R, Rajan D, Specht A, *et al*: **Semen-derived amyloid fibrils drastically enhance HIV infection.** *Cell* 2007, **131:**1059–1071.
4. Roan NR, Munch J, Arhel N, Mothes W, Neidleman J, Kobayashi A, Smith-McCune K, Kirchhoff F, Greene WC: **The cationic properties of SEVI underlie its ability to enhance human immunodeficiency virus infection.** *J Virol* 2009, **83:**73–80.
5. Capule CC, Brown C, Olsen JS, Dewhurst S, Yang J: **Oligovalent amyloid-binding agents reduce SEVI-mediated enhancement of HIV-1 infection.** *J Am Chem Soc* 2012, **134:**905–908.
6. Olsen JS, Brown C, Capule CC, Rubinshtein M, Doran TM, Srivastava RK, Feng C, Nilsson BL, Yang J, Dewhurst S: **Amyloid-binding small molecules efficiently block SEVI (semen-derived enhancer of virus infection)- and semen-mediated enhancement of HIV-1 infection.** *J Biol Chem* 2010, **285:**35488–35496.
7. Hauber I, Hohenberg H, Holstermann B, Hunstein W, Hauber J: **The main green tea polyphenol epigallocatechin-3-gallate counteracts semen-mediated enhancement of HIV infection.** *Proc Natl Acad Sci USA* 2009, **106:**9033–9038.
8. Sievers SA, Karanicolas J, Chang HW, Zhao A, Jiang L, Zirafi O, Stevens JT, Munch J, Baker D, Eisenberg D: **Structure-based design of non-natural amino-acid inhibitors of amyloid fibril formation.** *Nature* 2011, **475:**96–100.
9. Roan NR, Sowinski S, Munch J, Kirchhoff F, Greene WC: **Aminoquinoline surfen inhibits the action of SEVI (semen-derived enhancer of viral infection).** *J Biol Chem* 2010, **285:**1861–1869.
10. Funke AS, van Groen T, Kadish I, Bartnik D, Nagel-Steger L, Brener O, Sehl T, Batra-Safferling R, Moriscot C, Schoehn G, *et al*: **Oral treatment with the d-enantiomeric peptide D3 improves the pathology and behavior of Alzheimer's disease transgenic mice.** *ACS Chem Neurosci* 2010, **1:**639–648.
11. Polzer S, Dittmar MT, Schmitz H, Schreiber M: **The N-linked glycan g15 within the V3 loop of the HIV-1 external glycoprotein gp120 affects coreceptor usage, cellular tropism, and neutralization.** *Virology* 2002, **304:**70–80.
12. Chien P, Weissman JS, DePace AH: **Emerging principles of conformation-based prion inheritance.** *Annu Rev Biochem* 2004, **73:**617–656.
13. Daniel MD, Li Y, Naidu YM, Durda PJ, Schmidt DK, Troup CD, Silva DP, MacKey JJ, Kestler HW 3rd, Sehgal PK, *et al*: **Simian immunodeficiency virus from African green monkeys.** *J Virol* 1988, **62:**4123–4128.
14. Kikukawa R, Koyanagi Y, Harada S, Kobayashi N, Hatanaka M, Yamamoto N: **Differential susceptibility to the acquired immunodeficiency syndrome retrovirus in cloned cells of human leukemic T-cell line Molt-4.** *J Virol* 1986, **57:**1159–1162.
15. Abacioglu YH, Fouts TR, Laman JD, Claassen E, Pincus SH, Moore JP, Roby CA, Kamin-Lewis R, Lewis GK: **Epitope mapping and topology of baculovirus-expressed HIV-1 gp160 determined with a panel of murine monoclonal antibodies.** *AIDS Res Hum Retroviruses* 1994, **10:**371–381.
16. Widera M, Erkelenz S, Hillebrand F, Krikoni A, Widera D, Kaisers W, Deenen R, Gombert M, Dellen R, Pfeiffer T, *et al*: **An intronic G run within HIV-1 intron 2 is critical for splicing regulation of vif mRNA.** *J Virol* 2013, **87:**2707–2720.
17. van Groen T, Wiesehan K, Funke SA, Kadish I, Nagel-Steger L, Willbold D: **Reduction of Alzheimer's disease amyloid plaque load in transgenic mice by D3, A D-enantiomeric peptide identified by mirror image phage display.** *Chem Med Chem* 2008, **3:**1848–1852.
18. Shen R, Richter HE, Smith PD: **Early HIV-1 target cells in human vaginal and ectocervical mucosa.** *Am J Reprod Immunol* 2011, **65:**261–267.

doi:10.1186/1742-6405-11-1
Cite this article as: Widera *et al.*: The D-amino acid peptide D3 reduces amyloid fibril boosted HIV-1 infectivity. *AIDS Research and Therapy* 2014 **11**:1.

4. Diskussion und Zusammenfassung

Inhalt der hier vorgelegten Arbeit ist die Entwicklung und Optimierung potentiell therapeutisch aktiver D-Peptide für die Behandlung der Alzheimerschen Demenz (AD).

In **Kapitel 1** wurde ein genereller Überblick über die Alzheimersche Demenz (AD) und die therapeutischen Strategien gegeben. Laut Prognosen wird die Anzahl der an Demenz erkrankten Personen von über 36 Mio. im Jahr 2010 auf über 115 Mio. bis 2050 ansteigen. Zurzeit gibt es weder eine zweifelsfreie Diagnose noch eine kausale Therapie für die AD. Der Auslöser der AD ist eine Mutation oder ein bisher unbekannter Auslöser, in Folge dessen es zu Fehlfaltungen und zur Selbstaggregation des Amyloid-β-Peptides (Aβ) kommt. Aβ-Oligomere haben pathologische Effekte auf den menschlichen Organismus, die schlussendlich zur AD führen. Bereits vor Beginn dieser Arbeit wurde an der Entwicklung eines Wirkstoff-Kandidaten, der toxische Aβ-Oligomere eliminiert, geforscht. Hierbei wurde mittels Spiegelbild-Phagendisplay das D-enantiomere Peptid D3 entdeckt. D3 (rprtrlhthrnr-NH_2) und einige D3-Derivate entfernen Aβ-Oligomere *in vitro* ohne den Anteil an physiologisch relevanten Aβ-Monomeren zu beeinflussen, reduzieren die Aβ-induzierte Zytotoxizität und wandeln vorgeformte Aβ-Aggregate in amorphe Aggregate um. In verschiedenen AD Mausmodellen konnte ein positiver Effekt auf die Kognition und die inflammatorische Zellantwort durch D3 erzielt werden.

Das Hauptziel dieser Arbeit war es systematisch die Aminosäuresequenz von D3 hinsichtlich seiner *in vitro* Effektivität zu optimieren. Es wurden Optimierungen zum einen bezüglich der Affinität der D3-Derivate an HFIP-vorbehandeltes Aβ, bestehend aus Aβ-Monomeren und -Oligomeren (**Kapitel 3.1.1**), und zum anderen bezügliche der Affinität und Spezifität gegen Aβ-Monomere (**Kapitel 3.1.2**) durchgeführt. Diese neu selektierten D3-Derivate sollen Aβ-Monomere binden, sie dadurch stabilisieren und somit die Selbstaggregation von Aβ verhindern. Für die Selektion der optimierten D3-Derivate wurde eine Zwei-Schritt-Prozedur unter Verwendung von Peptid-Mikroarrays etabliert.

Als erster Schritt wurde die Interaktion zwischen verschiedenen D3-Derivaten und HFIP-vorbehandeltem Aβ mit Hilfe von Peptid-Mikroarrays untersucht

(**Kapitel 3.1.1)**. Jedes der verwendeten D3-Derivate entstand durch Austausch einer Aminosäure an einer Position der Aminosäuresequenz von D3 gegen alle anderen 19 Aminosäuren. In **Kapitel 3.1.1** wurde die Optimierung von D3 bezogen auf die Affinität an HFIP-vorbehandeltem Aβ mit Hilfe eines Peptid-Mikroarrays untersucht. Die Messung der Aβ-Peptid-Interaktion erfolgte bei diesem Peptid-Mikroarray über einen Aβ spezifischen Antikörper und einen sekundären Meerrettichperoxidase-konjugierten Antikörper. Vielversprechende Aminosäureaustausche wurden in einem zweiten Schritt miteinander kombiniert und die entstandenen D3-Derivate hinsichtlich ihrer Affinität zu HFIP-vorbehandelten und mit Fluoresceinisothiocyanat (FITC) markiertem Aβ untersucht. Die Messung der FITC-Aβ-Peptid-Interaktion erfolgte in diesem zweiten Schritt über das Fluorochrom FITC. Fünf Peptide, genannt DB1 bis DB5, wurden aufgrund ihrer gemessenen hohen Affinität zu den eingesetzten Aβ-Spezies selektiert. Innerhalb der Aminosäuresequenz von den D3-Derivaten DB1 bis DB5 wurden zwei bis vier Aminosäuren im Vergleich zum Ursprungspeptid D3 ausgetauscht. Folgende Aminosäuren wurden in verschiedenen Kombinationen ausgetauscht: Arg3Ile, Arg5Thr, His7Gln, His7Arg His9Asp, Arg10Gln und Arg10Glu. Die DB-Peptide mit Ausnahme von DB4 besitzen im Vergleich zu D3 eine bis drei positiven Ladungen weniger. DB2 bis DB5 besitzen mindestens eine aromatische Aminosäure.

DB3 (rpitrlrthqnr-NH_2) und ein C- an N-terminal (*head-to-tail*) verknüpftes Tandempeptid DB3DB3 (rpitrlrthqnrrpitrlrthqnr-NH_2) wurden detailliert *in vitro* charakterisiert. Dabei wurden folgende Methoden verwendet: Thioflavin T (ThT)-Assay, Oberflächenplasmonenresonanzspektroskopie (SPR), ein Aβ-Aggregationsinhibierungs- und ein Aβ-Disassemblierungs-*enzyme-linked immunosorbent assay* (ELISA), ein Assay zur quantitativen Bestimmung des Einflusses der D-Peptide auf die Größenverteilung von Aβ Aggregaten (QIAD), 3-(4,5-Dimethylthiazol-2-yl)-2,5-diphenyltetrazoliumbromid (MTT) Zytotoxizitäts-assay und Transmissionenelektronenmikroskopie (TEM). Mittels SPR wurde einer Affinität von DB3 an monomeres Aβ mit einem K_D von 422 µM und an oligomeres Aβ mit einem K_D von 375 µM gemessen. DB3DB3 bindet dagegen mit einem K_D von 10 µM an monomeres Aβ und einem K_D von 11 µM an oligomeres Aβ. Die Aβ-Fibrillenaggregation wird mit einer mittleren effektiven Konzentration

(EC_{50}) von 6 µM durch DB3 bzw. 7 nM durch DB3DB3 inhibiert. Bei der Koinkubation von 80 µM Aβ mit 20 µM DB3 bzw. 10 µM DB3DB3 werden 28 % bzw. 82 % der Aβ-Oligomere durch DB3 bzw. DB3DB3 eliminiert. Des Weiteren wird die Aβ-induzierte Zytotoxizität um 3 % bzw. 36 % bei fünffachem Peptidüberschuss im Vergleich zu Aβ reduziert. Mittels Aβ-Aggregat Dissassemblierungs-ELISA konnte gezeigt werden, dass vorgeformte Aβ-Aggregate durch DB3 und DB3DB3 zerstört werden. Für DB3 konnte hierfür eine EC_{50} von 2.5 µM bestimmt werden, für DB3DB3 war hier keine Bestimmung mögliche (s. Kapitel **3.1.1**). Es wird deutlich, dass die therapeutische Effektivität mit dem Tandempeptid DB3DB3 im Vergleich zu DB3 um ein vielfaches verstärkt werden konnte, z. B. bei einer 40 x erhöhten Affinität gegen monomeres und oligomeres Aβ und einer 750 x niedrigeren EC_{50} der Aβ-Aggregationsinhibierung. Der höhere Wirkungsgrad von DB3DB3 im Vergleich zu DB3 kommt vermutlich durch Aviditätseffekte zustande.

In einer weiteren Optimierung wurde die Aminosäuresequenz von D3-Derivaten hinsichtlich ihrer spezifischen Bindung an Aβ-Monomere verändert **(Kapitel 3.1.2)**. Dafür wurde die etablierte Peptid-Mikroarray-Prozedur modifiziert. Die Aminosäureaustausche wurden, um die Sequenzvariabilität zu steigern, zusätzlich zu den 18 natürlichen Aminosäuren (alle mit Ausnahme von Cys) mit 13 nichtnatürlich vorkommenden Aminosäuren durchgeführt. Des Weiteren wurden Aβ-Monomere durch Größenausschlusschromatographie von Aβ-Oligomeren und größeren Aβ-Aggregaten getrennt, um somit, im Gegensatz zur Selektierung der DB-Peptide, definierte Aβ-Spezies zu verwenden. Peptid-Mikroarrays wurden mit Aβ-Monomeren, -Oligomeren, -Fibrillen und, da FITC markiertes Aβ verwendet wurde, mit freiem FITC als Kontrolle inkubiert. Die Bindungssignale wurden normiert, um mehrere Slides miteinander vergleichen zu können. Um D3-Derivate nicht zu berücksichtigen, die nur mit FITC, jedoch nicht an Aβ interagieren, wurde das Bindungssignal der FITC-Kontrolle von den detektierten Fluoreszenzsignalen der D3-Derivate nach Inkubation der Peptid-Mikroarrays mit den verschiedenen FITC-markierten Aβ-Spezies subtrahiert. Um nur D3-Derivate zu selektieren, die eine hohe Affinität an Aβ-Monomere, aber nicht an Aβ-Oligomere und -Fibrillen besitzen, wurde außerdem das gemessene Bindungssignal von Aβ-Monomeren durch Subtrahieren der Signale von Aβ-

Oligomeren und Aβ-Fibrillen reduziert. Es wurden sieben verschiedene Peptide, genannt ANK1 bis ANK7, selektiert. Im Vergleich zu D3 wurden bei den ANK-Peptiden fünf oder sechs Aminosäuren ausgetauscht, wobei bei allen ANK-Peptiden Arg2 gegen Lys, Thr4 gegen Ile oder Val und His7 gegen Val, 4-Fluoro-D-Phenylalanin oder D-Phenylglycin ausgetauscht wurde. Weitere Austausche in einzelnen ANK-Peptiden sind: Thr8 gegen Tyr, His9 gegen Lys, Arg10 gegen Ile, Trp oder Lys und Asn11 gegen Lys. ANK1 bis ANK7 wurden *in vitro* charakterisiert und ihre möglicherweise therapeutische Effektivität mit der von D3 verglichen.

Im Vergleich zu D3 besitzen die D3-Derivate ANK1 bis ANK7 mit einem K_D von 8 bis 13 µM eine sechsfach höhere Affinität zu Aβ-Monomeren, inhibieren effizienter die Aβ-Aggregation im ThT-Assay und reduzieren effizienter die Aβ-induzierte Zytotoxizität, wie mittels MTT-Zytotoxizitätsassay gezeigt wurde. ANK1 bis ANK3 entfernen den toxischen Effekt von Aβ auf neuronale Zellen vollständig wenn sie im fünffachen Peptidüberschuss verglichen mit Aβ-Monomeren eingesetzt werden. Das dynamische Gleichgewicht von Aβ wird durch die D-Peptide ANK1 bis ANK7 und D3 weg von Aβ-Oligomeren hin zu Aβ-Monomeren und größeren Aggregaten verschoben. ANK5 bis ANK7 eliminieren 22 bis 31 % effizienter Aβ-Oligomere als D3 bei Koinkubation von 80 µM Aβ mit 10 µM D-Peptid, wie mittels QIAD-Assay gezeigt wurde. Durch TEM-Aufnahmen konnte gezeigt werden, dass die größeren Aβ-Aggregate, die bei einer Koinkubation von Aβ-Aggregaten mit ANK6 entstehen, eine geringere amyloide Struktur aufweisen. Des Weiteren konnte gezeigt werden, dass vorhandene Aβ-Aggregate nach einer Koinkubation mit ANK6 einen reduzierten Prion-ähnlichen *Seeding*mechanismus im Vergleich zu Aβ alleine besitzen. Der vielversprechendste therapeutische Wirkstoff ANK6 (rkrirlvtkkkr-NH_2) wurde *in vivo* untersucht. Durch intraperitoneale Verabreichung von ANK6 konnten die kognitiven Fähigkeiten von tg-APPSwDI Mäusen im *Object recognition*-Test gesteigert werden.

Innerhalb dieser Arbeit wurden fünf D3-Derivate, genannt DB1 bis DB5, aufgrund ihrer höheren Affinität an HFIP-vorbehandeltes Aβ identifiziert. Sieben weitere D3-Derivate, genannt ANK1 bis ANK7, wurden nicht nur aufgrund einer höheren Affinität, sondern auch einer höheren Spezifität an monomeres Aβ mit Hilfe von Peptid-Mikroarrays identifiziert. All diese D3-Derivate zeigen eine therapeutische

Effektivität gegenüber Aβ, wobei die ANK-Peptide eine höhere Effizienz als die DB-Peptide besitzen. Eine mögliche Ursache hierfür ist, dass bei der Selektion der DB-Peptide nur die Affinität der Bindung an HFIP-vorbehandeltes Aβ, bestehend aus Aβ-Monomere und -Oligomere, gemessen wurde. Bei der Selektion der ANK-Peptide wurde nicht nur die Affinität der Bindung an Aβ-Monomere berücksichtigt, sondern auch eine spezifische Bindung an Aβ-Monomere. Des Weiteren wurden bei den DB-Peptiden zwei verschiedene Peptid-Mikroarraysysteme mit unterschiedlichen Detektionssystemen verwendet. Auffallend ist auch, dass die veränderte Aminosäuresequenz der DB-Peptide mit Ausnahme von DB4 im Vergleich zu sechs positiven Ladungen bei D3 eine Reduktion der positiven Ladungen auf drei bis fünf positiven Ladungen bewirkt. Die Aminosäuresequenzen der ANK-Peptide dagegen beinhalten sechs bis neun positive Ladungen. *In silico* Studien haben gezeigt, dass das Ursprungspeptid D3 über elektrostatische Wechselwirkungen an Aβ bindet. Die höhere Anzahl der positiven Ladungen in der Sequenz der ANK-Peptide kann somit die höhere Affinität dieser Peptide zu Aβ im Vergleich zu den DB-Peptiden erklären. Allerdings ist die Steigerung der Affinität der ANK-Peptide im Vergleich zu D3 nicht nur über die größere Anzahl an positiven Ladungen zu erklären, da ANK1 bis ANK4 genauso viele Ladungen wie D3 besitzt, aber eine höhere Affinität an Aβ-Monomere besitzen und z. B. im MTT-Zytotoxizitätsassay und ThT-Assay einen höhere *in vitro* Effektivität zeigen.

Den stärksten *in vitro* Effekt zur Verringerung der Aβ-Oligomer-Konzentration zeigt ANK6. Dieses D3-Derivat konnte bereits im AD-Tiermodel eine therapeutische Wirkung zeigen und stellt somit einen guten Ausgangspunkt für die Entwicklung eines Medikaments gegen AD dar (s. **Kapitel 5**).

Ein weiterer Ansatz für die Entwicklung eines effizienten therapeutischen Wirkstoffs gegen die AD wurde in **Kapitel 3.1.3** durch die Entwicklung des kompetitiven Spiegelbild-Phagendisplays und die Selektion von spezifischen Aβ Monomer-bindenden Peptiden durchgeführt. Die Selektion von Peptiden erfolgte gegen immobilisierte Aβ-Monomere. Die Kompetition in diesem Spiegelbild-Phagendisplay wurde durch Zugabe von freien Aβ-Oligomeren und größeren Aβ-Aggregaten ab der zweiten Amplifizierungsrunde erzielt. Das durch dieses Verfahren selektierte, möglicherweise Aβ-Monomer spezifische D-Peptid Mosd1

(ysyltsyhmwvr-NH_2) wurde *in vitro* hinsichtlich seines Einflusses auf Aβ-Oligomere und der Zytotoxizität untersucht. Durch einen ELISA wurde nachgewiesen, das Mosd1 bevorzugt an Aβ-Monomere im Vergleich zu anderen Aβ-Aggregaten bindet. Aβ, das mit Mosd1 über 24 h koinkubiert wurde, bildet unstrukturierte, amorphe Aggregate. Mosd1 eliminiert Aβ-Oligomere bei einer Koinkubation von 80 µM Aβ mit 10 bis 40 µM Mosd1, reduziert die Aβ-induzierte Zytotoxizität bei equimolaren Konzentrationen, sowie bei 0,5 x Unterschuss von Mosd1 im Vergleich zu monomerem Aβ. Es hat keinen Einfluss auf die γ-Sekretase. Der Phänotyp stabil mit APP transfizierter neuronaler Zellen konnte durch Verabreichung von Mosd1 verbessert werden.

In einem Nebenprojekt wurde D3 hinsichtlich seines Einflusses auf SEVI-Fibrillen bei der Übertragung von HIV untersucht. Die Ergebnisse zu diesem Projekt sind in **Kapitel 3.1.4** dargestellt. Teile der prostataspezifische saure Phosphatase (PAP) bilden amyloide Strukturen (*semen-derived enhancer of viral infection*, SEVI) und steigert dadurch die sexuelle Übertragungseffizienz. Durch D3 kann die Amyloid-vermittelte Steigerung der Infektiösität inhibiert werden.

5. Ausblick

In dieser Arbeit wurden fünf an HFIP-vorbehandeltem Aβ bindende (DB1 bis DB5) und sieben spezifisch an monomeres Aβ bindende D3-Derivate (ANK1 bis ANK7) selektiert. Dafür wurden drei Sets an Peptid-Mikroarrays verwendet. Ein Set beinhaltete 228 verschiedene D3-Derivate mit mehr als einem Aminosäureaustausch, basierend auf vorherigen Ergebnissen der Arbeitsgruppe. Aus diesem Set wurden 5 Peptide, genannt DB1 bis DB5, selektiert. Ein zweites Set beinhaltete D3-Derivate mit einem kompletten Austausch von allen Aminosäuren gegen 18 natürliche Aminosäuren und 13 nicht-natürlich vorkommende Aminosäuren. Dem zu Folge wurden mit diesem Set 384 verschiedene D3-Derivate untersucht. Anhand der Ergebnisse dieser Peptid-Mikroarray-Sets wurde ein drittes Set mit mehr als 1.000 verschiedenen D3-Derivaten erstellt, davon sieben D3-Derivate selektiert, genannt ANK1 bis ANK7, und näher *in vitro* charakterisiert. Insgesamt sind also über 1.500 verschiedene D3-Derivate hinsichtlich ihrer Affinität zu verschiedenen Aβ-Spezies gescreent worden. Die Auswahl der D3-Derivate, die näher untersucht wurden, war aufgrund des hohen Arbeitsaufwands nur limitiert möglich. Aus diesem Grund können evtl. noch andere der auf den Mikroarrays vorhandenen D3-Derivate von Interesse sein. Diese D3-Derivate können noch näher untersucht werden. Auch können durch andere Auswertemethoden der Peptid-Mikroarray-Daten weitere D3-Derivate ermittelt werden, die möglicherweise interessante Eigenschaften für die Modulation der Aβ-Aggregation zeigen.

Die Charakterisierung der bereits selektierten D3-Derivate ist noch nicht abgeschlossen. Eine offene Frage ist der Wirkmechanismus der D3-Derivate. An welche Aminosäuresequenz von Aβ binden die D3-Derivate? Dies kann zum Beispiel durch ein Epitopmapping untersucht werden. Wie wird die Sekundärstruktur von Aβ durch die D3-Derivate verändert? Diese Frage kann durch Fourier-Transformations-Infrarotspektroskopie (FTIR) untersucht werden. Auch die exakte Tertiärstruktur des Aβ-Peptid-Komplexes ist von Interesse und kann zum Beispiel mit Kernspinresonanzspektroskophie (engl. *Nuclear magnetic resonance*, NMR) untersucht werden.

Auch interessant ist die Wirkung der D3-Derivate auf andere Komponenten, die in der Pathologie von AD involviert sind. Wie wirken die D3-Derivate auf die Sekretasen? Haben die D3-Derivate einen Einfluss auf inflammatorische Komponenten, wie z. B. IL-10?

In 3.1.4 konnte gezeigt werden, das das Ursprungspeptid D3 einen Einfluss auf die SEVI-Fibrillen bei der sexuellen Übertragung von HIV-1 hat. Daraufhin ist es naheliegend zu untersuchen, ob die D3-Derivate ebenfalls einen Einfluss auf die SEVI-Fibrillen oder andere amyloide Fibrillen haben. Ein Einfluss von den Peptiden auf Tau wäre wünschenswert und könnte ebenfalls untersucht werden. In der Fachwelt wird eine Kombinationstherapie von AD mit Wirkmechanismen gegen Aβ und Tau stark diskutiert (Wisniewski *et al.*, 2015). Evtl. wird durch eine Wirkung der D3-Derivate auf andere amyloide Fibrillen eine Therapie von anderen amyloiden Erkrankungen, zum Beispiel PD oder ALS, möglich.

Des Weiteren können die bereits selektierten D3-Derivate noch weiter optimiert werden, zum Beispiel durch die Synthese von Tandempeptiden (zweimal dieselbe Peptidsequenz hintereinander), um die Avidität zu steigern oder von zyklisierten Peptiden (z. B. C- an N-terminale-Zyklisierung), um die Freiheitsgerade und die Entropie zu verringern. Des Weiteren sind auch Kombinationen von verschiedenen Peptiden/ D3-Derivate denkbar (z. B. vom bereits *in vitro* getesteten RD2 mit einem der ANK-Peptide).

Die in dieser Arbeit identifizierten und selektierten D3-Derivate ANK1 bis ANK7 stellen vielversprechende Wirkstoffe für die Behandlung der AD dar, deren Wirkmechanismus noch weiter identifiziert werden muss.

Abkürzungsverzeichnis

Alle Einheiten entsprechen dem internationalen Einheitssystem (SI) und werden hier nicht gesondert aufgelistet.

4HNE	4-hyroxynonenal
Aβ	Amyloid-β-Peptid
AD	Alzheimersche Demenz
ADDL	Aβ bestehende diffuse Liganden
AICD	APP intrazelluläre Domaine (*APP intracellular domain*)
ALS	Amyotrophe Lateralsklerose
ANK	D3-Derivate selektiert mit Hilfe von Peptid-Mikroarrays
APP	Amyloid-Vorläufer-Protein (*amyloid precursor protein*)
ApoE	Apolipoprotein E
ATP	Adenosintriphosphat
BACE	*beta-site APP cleaving enzyme*
BBB	Blut-Hirn-Schranke (b*lood brain barrier*)
ChAT	Cholineacetyltransferase
CJK	Creutzfeld-Jakob-Krankheit
CSF	Zerebrospinalflüssigkeit (*cerebrospinal fluid*)
CT	Computertomografie
D3	D-enantiomeres Peptid selektiert mit Hilfe von Spiegelbild-Phagendisplay
DB	D3-Derivate selektiert mit Hilfe von Peptid-Mikroarrays
EC_{50}	mittlere effektive Konzentration

EGCG	Epigallocatechingallate
ELISA	*enzyme-linked immunosorbent assay*
fAD	familiäre Alzheimersche Demenz
FITC	Fluoresceinisothiocyanat
FTIR	Fourier-Transformations-Infrarotspektroskopie
GTP	Guanosintriphosphat
HD	Chorea Huntington
HFIP	1,1,1,3,3,3-Hexafluor-2-propanol
HIV	humanes Immundefizienz-Virus
IDE	Insulin degenerierendes Enzym
IgG	Immunglobulin G
LRP1	l*ow-density lipoprotein receptor related protein*
LTP	Langzeit-Potential (*long time potential*)
LTD	Langzeit-Depression (*long time depression*)
MRT	Magnetresonanztomografie
MTT	3-(4,5-Dimethylthiazol-2-yl)-2,5-diphenyltetrazoliumbromid
NFT	neurofibrilläre Bündel (*neurofibrillary tangles*)
NMDAR	N-Methyl-D-Aspartat-Rezeptor
NMR	Kernspinresonanzspektroskopie (*nuclear magnetic resonance*)
NRG1	Neuregulin 1
PAP	prostataspezifische saure Phosphatase (p*rostatic acidic phosphatase)*
PD	Parkinsonkrankheit
PET	Positronen-Elektronen-Tomografie

PHF	*paired helical fibrils*
polyQ	Polyglutamat
QIAD	Assay zur quantitativen Bestimmung des Einflusses von Substanzen auf die Größenverteilung von Aβ-Aggregaten (engl. *quantitative determination of interference with Aβ aggregate size distribution)*
RAGE	*receptor for advanced glycation endproducts*
RD2	D-enantiomeres Peptid selektiert durch rationales Design
sAD	sporadische Alzheimersche Demenz
SEVI	*semen-derived enhancer of viral infection*
tg-APPSwDI	transgene APP *Swedish Dutch Iowa* Mäuse
ThT	Thioflavin T

Natürlich vorkommende Aminosäuren (Drei- und Ein-Buchstabencode):

A	Ala	Alanin	M	Met	Methionin
C	Cys	Cystein	N	Asn	Asparagin
D	Asp	Asparaginsäure	P	Pro	Prolin
E	Glu	Glutaminsäure	Q	Gln	Glutamin
F	Phe	Phenylalanin	R	Arg	Arginin
G	Gly	Glycin	S	Ser	Serin
H	His	Histidin	T	Thr	Threonin
I	Ile	Isoleucin	V	Val	Valin
K	Lys	Lysin	W	Trp	Tryptophan
L	Leu	Leucin	Y	Tyr	Tyrosin

Liste der Publikationen, Patentbeteiligungen und Posterpräsentationen

Publikationen

Grüning CS, Klinker S, Wolff M, Schneider M, Toksöz K, Klein AN, Nagel-Steger L, Willbold D, Hoyer W; The off-rate of monomers dissociating from amyloid-beta protofibrils.; J. Biol. Chem. 288, 37104-37111 (2013).

Widera M, Klein AN, Cinar Y, Funke SA, Willbold D, Schaal H; The D-amino acid peptide D3 reduces amyloid fibril boosted HIV-1 infectivity.; AIDS Research and Therapy 01/2014; 11(1):1 (2014).

Grüning CS, Mirecka EA, Klein AN, Mandelkow E, Willbold D, Marino SF, Stoldt M, Hoyer W; Alternative conformations of the tau repeat domain in complex with an engineered binding protein.; J. Biol. Chem. 289, 23209-23218 (2014).

Shaykhalishahi H, Gauhar A, Wördehoff MM, Grüning CSR, Klein AN, Bannach O, Stoldt M, Willbold D, Härd T, Hoyer W; Contact between the β-1 and β-2 segments of α-synuclein entails inhibition of amyloid formation.; Angew. Chem. Int. Ed. 54, 8837-8840 (2015).

Pattky M, Nicolardi S, Santiago-Schübell B, Sydes D, van der Burget YEM, Klein AN, Jiang N, Mohrlüder J, Händel K, Kutzsche J, Funke SA, Willbold D, Willbold S, Huhn C; Structure characterization of unexpected covalent O-sulfonation and ion pairing on an extremely hydrophilic peptide with CE-MS and FT-ICR-MS.; Anal. Bioanal. Chem. 407, 6637-6655 (2015).

Dammers C, Gremer L, Reiß K, Klein AN, Neudecker P, Hartmann R, Demuth H-U, Schwarten M and Willbold D; Structural analysis and aggregation propensity of pyroglutamate Aβ(3-40) in aqueous trifluoroethanol.; im Druck.

Klein AN, Ziehm T, Tusche M, Buithuis J, Bartnik D, Boeddrich A, Wiglenda T, Wanker E, Funke SA, Thomaier M, Brener O, Gremer L, Kutzsche J, Willbold D; Optimization of the all-D peptide D3 for Aβ oligomer elimination.; Eingereicht bei PlosOne.

Klein AN, Ziehm T, van Groen T, Kadish I, Elfgen A, Tusche M, Reiß K, Brener O, Gremer L, Kutzsche J, Willbold D; Optimization of D-peptides for Aβ monomer binding specificity enhances their potential to eliminate toxic Aβ oligomers; Eingereicht bei JACs.

Rudolph S, Klein AN, Tusche AN, Schlosser C, Funke SA, Kutzsche J, Willbold D.; Competitive mirror image phage display derived peptides modulates amyloid beta aggregation and decreases toxicity; Eingereicht bei PlosOne.

Patentbeteiligungen (zum Patent eingereicht)

Funke SA, Brener O, Willbold D, Bartnik D, Nagel-Steger L, Klein AN
Neue, von D3 abgeleitete D-enantiomere Peptide und deren Verwendung
14. September 2012, DE 10 2012 108598 A1 & WO2014041115A3

Willbold D, Klein AN, Kutzsche J,
Spezifisch A-Beta-Spezies bindende Peptide für die Therapie und/oder die Diagnose der Alzheimerschen Demenz
18. März 2016, DE 10 2015 003676.9

Posterpräsentationen (nur Erstautorenschaften aufgelistet)

Klein AN, Tusche M, Schlosser C, Bartnik D, Kutzsche J, Willbold D
Characterization of D-enantiomeric peptides derived from D3 for treatment of Alzheimer's disease.
Alzheimer's Association International Conference 2014, 12.-17. Juli 2014, Kopenhagen, Dänemark

Klein AN, Ziehm T, Tusche M, Kutzsche J, Willbold D
Characterization of a novel d-enatimoneric peptide that is able to eliminate Abeta oligomers.
12th International Conference on Alzheimer's & Parkinson's Diseases, 18.-22. März 2015 Nizza, Frankreich

Literaturverzeichnis

Andersson, E. R., Sandberg, R. & Lendahl, U. (2011). *Notch signaling: simplicity in design, versatility in function*. Development, 138**,** 3593-612.

Andresen, H., Zarse, K., Grötzinger, C., Hollidt, J.-M., Ehrentreich-Förster, E., Bier, F. F. & Kreuzer, O. J. (2006). *Development of peptide microarrays for epitope mapping of antibodies against the human TSH receptor*. Journal of Immunological Methods, 315**,** 11-18.

Bard, F., Barbour, R., Cannon, C., Carretto, R., Fox, M., Games, D., Guido, T., Hoenow, K., Hu, K., Johnson-Wood, K., Khan, K., Kholodenko, D., Lee, C., Lee, M., Motter, R., Nguyen, M., Reed, A., Schenk, D., Tang, P., Vasquez, N., Seubert, P. & Yednock, T. (2003). *Epitope and isotype specificities of antibodies to beta -amyloid peptide for protection against Alzheimer's disease-like neuropathology*. Proc Natl Acad Sci U S A, 100**,** 2023-8.

Bard, F., Cannon, C., Barbour, R., Burke, R. L., Games, D., Grajeda, H., Guido, T., Hu, K., Huang, J., Johnson-Wood, K., Khan, K., Kholodenko, D., Lee, M., Lieberburg, I., Motter, R., Nguyen, M., Soriano, F., Vasquez, N., Weiss, K., Welch, B., Seubert, P., Schenk, D. & Yednock, T. (2000). *Peripherally administered antibodies against amyloid β-peptide enter the central nervous system and reduce pathology in a mouse model of Alzheimer disease*. Nature Medicine, 6**,** 916-919.

Bartnik, D., Funke, S. A., Andrei-Selmer, L.-C., Bacher, M., Dodel, R. & Willbold, D. (2009). *Differently Selected d-Enantiomeric Peptides Act on Different Aβ Species*. Rejuvenation Research, 13**,** 202-205.

Begum, A. N., Jones, M. R., Lim, G. P., Morihara, T., Kim, P., Heath, D. D., Rock, C. L., Pruitt, M. A., Yang, F., Hudspeth, B., Hu, S., Faull, K. F., Teter, B., Cole, G. M. & Frautschy, S. A. (2008). *Curcumin Structure-Function, Bioavailability, and Efficacy in Models of Neuroinflammation and Alzheimer's Disease*. Journal of Pharmacology and Experimental Therapeutics, 326**,** 196-208.

Beydoun, M., Beydoun, H., Gamaldo, A., Teel, A., Zonderman, A. & Wang, Y. (2014). *Epidemiologic studies of modifiable factors associated with cognition and dementia: systematic review and meta-analysis*. BMC Public Health, 14**,** 643.

Blennow, K., de Leon, M. J. & Zetterberg, H. (2006). *Alzheimer's disease*. Lancet, 368**,** 387-403.

Blennow, K., Hampel, H., Weiner, M. & Zetterberg, H. (2010). *Cerebrospinal fluid and plasma biomarkers in Alzheimer disease*. Nat Rev Neurol, 6**,** 131-144.

Bocci, V. (1989). *Catabolism of therapeutic proteins and peptides with implications for drug delivery*. Advanced Drug Delivery Reviews, 4**,** 149-169.

Braak, H. & Braak, E. (1991). *Neuropathological stageing of Alzheimer-related changes*. Acta Neuropathologica, 82**,** 239-259.

Brodaty, H., Ames, D., Snowdon, J., Woodward, M., Kirwan, J., Clarnette, R., Lee, E., Lyons, B. & Grossman, F. (2003). *A randomized placebo-controlled trial of risperidone for the treatment of aggression, agitation, and psychosis of dementia*. Journal of Clinical Psychiatry, 64**,** 134-143.

Bullock, R., Touchon, J., Bergman, H., Gambina, G., He, Y., Rapatz, G., Nagel, J. & Lane, R. (2005). *Rivastigmine and donepezil treatment in moderate to moderately-severe Alzheimer's disease over a 2-year period*. Curr Med Res Opin, 21**,** 1317-27.

Butterfield, A. D. (2002). *Amyloid β-peptide (1-42)-induced Oxidative Stress and Neurotoxicity: Implications for Neurodegeneration in Alzheimer's Disease Brain. A Review*. Free Radical Research, 36**,** 1307-1313.

Cabrol, C., Huzarska, M. A., Dinolfo, C., Rodriguez, M. C., Reinstatler, L., Ni, J., Yeh, L.-A., Cuny, G. D., Stein, R. L., Selkoe, D. J. & Leissring, M. A. (2009). *Small-Molecule Activators of Insulin-Degrading Enzyme Discovered through High-Throughput Compound Screening*. PLoS ONE, 4**,** e5274.

Caccamo, A., Oddo, S., Sugarman, M. C., Akbari, Y. & LaFerla, F. M. (2005). *Age- and region-dependent alterations in Aβ-degrading enzymes: implications for Aβ-induced disorders*. Neurobiology of Aging, 26**,** 645-654.

Carrell, R. W. & Lomas, D. A. (1997). *Conformational disease*. The Lancet, 350**,** 134-138.

Chiti, F. & Dobson, C. M. (2006). *Protein Misfolding, Functional Amyloid, and Human Disease*. Annual Review of Biochemistry, 75**,** 333-366.

Cleveland, D. W., Hwo, S. Y. & Kirschner, M. W. (1977). *Physical and chemical properties of purified tau factor and the role of tau in microtubule assembly*. J Mol Biol, 116**,** 227-47.

Cohen, S. I. A., Linse, S., Luheshi, L. M., Hellstrand, E., White, D. A., Rajah, L., Otzen, D. E., Vendruscolo, M., Dobson, C. M. & Knowles, T. P. J. (2013). *Proliferation of amyloid-β42 aggregates occurs through a secondary nucleation mechanism*. Proceedings of the National Academy of Sciences of the United States of America, 110**,** 9758-9763.

Courtney, C., Farrell, D., Gray, R., Hills, R., Lynch, L., Sellwood, E., Edwards, S., Hardyman, W., Raftery, J., Crome, P., Lendon, C., Shaw, H. & Bentham, P. (2004). *Long-term donepezil treatment in 565 patients with Alzheimer's disease (AD2000): randomised double-blind trial*. Lancet, 363**,** 2105-15.

De Strooper, B. (2010). *Proteases and Proteolysis in Alzheimer Disease: A Multifactorial View on the Disease Process*.

De Strooper, B., Annaert, W., Cupers, P., Saftig, P., Craessaerts, K., Mumm, J. S., Schroeter, E. H., Schrijvers, V., Wolfe, M. S., Ray, W. J., Goate, A. & Kopan, R. (1999). *A presenilin-1-dependent [gamma]-secretase-like protease mediates release of Notch intracellular domain*. Nature, 398**,** 518-522.

Deane, R., Bell, R., Sagare, A. & Zlokovic, B. (2009). *Clearance of amyloid-β peptide across the blood-brain barrier: implication for therapies in Alzheimer's disease*. CNS & neurological disorders drug targets, 8**,** 16.

Deane, R., Du Yan, S., Submamaryan, R. K., LaRue, B., Jovanovic, S., Hogg, E., Welch, D., Manness, L., Lin, C., Yu, J., Zhu, H., Ghiso, J., Frangione, B., Stern, A., Schmidt, A. M., Armstrong, D. L., Arnold, B., Liliensiek, B., Nawroth, P., Hofman, F., Kindy, M., Stern, D. & Zlokovic, B. (2003). *RAGE mediates amyloid-beta peptide transport across the blood-brain barrier and accumulation in brain*. Nat Med, 9**,** 907-13.

Devlin, J., Panganiban, L. & Devlin, P. (1990). *Random peptide libraries: a source of specific protein binding molecules*. Science, 249**,** 404-406.

Doody, R. S., Thomas, R. G., Farlow, M., Iwatsubo, T., Vellas, B., Joffe, S., Kieburtz, K., Raman, R., Sun, X., Aisen, P. S., Siemers, E., Liu-Seifert, H. & Mohs, R. (2014). *Phase 3 Trials of Solanezumab for Mild-to-Moderate Alzheimer's Disease*. New England Journal of Medicine, 370**,** 311-321.

Eckman, E. & Eckman, C. (2005). *Abeta-degrading enzymes: modulators of Alzheimer's disease pathogenesis and targets for therapeutic intervention*. Biochemical Society Transactions, 33**,** 1101.

Ehrnhoefer, D. E., Bieschke, J., Boeddrich, A., Herbst, M., Masino, L., Lurz, R., Engemann, S., Pastore, A. & Wanker, E. E. (2008). *EGCG redirects amyloidogenic polypeptides into unstructured, off-pathway oligomers*. Nat Struct Mol Biol, 15**,** 558-566.

Ferri, C. P., Prince, M., Brayne, C., Brodaty, H., Fratiglioni, L., Ganguli, M., Hall, K., Hasegawa, K., Hendrie, H., Huang, Y., Jorm, A., Mathers, C., Menezes, P. R., Rimmer, E., Scazufca, M. & Alzheimer's Disease, I. (2005). *Global prevalence of dementia: a Delphi consensus study*. Lancet, 366**,** 2112-2117.

Finder, V. H. & Glockshuber, R. (2007). *Amyloid-β Aggregation*. Neurodegenerative Diseases, 4**,** 13-27.

Fodor, S. P., Read, J. L., Pirrung, M. C., Stryer, L., Lu, A. T. & Solas, D. (1991). *Light-directed, spatially addressable parallel chemical synthesis*. Science, 251**,** 767-73.

Foong, Y. M., Fu, J., Yao, S. Q. & Uttamchandani, M. (2012). *Current advances in peptide and small molecule microarray technologies*. Current Opinion in Chemical Biology, 16**,** 234-242.

Forman, M., Kleijn, H.-J., Dockendorf, M., Palcza, J., Tseng, J., Canales, C., Egan, M., Kennedy, M., Laterza, O., Ma, L., Scott, J., Tanen, M., Apter, J., Backonja, M., Ereshefsky, L., Gevorkyan, H., Jhee, S., Rynders, R., Zari, A., Bryan, E., Wagner, J., Troyer, M. & Stone, J. *The novel BACE inhibitor MK-8931 dramatically lowers CSF beta-amyloid in patients with mild-to-moderate Alzheimer's disease*. Alzheimer's & Dementia: The Journal of the Alzheimer's Association, 9**,** P139.

Fraering, P. C., Ye, W., LaVoie, M. J., Ostaszewski, B. L., Selkoe, D. J. & Wolfe, M. S. (2005). *γ-Secretase Substrate Selectivity Can Be Modulated Directly via Interaction with a Nucleotide-binding Site*. Journal of Biological Chemistry, 280**,** 41987-41996.

Funke, S. A., van Groen, T., Kadish, I., Bartnik, D., Nagel-Steger, L., Brener, O., Sehl, T., Batra-Safferling, R., Moriscot, C., Schoehn, G., Horn, A. H. C., Müller-Schiffmann, A., Korth, C., Sticht, H. & Willbold, D. (2010). *Oral Treatment with the d-Enantiomeric Peptide D3 Improves the Pathology and Behavior of Alzheimer's Disease Transgenic Mice*. ACS Chemical Neuroscience, 1**,** 639-648.

Funke, S. A. & Willbold, D. (2009). *Mirror image phage display-a method to generate d-peptideligands for use in diagnostic or therapeutical applications*. Molecular BioSystems, 5**,** 783-786.

Giuffrida, M. L., Caraci, F., Pignataro, B., Cataldo, S., De Bona, P., Bruno, V., Molinaro, G., Pappalardo, G., Messina, A., Palmigiano, A., Garozzo, D., Nicoletti, F., Rizzarelli, E. & Copani, A. (2009). *β-Amyloid Monomers Are Neuroprotective*. The Journal of Neuroscience, 29**,** 10582-10587.

Glenner, G. G. & Wong, C. W. (1984). *Alzheimer's disease: Initial report of the purification and characterization of a novel cerebrovascular amyloid protein*. Biochemical and Biophysical Research Communications, 120**,** 885-890.

Goure, W., Krafft, G., Jerecic, J. & Hefti, F. (2014). *Targeting the proper amyloid-beta neuronal toxins: a path forward for Alzheimer's disease immunotherapeutics*. Alzheimer's Research & Therapy, 6**,** 42.

Gray, R. H., Wawer, M. J., Brookmeyer, R., Sewankambo, N. K., Serwadda, D., Wabwire-Mangen, F., Lutalo, T., Li, X., vanCott, T. & Quinn, T. C. (2001). *Probability of HIV-1 transmission per coital act in monogamous, heterosexual, HIV-1-discordant couples in Rakai, Uganda*. Lancet, 357**,** 1149-53.

Grundke-Iqbal, I., Iqbal, K., Tung, Y. C., Quinlan, M., Wisniewski, H. M. & Binder, L. I. (1986). *Abnormal phosphorylation of the microtubule-associated protein tau (tau) in Alzheimer cytoskeletal pathology*. Proc Natl Acad Sci U S A, 83**,** 4913-7.

Haass, C. & Selkoe, D. J. (2007). *Soluble protein oligomers in neurodegeneration: lessons from the Alzheimer's amyloid [beta]-peptide*. Nat Rev Mol Cell Biol, 8**,** 101-112.

Hardy, J. & Selkoe, D. J. (2002). *The Amyloid Hypothesis of Alzheimer's Disease: Progress and Problems on the Road to Therapeutics*. Science, 297**,** 353-356.

Hartley, D. M., Walsh, D. M., Ye, C. P., Diehl, T., Vasquez, S., Vassilev, P. M., Teplow, D. B. & Selkoe, D. J. (1999). *Protofibrillar Intermediates of Amyloid β-Protein Induce Acute Electrophysiological Changes and Progressive Neurotoxicity in Cortical Neurons*. The Journal of Neuroscience, 19**,** 8876-8884.

Iadecola, C. (2004). *Neurovascular regulation in the normal brain and in Alzheimer's disease*. Nat Rev Neurosci, 5**,** 347-360.

Ikonomovic, M. D., Klunk, W. E., Abrahamson, E. E., Mathis, C. A., Price, J. C., Tsopelas, N. D., Lopresti, B. J., Ziolko, S., Bi, W., Paljug, W. R., Debnath, M. L., Hope, C. E., Isanski, B. A., Hamilton, R. L. & DeKosky, S. T. (2008). *Post-mortem correlates of in vivo PiB-PET amyloid imaging in a typical case of Alzheimer's disease*.

Itagaki, S., McGeer, P. L., Akiyama, H., Zhu, S. & Selkoe, D. (1989). *Relationship of microglia and astrocytes to amyloid deposits of Alzheimer disease*. Journal of Neuroimmunology, 24**,** 173-182.

Jakes, R., Novak, M., Davison, M. & Wischik, C. M. (1991). *Identification of 3- and 4-repeat tau isoforms within the PHF in Alzheimer's disease*. The EMBO Journal, 10**,** 2725-2729.

Jakob-Roetne, R. & Jacobsen, H. (2009). *Alzheimer's Disease: From Pathology to Therapeutic Approaches*. Angewandte Chemie International Edition, 48**,** 3030-3059.

Jin, M., Shepardson, N., Yang, T., Chen, G., Walsh, D. & Selkoe, D. J. (2011). *Soluble amyloid β-protein dimers isolated from Alzheimer cortex directly induce Tau hyperphosphorylation and neuritic degeneration*. Proceedings of the National Academy of Sciences, 108**,** 5819-5824.

Johnson, G. V. & Stoothoff, W. H. (2004). *Tau phosphorylation in neuronal cell function and dysfunction*. J Cell Sci, 117**,** 5721-9.

Jonsson, T., Atwal, J. K., Steinberg, S., Snaedal, J., Jonsson, P. V., Bjornsson, S., Stefansson, H., Sulem, P., Gudbjartsson, D., Maloney, J., Hoyte, K., Gustafson, A., Liu, Y., Lu, Y., Bhangale, T., Graham, R. R., Huttenlocher, J., Bjornsdottir, G., Andreassen, O. A., Jonsson, E. G., Palotie, A., Behrens, T. W., Magnusson, O. T., Kong, A., Thorsteinsdottir, U., Watts, R. J. & Stefansson, K. (2012). *A mutation in APP protects against Alzheimer/'s disease and age-related cognitive decline*. Nature, 488**,** 96-99.

Kanemitsu, H., Tomiyama, T. & Mori, H. (2003). *Human neprilysin is capable of degrading amyloid β peptide not only in the monomeric form but also the pathological oligomeric form.* Neuroscience Letters, 350**,** 113-116.

Katz, C., Levy-Beladev, L., Rotem-Bamberger, S., Rito, T., Rüdiger, S. G. & Friedler, A. (2011). *Studying protein–protein interactions using peptide arrays*. Chemical Society Reviews, 40**,** 2131-2145.

Kirsten, C. N. & Schrader, T. H. (1997). *Intermolecular β-Sheet Stabilization with Aminopyrazoles*. Journal of the American Chemical Society, 119**,** 12061-12068.

Knowles, T. P. J., Vendruscolo, M. & Dobson, C. M. (2014). *The amyloid state and its association with protein misfolding diseases*. Nat Rev Mol Cell Biol, 15**,** 384-396.

Kumar, S., Rezaei-Ghaleh, N., Terwel, D., Thal, D. R., Richard, M., Hoch, M., Mc Donald, J. M., Wüllner, U., Glebov, K., Heneka, M. T., Walsh, D. M., Zweckstetter, M. & Walter, J. (2011). *Extracellular phosphorylation of the amyloid β-peptide promotes formation of toxic aggregates during the pathogenesis of Alzheimer's disease*.

Kuperstein, I., Broersen, K., Benilova, I., Rozenski, J., Jonckheere, W., Debulpaep, M., Vandersteen, A., Segers-Nolten, I., Van Der Werf, K., Subramaniam, V., Braeken, D., Callewaert, G., Bartic, C., D'Hooge, R., Martins, I. C., Rousseau, F., Schymkowitz, J. & De Strooper, B. (2010). *Neurotoxicity of Alzheimer's disease Aβ peptides is induced by small changes in the Aβ42 to Aβ40 ratio*.

Lashuel, H. A., Hartley, D., Petre, B. M., Walz, T. & Lansbury, P. T. (2002). *Neurodegenerative disease: Amyloid pores from pathogenic mutations*. Nature, 418**,** 291-291.

Lee, V. H. L. & Yamamoto, A. (1989). *Penetration and enzymatic barriers to peptide and protein absorption*. Advanced Drug Delivery Reviews, 4**,** 171-207.

Leivonen, S. K., Makela, R., Ostling, P., Kohonen, P., Haapa-Paananen, S., Kleivi, K., Enerly, E., Aakula, A., Hellstrom, K., Sahlberg, N., Kristensen, V. N., Borresen-Dale, A. L., Saviranta, P., Perala, M. & Kallioniemi, O. (2009). *Protein lysate microarray analysis to identify microRNAs regulating estrogen receptor signaling in breast cancer cell lines*. Oncogene, 28**,** 3926-3936.

Levine, H. (1993). *Thioflavine T interaction with synthetic Alzheimer's disease β-amyloid peptides: Detection of amyloid aggregation in solution*. Protein Science, 2**,** 404-410.

Liu, H., Funke, S. A. & Willbold, D. (2009). *Transport of Alzheimer Disease Amyloid-β-Binding d-Amino Acid Peptides across an In Vitro Blood–Brain Barrier Model*. Rejuvenation Research, 13**,** 210-213.

Lokate, A. M. C., Beusink, J. B., Besselink, G. A. J., Pruijn, G. J. M. & Schasfoort, R. B. M. (2007). *Biomolecular Interaction Monitoring of Autoantibodies by Scanning Surface Plasmon Resonance Microarray Imaging*. Journal of the American Chemical Society, 129**,** 14013-14018.

Lundkvist, J. & Näslund, J. (2007). *γ-Secretase: a complex target for Alzheimer's disease*. Current Opinion in Pharmacology, 7**,** 112-118.

Masterman, D. (2003). *Treatment of the Neuropsychiatric Symptoms in Alzheimer's Disease*. Journal of the American Medical Directors Association, 4**,** S146-S154.

Masters, C. L., Simms, G., Weinman, N. A., Multhaup, G., McDonald, B. L. & Beyreuther, K. (1985). *Amyloid plaque core protein in Alzheimer disease and Down syndrome*. Proceedings of the National Academy of Sciences of the United States of America, 82**,** 4245-4249.

Mattson, M. P. (2004). *Pathways towards and away from Alzheimer's disease*. Nature, 430**,** 631-639.

Mayeux, R. (2003). *Epidemiology of neurodegeneration*. Annual Review of Neuroscience, 26**,** 81-104.

McGregor, D. P. (2008). *Discovering and improving novel peptide therapeutics*. Current Opinion in Pharmacology, 8**,** 616-619.

McLean, C. A., Cherny, R. A., Fraser, F. W., Fuller, S. J., Smith, M. J., Konrad, V., Bush, A. I. & Masters, C. L. (1999). *Soluble pool of Aβ amyloid as a determinant of severity of neurodegeneration in Alzheimer's disease*. Annals of Neurology, 46**,** 860-866.

Mullard, A. (2012). *Sting of Alzheimer's failures offset by upcoming prevention trials*. Nat Rev Drug Discov, 11**,** 657-660.

Müller-Schiffmann, A., März-Berberich, J., Andreyeva, A., Rönicke, R., Bartnik, D., Brener, O., Kutzsche, J., Horn, A. H. C., Hellmert, M., Polkowska, J., Gottmann, K., Reymann, K. G., Funke, S. A., Nagel-Steger, L., Moriscot, C., Schoehn, G., Sticht, H., Willbold, D., Schrader, T. & Korth, C. (2010). *Combining Independent Drug Classes into Superior, Synergistically Acting Hybrid Molecules*. Angewandte Chemie International Edition, 49**,** 8743-8746.

Münch, J., Rücker, E., Ständker, L., Adermann, K., Goffinet, C., Schindler, M., Wildum, S., Chinnadurai, R., Rajan, D., Specht, A., Giménez-Gallego, G., Sánchez, P. C., Fowler, D. M., Koulov, A., Kelly, J. W., Mothes, W., Grivel, J.-C., Margolis, L., Keppler, O. T., Forssmann, W.-G. & Kirchhoff, F. (2007). *Semen-Derived Amyloid Fibrils Drastically Enhance HIV Infection*. Cell, 131**,** 1059-1071.

Nagel-Steger, L., Demeler, B., Meyer-Zaika, W., Hochdörffer, K., Schrader, T. & Willbold, D. (2010). *Modulation of aggregate size- and shape-distributions of the amyloid-β peptide by a designed β-sheet breaker*. European Biophysics Journal, 39**,** 415-422.

Nelson, P. T., Alafuzoff, I., Bigio, E. H., Bouras, C., Braak, H., Cairns, N. J., Castellani, R. J., Crain, B. J., Davies, P., Tredici, K. D., Duyckaerts, C., Frosch, M. P., Haroutunian, V., Hof, P. R., Hulette, C. M., Hyman, B. T., Iwatsubo, T., Jellinger, K. A., Jicha, G. A., Kövari, E., Kukull, W. A., Leverenz, J. B., Love, S., MacKenzie, I. R., Mann, D. M., Masliah, E., McKee, A. C., Montine, T. J., Morris, J. C., Schneider, J. A., Sonnen, J. A., Thal, D. R., Trojanowski, J. Q., Troncoso, J. C., Wisniewski, T., Woltjer, R. L. & Beach, T. G. (2012). *Correlation of alzheimer disease neuropathologic changes with cognitive status: A review of the literature*. Journal of Neuropathology and Experimental Neurology, 71**,** 362-381.

Nelson, R., Sawaya, M. R., Balbirnie, M., Madsen, A. O., Riekel, C., Grothe, R. & Eisenberg, D. (2005). *Structure of the cross-[beta] spine of amyloid-like fibrils*. Nature, 435**,** 773-778.

Nunes-Tavares, N., Santos, L. E., Stutz, B., Brito-Moreira, J., Klein, W. L., Ferreira, S. T. & de Mello, F. G. (2012). *Inhibition of Choline Acetyltransferase as a Mechanism for Cholinergic Dysfunction Induced by Amyloid-β Peptide Oligomers*. Journal of Biological Chemistry, 287**,** 19377-19385.

O'Nuallain, B., Williams, A. D., Westermark, P. & Wetzel, R. (2004). *Seeding Specificity in Amyloid Growth Induced by Heterologous Fibrils*. Journal of Biological Chemistry, 279**,** 17490-17499.

Olsen, J. S., Brown, C., Capule, C. C., Rubinshtein, M., Doran, T. M., Srivastava, R. K., Feng, C., Nilsson, B. L., Yang, J. & Dewhurst, S. (2010). *Amyloid-binding Small Molecules Efficiently Block SEVI (Semen-derived Enhancer of Virus Infection)- and Semen-mediated Enhancement of HIV-1 Infection*. Journal of Biological Chemistry, 285**,** 35488-35496.

Olsson, F., Schmidt, S., Althoff, V., Munter, L. M., Jin, S., Rosqvist, S., Lendahl, U., Multhaup, G. & Lundkvist, J. (2014). *Characterization of Intermediate Steps in Amyloid Beta (Aβ) Production under Near-native Conditions*. Journal of Biological Chemistry, 289**,** 1540-1550.

Olubiyi, O. O., Frenzel, D., Bartnik, D., Gluck, J. M., Brener, O., Nagel-Steger, L., Funke, S. A., Willbold, D. & Strodel, B. (2014). *Amyloid Aggregation Inhibitory Mechanism of Arginine-rich D-peptides*. Current Medicinal Chemistry, 21**,** 1448-1457.

Olubiyi, O. O. & Strodel, B. (2012). *Structures of the Amyloid β-Peptides Aβ1–40 and Aβ1–42 as Influenced by pH and a d-Peptide*. The Journal of Physical Chemistry B, 116**,** 3280-3291.

Orgogozo, J. M., Gilman, S., Dartigues, J. F., Laurent, B., Puel, M., Kirby, L. C., Jouanny, P., Dubois, B., Eisner, L., Flitman, S., Michel, B. F., Boada, M., Frank, A. & Hock, C. (2003). *Subacute meningoencephalitis in a subset of patients with AD after Aβ42 immunization*. Neurology, 61**,** 46-54.

Oster-Granite, M. L., McPhie, D. L., Greenan, J. & Neve, R. L. (1996). *Age-Dependent Neuronal and Synaptic Degeneration in Mice Transgenic for the C Terminus of the Amyloid Precursor Protein*. The Journal of Neuroscience, 16**,** 6732-6741.

Permanne, B., Adessi, C., Saborio, G. P., Fraga, S., Frossard, M. J., Van Dorpe, J., Dewachter, I., Banks, W. A., Van Leuven, F. & Soto, C. (2002). *Reduction of amyloid load and cerebral damage in a transgenic mouse model of Alzheimer's disease by treatment with a beta-sheet breaker peptide*. FASEB J, 16**,** 860-2.

Petkova, A. T., Leapman, R. D., Guo, Z., Yau, W.-M., Mattson, M. P. & Tycko, R. (2005). *Self-Propagating, Molecular-Level Polymorphism in Alzheimer's ß-Amyloid Fibrils*. Science, 307**,** 262-265.

Poduslo, J. F., Curran, G. L., Kumar, A., Frangione, B. & Soto, C. (1999). *β-sheet breaker peptide inhibitor of Alzheimer's amyloidogenesis with increased blood–brain barrier permeability and resistance to proteolytic degradation in plasma*. Journal of Neurobiology, 39**,** 371-382.

Poojari, C. & Strodel, B. (2013). *Stability of Transmembrane Amyloid β-Peptide and Membrane Integrity Tested by Molecular Modeling of Site-Specific $Aβ_{42}$ Mutations*. PLoS ONE, 8**,** e78399.

Prince, M., Bryce, R., Albanese, E., Wimo, A., Ribeiro, W. & Ferri, C. P. (2013). *The global prevalence of dementia: A systematic review and metaanalysis*. Alzheimer's & Dementia, 9**,** 63-75.e2.

Puchtler, H. & Sweat, F. (1965). *Congo red as a stain for fluorescence microscopy of amyloid*. J Histochem Cytochem, 13**,** 693-4.

Qiu, C., Kivipelto, M. & von Strauss, E. (2009). *Epidemiology of Alzheimer's disease: occurrence, determinants, and strategies toward intervention*. Dialogues in Clinical Neuroscience, 11**,** 111-128.

Qiu, W. Q., Walsh, D. M., Ye, Z., Vekrellis, K., Zhang, J., Podlisny, M. B., Rosner, M. R., Safavi, A., Hersh, L. B. & Selkoe, D. J. (1998). *Insulin-degrading Enzyme Regulates Extracellular Levels of Amyloid β-Protein by Degradation*. Journal of Biological Chemistry, 273**,** 32730-32738.

Querfurth, H. W. & LaFerla, F. M. (2010). *Alzheimer's Disease*. New England Journal of Medicine, 362**,** 329-344.

Quist, A., Doudevski, I., Lin, H., Azimova, R., Ng, D., Frangione, B., Kagan, B., Ghiso, J. & Lal, R. (2005). *Amyloid ion channels: A common structural link for protein-misfolding disease*. Proceedings of the National Academy of Sciences of the United States of America, 102**,** 10427-10432.

Rhein, V., Baysang, G., Rao, S., Meier, F., Bonert, A., Müller-Spahn, F. & Eckert, A. (2009). *Amyloid-beta Leads to Impaired Cellular Respiration, Energy Production and Mitochondrial Electron Chain Complex Activities in Human Neuroblastoma Cells*. Cellular and Molecular Neurobiology, 29**,** 1063-1071.

Roan, N. R., Munch, J., Arhel, N., Mothes, W., Neidleman, J., Kobayashi, A., Smith-McCune, K., Kirchhoff, F. & Greene, W. C. (2009). *The cationic properties of SEVI underlie its ability to enhance human immunodeficiency virus infection*. J Virol, 83**,** 73-80.

Rzepecki, P., Nagel-Steger, L., Feuerstein, S., Linne, U., Molt, O., Zadmard, R., Aschermann, K., Wehner, M., Schrader, T. & Riesner, D. (2004). *Prevention of Alzheimer's disease-associated Abeta aggregation by rationally designed nonpeptidic beta-sheet ligands*. J Biol Chem, 279**,** 47497-505.

Saido, T. C., Iwatsubo, T., Mann, D. M., Shimada, H., Ihara, Y. & Kawashima, S. (1995). *Dominant and differential deposition of distinct β-amyloid peptide species, Aβ N3 (pE), in senile plaques*. Neuron, 14**,** 457-466.

Salloway, S., Sperling, R., Fox, N. C., Blennow, K., Klunk, W., Raskind, M., Sabbagh, M., Honig, L. S., Porsteinsson, A. P., Ferris, S., Reichert, M., Ketter, N., Nejadnik, B., Guenzler, V., Miloslavsky, M., Wang, D., Lu, Y., Lull, J., Tudor, I. C., Liu, E., Grundman, M., Yuen, E., Black, R. & Brashear, H. R. (2014). *Two Phase 3 Trials of Bapineuzumab in Mild-to-Moderate Alzheimer's Disease*. New England Journal of Medicine, 370**,** 322-333.

Savonenko, A. V., Melnikova, T., Laird, F. M., Stewart, K. A., Price, D. L. & Wong, P. C. (2008). *Alteration of BACE1-dependent NRG1/ErbB4 signaling and schizophrenia-like phenotypes in BACE1-null mice*. Proceedings of the National Academy of Sciences of the United States of America, 105**,** 5585-5590.

Schena, M., Shalon, D., Davis, R. W. & Brown, P. O. (1995). *Quantitative monitoring of gene expression patterns with a complementary DNA microarray*. Science, 270**,** 467-70.

Schenk, D., Barbour, R., Dunn, W., Gordon, G., Grajeda, H., Guldo, T., Hu, K., Huang, J., Johnson-Wood, K., Khan, K., Kholodenko, D., Lee, M., Liao, Z., Lieberburg, I., Motter, R., Mutter, L., Soriano, F., Shopp, G., Vasquez, N., Vandevert, C., Walker, S., Wogulis, M., Yednock, T., Games, D. & Seubert, P. (1999). *Immunization with amyloid-β attenuates Alzheimer disease-like pathology in the PDAPP mouse*. Nature, 400**,** 173-177.

Schumacher, T. N., Mayr, L. M., Minor, D. L., Jr., Milhollen, M. A., Burgess, M. W. & Kim, P. S. (1996). *Identification of D-peptide ligands through mirror-image phage display*. Science, 271**,** 1854-7.

Sciarretta, K. L., Gordon, D. J. & Meredith, S. C. (2006). *Peptide-Based Inhibitors of Amyloid Assembly*. Methods in Enzymology, Volume 413**,** 273-312.

Scott, J. & Smith, G. (1990). *Searching for peptide ligands with an epitope library*. Science, 249**,** 386-390.

Selkoe, D. J. (2001). *Alzheimer's Disease: Genes, Proteins, and Therapy*.

Seward, M. E., Swanson, E., Norambuena, A., Reimann, A., Cochran, J. N., Li, R., Roberson, E. D. & Bloom, G. S. (2013). *Amyloid-β signals through tau to drive ectopic neuronal cell cycle re-entry in Alzheimer's disease*. Journal of Cell Science, 126**,** 1278-1286.

Shankar, G. M., Li, S., Mehta, T. H., Garcia-Munoz, A., Shepardson, N. E., Smith, I., Brett, F. M., Farrell, M. A., Rowan, M. J., Lemere, C. A., Regan, C. M., Walsh, D. M., Sabatini, B. L. & Selkoe, D. J. (2008). *Amyloid β-Protein Dimers Isolated Directly from Alzheimer Brains Impair Synaptic Plasticity and Memory*. Nature medicine, 14**,** 837-842.

Shelanski, M., Shin, W., Aubry, S., Sims, P., Alvarez, M. & Califano, A. (2015). *A Systems Approach to Drug Discovery in Alzheimer's Disease*. Neurotherapeutics, 12**,** 126-131.

Sheridan, C. (2015). *Pivotal trials for [beta]-secretase inhibitors in Alzheimer's*. Nat Biotech, 33**,** 115-116.

Smith, G. P. & Petrenko, V. A. (1997). *Phage Display*. Chemical Reviews, 97**,** 391-410.

Sondag, C. M., Dhawan, G. & Combs, C. K. (2009). *Beta amyloid oligomers and fibrils stimulate differential activation of primary microglia*. J Neuroinflammation, 6**,** 1.

Soscia, S. J., Kirby, J. E., Washicosky, K. J., Tucker, S. M., Ingelsson, M., Hyman, B., Burton, M. A., Goldstein, L. E., Duong, S. & Tanzi, R. E. (2010). *The Alzheimer's disease-associated amyloid β-protein is an antimicrobial peptide*. PloS one, 5**,** e9505.

Soto, C. (2003). *Unfolding the role of protein misfolding in neurodegenerative diseases*. Nat Rev Neurosci, 4**,** 49-60.

van Groen, T., Kadish, I., Funke, S. A., Bartnik, D. & Willbold, D. (2013). *Treatment with D3 Removes Amyloid Deposits, Reduces Inflammation, and Improves Cognition in Aged AβPP/PS1 Double Transgenic Mice*. Journal of Alzheimer's Disease, 34**,** 609-620.

van Groen, T., Wiesehan, K., Funke, S. A., Kadish, I., Nagel-Steger, L. & Willbold, D. (2008). *Reduction of Alzheimer's Disease Amyloid Plaque Load in Transgenic Mice by D3, a D-Enantiomeric Peptide Identified by Mirror Image Phage Display*. ChemMedChem, 3**,** 1848-1852.

van Groen, T., Kadish, I., Wiesehan, K., Funke, S. A. & Willbold, D. (2009). *In vitro and in vivo Staining Characteristics of Small, Fluorescent, Aβ42-Binding D-Enantiomeric Peptides in Transgenic AD Mouse Models*. ChemMedChem, 4**,** 276-282.

Varvel, N. H., Bhaskar, K., Kounnas, M. Z., Wagner, S. L., Yang, Y., Lamb, B. T. & Herrup, K. (2009). *NSAIDs prevent, but do not reverse, neuronal cell cycle reentry in a mouse model of Alzheimer disease*. J Clin Invest, 119**,** 3692-702.

Viola, K. & Klein, W. (2015). *Amyloid β oligomers in Alzheimer's disease pathogenesis, treatment, and diagnosis*. Acta Neuropathologica, 129**,** 183-206.

Vlieghe, P., Lisowski, V., Martinez, J. & Khrestchatisky, M. (2010). *Synthetic therapeutic peptides: science and market*. Drug Discovery Today, 15**,** 40-56.

Wang-Dietrich, L., Funke, S. A., Kuhbach, K., Wang, K., Besmehn, A., Willbold, S., Cinar, Y., Bannach, O., Birkmann, E. & Willbold, D. (2013). *The amyloid-beta oligomer count in cerebrospinal fluid is a biomarker for Alzheimer's disease*. J Alzheimers Dis, 34**,** 985-94.

Wang, D.-S., Iwata, N., Hama, E., Saido, T. C. & Dickson, D. W. (2003). *Oxidized neprilysin in aging and Alzheimer's disease brains*. Biochemical and Biophysical Research Communications, 310**,** 236-241.

White, J. A., Manelli, A. M., Holmberg, K. H., Van Eldik, L. J. & LaDu, M. J. (2005). *Differential effects of oligomeric and fibrillar amyloid-β1–42 on astrocyte-mediated inflammation*. Neurobiology of Disease, 18**,** 459-465.

Wisniewski, T. & Goñi, F. (2015). *Immunotherapeutic Approaches for Alzheimer's Disease*. Neuron, 85**,** 1162-1176.

Wolfe, M. S. (2006). *The γ-Secretase Complex: Membrane-Embedded Proteolytic Ensemble*. Biochemistry, 45**,** 7931-7939.

Zhang, W., Arteaga, J., Cashion, D. K., Chen, G., Gangadharmath, U., Gomez, L. F., Kasi, D., Lam, C., Liang, Q., Liu, C., Mocharla, V. P., Mu, F., Sinha, A., Szardenings, A. K., Wang, E., Walsh, J. C., Xia, C., Yu, C., Zhao, T. & Kolb, H. C. (2012). *A Highly Selective and Specific PET Tracer for Imaging of Tau Pathologies*. Journal of Alzheimer's Disease, 31**,** 601-612.

Zhang, Y.-w., Thompson, R., Zhang, H. & Xu, H. (2011). *APP processing in Alzheimer's disease*. Molecular Brain, 4**,** 3-3.

Zhao, W.-Q., De Felice, F. G., Fernandez, S., Chen, H., Lambert, M. P., Quon, M. J., Krafft, G. A. & Klein, W. L. (2008). *Amyloid beta oligomers induce impairment of neuronal insulin receptors*. The FASEB Journal, 22**,** 246-260.

Zhu, H. & Snyder, M. (2003). *Protein chip technology*. Current Opinion in Chemical Biology, 7**,** 55-63.

Danksagung

An dieser Stelle möchte ich mich bei allen, die mich während meiner Promotion unterstützt haben, bedanken.

Prof. Dr. Dieter Willbold danke ich für die Bereitstellung des interessanten Themas, fachlichen Diskussionen, die Möglichkeit der Weiterbildung auf internationalen Konferenzen und Projektbesprechungen und seiner generellen Unterstützung. Ich danke Ihm auch für die Bereitstellung der wissenschaftlichen Ausrüstung und meines Verbrauchsmaterials im Institut.

Vielen Dank an Dr. Janine Kutzsche für viele fachliche Diskussionen und eine immer offene Bürotür.

Markus Tusche, Tamar Ziehm, Stephan Rudolph und der restlichen Alzheimer-Therapie-Gruppe danke ich für die hilfsbereite, freundliche und angenehme Zusammenarbeit.

Bei Dr. Aileen Funke und Dr. Dirk Bartnik möchte ich mich für die fachliche Unterstützung und Diskussionen während den Anfängen meiner Doktorarbeit bedanken.

Vielen Dank auch an das sFida-Büro für aufmunternde Worte und eine schöne Zeit.

Den vielen helfenden Händen (TAs, Doktoranden, Masteranden…) während meiner Promotion möchte ich herzlich für ihre Unterstützung danken.

Dem gesamten ICS-6 und Institut für Physikalische Biologie danke ich für die fachliche Unterstützung und die gute Zusammenarbeit.

Zum Schluss danke ich meinen Eltern, ohne die die ganze Promotion nicht möglich gewesen wäre.

Eidesstattliche Erklärung

Hiermit erkläre ich an Eides statt, dass ich die vorliegende Dissertation selbständig verfasst und keine anderen als die von mir angegebenen Quellen und Hilfsmittel verwendet und Zitate kenntlich gemacht habe.

Ferner erkläre ich, dass ich in keinem anderen Dissertationsverfahren mit oder ohne Erfolg versucht habe, diese Dissertation einzureichen.

Düsseldorf, den

(Antonia Nicole Klein)